

# An investigation of combing forces and related fibre breakage

**Author:**

Wang, Xungai

**Publication Date:**

1991

**DOI:**

<https://doi.org/10.26190/unsworks/11419>

**License:**

<https://creativecommons.org/licenses/by-nc-nd/3.0/au/>

Link to license to see what you are allowed to do with this resource.

Downloaded from <http://hdl.handle.net/1959.4/66611> in <https://unsworks.unsw.edu.au> on 2024-04-20



UNSW LIBRARY  
PT677.31/40



>009523243

X. WANG

STACK

PhD

1991

P  
T 677-31  
40

UNSW



THE UNIVERSITY OF NEW SOUTH WALES

DECLARATION RELATING TO DISPOSITION  
OF  
PROJECT REPORT/THESIS

This is to certify that I .....XUINGHAI WANG..... being a  
candidate for the degree of .....Ph.D..... am fully  
aware of the policy of the University relating to the retention and use of higher  
degree project reports and theses, namely that the University retains the copies  
submitted for examination and is free to allow them to be consulted or borrowed.  
Subject to the provisions of the Copyright Act, 1968, the University may issue a  
project report or thesis in whole or in part, in photostat or microfilm or other  
copying medium.

In the light of these provisions I grant the University Librarian permission to  
publish, or to authorize the publication of my project report/thesis, in whole or in  
part.

I also authorize the publication by University Microfilms of a 350 word abstract  
in *Dissertation Abstracts International* (applicable to doctorates only).

Signature .....

Witness.....

Date .....July 25, 1991.....

---

**AN INVESTIGATION OF COMBING FORCES  
AND RELATED FIBRE BREAKAGE**

---

**A thesis submitted to  
The University of New South Wales  
for the degree of  
Doctor of Philosophy**

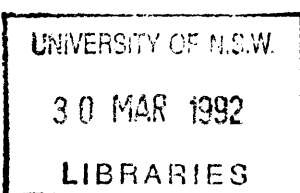
**by**

**Xungai Wang**

**Department of Textile Technology  
School of Fibre Science and Technology  
The University of New South Wales**

**July 1991**





**CERTIFICATE OF ORIGINALITY**

---

I hereby declare that this submission is my own work and that, to the best of my knowledge and belief, it contains no material previously published or written by another person nor material which to a substantial extent has been accepted for the award of any other degree or diploma of a university or other institute of higher learning, except where due acknowledgement is made in the text.

(Signed) .....



## ACKNOWLEDGEMENTS

---

I would like to express my sincere appreciation to my supervisor Dr. Nigel Johnson for his responsible guidance, close co-operation and friendly encouragement throughout the course of this research.

Special thanks are due to Dr. Michael Young for his valuable suggestions and generous help, and to Ms. Ursula Wohnlich and Mrs. Vera Seder for their tremendous assistance and friendship.

Thanks are also due to all my friends and colleagues, especially those in the Yarn Technology group and Textile Physics group, for their useful discussions and encouragement. Support from the administration of this school, and from the faculty workshop of Applied Science, has been invaluable as well.

I am very grateful to my family, to Julie Zhang and her family for their sacrifice and understanding.

I am also very grateful to the Northwest Institute of Textile Science and Technology in Xi'an, the State Education Commission of China, the Australian Wool Research & Development Fund and the Australia China Education Co-operation Program for making this research possible.

## ABSTRACT

---

Fibre breakage and low production rate of worsted combs have been two major barriers for a more efficient worsted topmaking practice in the wool industry. This project has been carried out to investigate the incidence and mechanisms of fibre breakage in woolcombing, and to explore fundamentally the possibilities of increasing the combing production rate without excessive fibre breakage.

Two sets of apparatus have been developed, using real time data acquisition and strain gauge techniques, to measure respectively the tension experienced by individual fibres, and the forces acting on a single pin during combing.

The results from the fibre tension measurement suggest that the tension peaks experienced by individual fibres, can give a better indication to the extent of fibre breakage than can the average fibre tension levels, which are usually much lower than the fibre breakage strength.

In the pin force investigation, general pictures regarding the effect on fibre breakage of various fibre entanglements have been obtained. This investigation also indicates that detailed examination of the mechanism of fibre breakage and its prevention requires more fundamental knowledge about whether or not, and how, an individual fibre entanglement contributes to the total fibre breakage level.

The major types of entanglement in a fibre assembly are parallel fibres, looped fibres, hooked fibres, twisted fibres and fibre neps. The first three entanglement types have

---



been theoretically analyzed by previous researchers. In this thesis, a theory has been developed to examine how a combing pin can disentangle two twisted fibres without breaking them. The theory elucidates that, if the pin speed exceeds a critical value, the twisted fibres will not be able to untwist quickly enough, and the consequent increase in the helix angle of the twisted section leads to the inevitable consequences of buckling or snarling of that section; the fibres then simply stretch to break, such breakage being analogous to that of a looped fibre engaged by a combing pin. This critical pin speed value is predicted by the theory, and experimental results have generally confirmed predictions of this theory.

---

## LIST OF SYMBOLS

---

$a$	Radius of ply axis helix about cord axis
$b$	Radius of ply as it lies in the cord
$b_{pr}$	Pin arm width
$B$	Flexural rigidity
$d,$	Diameter
$E, E_1, E_2, E_f, E_{pr}$	Tensile Young's moduli
$F$	Tensile force
$F_{HL}$	Static friction of free fibre length
$F_{TL}$	Inertia of free fibre length
$F_R, F_{ZR}$	Restraining forces
$F_{max}$	Maximum fibre tension
$F_{pr}$	Maximum pin force
$F_{CWep}, F_{Cpr}$	Centrifugal forces
$f_1, f_2, f_3$	Functions of $V_p, \theta$ , etc.
$f_n$	Natural frequency of pin arm
$G, G_f$	Moduli of rigidity
$g$	Acceleration of gravity
$H, h$	Lengths
$h_{pr}$	Pin arm thickness
$I, I_f, I_z$	Moments of inertia
$I_p$	Polar moment of inertia
$K_1, K_2$	Constants
$K_f$	Effective torsional inertia of a fibre

---



List of Symbols

---

$L, L_{pr}, L'_{pr}, l, l', l_0, l_t, l_{sg}$	Lengths
$M, \Sigma M$	Torques
$M_b$	Bending moment
$M_t$	Twisting torque
$M_\theta, M_{\theta 0}$	Helix angle related torques
$M_{ZR}$	Restraint torque
$M_B, M_{Bz}$	Torques due to bending
$M_T, M_{Tz}$	Torques due to torsion
$M_{Fz}$	Torque due to tension
$m, m_F$	Masses
$N_0, N$	Twist numbers
$n$	Viscous coefficient
$n_b$	Rotational speed of beater
$n_p$	Number of plies in a cord
$R_a$	Radius of pin arm adaptor
$R_b, R_c$	Radii of curvature
$R_p$	Pin radius
$r, r_f$	Fibre radii
$T, T'$	Tensions
$T_c, T_f$	Twist levels in cord, fibre
$T_{limit}$	Maximum cord twist
$Tt_F$	Fibre fineness
$t$	Time
$V, V_p$	Pin speeds
$V_A$	Clothing element speed
$V_E$	Feeding speed

---

List of Symbols

$v$	Fibre free end velocity
$v_n, v_p$	Components of $v$ , normal and perpendicular to fibre axis
$v_b$	Limiting breaking velocity
$V_t$	Transverse wave velocity
$V_l$	Longitudinal wave velocity
$W_{ep}, W_{pr}$	Weights
$x, x_z, X_{pr}$	Distances
$\sigma, \sigma_1, \sigma_2, \sigma_t, \sigma_{AFpr}, \sigma_{AC}, \sigma_{prm}$	Stresses
$\epsilon, \epsilon_r, \epsilon_{AFpr}, \epsilon_{Ac}$	Strains
$\theta, \theta_0$	Cord helix angles
$\theta_{limit}$	Limit of cord helix angle
$\alpha, \alpha_b, \alpha_r, \alpha_t, \alpha_z$	Various angles
$\delta, \delta_c$	Angular accelerations
$\beta_t$	Angular deformation
$\varphi$	Rotational angle
$\omega_b$	Angular speed of beater
$\tau_b$	Breaking twist
$\rho, \rho_{pr}$	Densities
$\mu_{F/S}, \mu_s, \mu_k$	Coefficients of friction



## TABLE OF CONTENTS

---

***CERTIFICATE OF ORIGINALITY***

***ACKNOWLEDGEMENTS***

***ABSTRACT***

***LIST OF SYMBOLS***

<b>CHAPTER 1: INTRODUCTION .....</b>	<b>1</b>
1.1 THE COMBING PROCESS .....	1
1.1.1 The Importance and Objectives of Woolcombing .....	1
1.1.2 Combing Machine and Its Working Principle .....	2
1.1.3 Investigations of Rectilinear Combing .....	5
1.1.3.1 Theoretical works .....	6
1.1.3.2 Empirical works .....	7
1.1.4 Scope of the Present Work .....	9
1.2 MECHANICAL PROPERTIES OF WOOL FIBRES .....	11
1.2.1 Tensile Properties of Wool Fibres .....	12
1.2.1.1 General introduction .....	12
1.2.1.2 Stress-strain behaviour .....	13
1.2.1.3 Time effects .....	14
1.2.1.4 Effects of loading rate on breakage .....	16
1.2.2 Bending Properties .....	18
1.2.3 Torsional Properties .....	19
1.2.4 Frictional Properties .....	20
1.3 THEORETICAL ANALYSES OF FIBRE BREAKAGE .....	22

---

## Table of Contents

---

1.3.1	Introduction .....	22
1.3.2	Different Forms of Fibre--Combing Element Interaction .....	23
1.3.3	Theoretical Analysis of Individual Cases .....	24
1.3.3.1	Fibre loops .....	24
1.3.3.2	Fibre hooks .....	25
1.3.3.3	Parallel fibres .....	28
1.4	SUMMARY .....	31
 <b>CHAPTER 2: STUDY OF FIBRE TENSION IN COMBING .....</b>		<b>33</b>
2.1	INTRODUCTION .....	33
2.2	QUALITATIVE THEORY .....	35
2.3	EXPERIMENTAL .....	37
2.3.1	Apparatus .....	37
2.3.2	Preparations .....	38
2.3.3	Testing Procedure .....	39
2.3.4	Parameters Investigated .....	40
2.4	RESULTS AND DISCUSSION .....	41
2.4.1	Mean Tension Levels .....	41
2.4.1.1	Effect of test fibre length .....	41
2.4.1.2	Effect of combing speed .....	41
2.4.1.3	Effect of fringe length and fringe density .....	43
2.4.2	Peak Tensions .....	43
2.4.3	Fibre Breakage .....	45
2.5	CONCLUSION .....	47
 <b>CHAPTER 3: STUDY OF PIN FORCES IN COMBING .....</b>		<b>49</b>
3.1	INTRODUCTION .....	49
3.2	THEORETICAL CONSIDERATIONS .....	50

---

---

3.3	EXPERIMENTAL .....	54
3.3.1	Apparatus .....	54
3.3.2	Sample Preparation .....	55
3.3.3	Testing Procedure .....	56
3.3.4	Parameters Investigated .....	57
3.4	RESULTS AND DISCUSSION .....	58
3.4.1	Mean Levels of the Pin Force .....	58
3.4.1.1	Effect of fringe density .....	58
3.4.1.2	Effect of fringe length .....	58
3.4.1.3	Effect of processing stage .....	58
3.4.2	Individual Patterns of the Pin Force .....	59
3.5	CONCLUSION .....	61

<b>CHAPTER 4: THE BEHAVIOUR OF A PIN DISENTANGLING</b>	
	<b>TWO TWISTED FIBRES ..... 63</b>
4.1	INTRODUCTION ..... 63
4.2	THEORY ..... 66
4.2.1	Qualitative Description ..... 66
4.2.2	Physical Modelling ..... 67
4.2.3	Torque in Two Twisted Fibres ..... 69
4.2.4	Effect of Pin Movement on Helix Angle ..... 72
4.2.5	Tension in the Fibres Behind the Pin ..... 76
4.2.6	Limit of the Helix Angle ..... 77
4.2.7	Fibre Breakage and Maximum Pin Speed ..... 79
4.3	CASE ANALYSIS ..... 80
4.4	EXPERIMENTAL VERIFICATION OF THE THEORY ..... 83



Table of Contents

---

4.4.1	Material .....	83
4.4.2	Apparatus .....	84
4.4.3	Parameters Examined .....	84
4.4.4	Theoretical Predictions .....	85
4.4.5	Empirical Results and Discussion .....	86
4.4.5.1	Fast speed .....	86
4.4.5.2	Slow speed .....	86
4.4.5.3	Discrepancies .....	87
4.5	CONCLUSION .....	88
 <b>CHAPTER 5: CONCLUSION .....</b>		<b>91</b>
5.1	SUMMARY .....	91
5.2	FURTHER WORK .....	96
 <b>APPENDIX I: PIN ARM DESIGN .....</b>		<b>99</b>
 <b>APPENDIX II: TABLES OF EXPERIMENTAL DATA .....</b>		<b>107</b>
 <b>REFERENCE .....</b>		<b>115</b>

---

## CHAPTER 1

### INTRODUCTION

---

## 1.1 THE COMBING PROCESS

### 1.1.1 The Importance and Objectives of Woolcombing

The modern wool textile industry is dominated by three major systems for converting fibres into fabrics: the woollen, worsted and semi-worsted systems. Yarns made from these three systems are called woollen, worsted and semi-worsted yarns respectively. Worsted yarns, compared with woollen and semi-worsted yarns, differ a great deal in both their character and their end-use. Worsted yarns are smoother, stronger, more uniform and can be finer, and thus give the ultimate worsted fabric a neat, smooth appearance. On the other hand, the woollen fabric normally has a rough and bulky appearance, mainly because the woollen yarns are fuzzy and have the constituent fibres crossed in all directions [1]. Yarns produced from the semi-worsted system contain fibres of all lengths, and are much bulkier and lack the leanness and smoothness associated with worsted yarns; they are suitable for end uses such as carpets, blankets, upholstery and hand-knitting [2]. Generally speaking, these differences arise from the fact that the processing units and their arrangements in woollen, worsted and semi-worsted systems are quite different, and also because the worsted system uses a much longer processing route from raw material to resultant yarn. Detailed information on the whole range of operations involved in these three systems has been presented elsewhere [2,3]. More specifically, the key factor which

makes the difference between the worsted, woollen and semi-worsted systems is the operation of combing. Woolcombing is characteristic of the worsted system of fibre processing, and is generally regarded as being of major practical importance [4].

The main objectives of the combing process are:

- 1). to remove from the carded and gilled sliver, the short fibres, highly entangled fibres (eg. neps), and remaining foreign matters (eg. vegetable matters, etc.). Short fibres and neps arise because fibre breakage and nep formation in carding are almost inevitable, due to the tangled nature of the scoured wool normally fed into the card [5, 6, 7, 8]. The presence of too many short fibres, neps and impurities adversely affects the drafting during subsequent drawing stages and produces faults in the final yarn which eventually show up in the fabric; it also limits the fineness of the yarn which could be spun from the particular material [9].
- 2). to arrange the remaining long fibres into a more or less parallel formation and at the same time, assemble them into a continuous twistless sliver. This sliver is very crucial for the production of fine and strong worsted yarns.

### **1.1.2 Combing Machine and Its Working Principle**

Until the 1970's, two distinct comb types were of commercial importance in the textile industry, the rectilinear comb and the Noble comb. These two types of machine were invented in 1846 and 1853 respectively, and they both have their respective advantages and disadvantages in industrial applications. It is generally accepted that the rectilinear comb gives a superior combing action, while the Noble comb claims

some merit because of its continuous feeding and drawing-off system. Several workers [10, 11, 12] compared the Rectilinear comb and Noble comb from various aspects to establish possible differences in their performances, but no conclusive evidence exists that one is better than the other in all situations. The choice of different machines largely depends on the class and length of the wool to be combed, the amount of vegetable matter present, and the kind of combed sliver (top) required [2]. Aldrich [9] pointed out that traditionally, the Noble comb was reserved for wools longer than about 65 to 70 mm mean fibre length (m.f.l) and free or nearly free from vegetable matter; while the rectilinear comb was reserved for short and medium length wool (although there is no reason why it can not deal satisfactorily with long wools), whether it be free from vegetable matter or not. The same person then mentioned that the rectilinear comb seemed to be a more versatile comb in that it could comb a wider fibre length range than could the Noble comb, and it could comb both burr-free and burry wools as well. Chaikin and Collins [13] also shared this point of view. They discussed many reasons why Noble combing had virtually disappeared, and concluded that the major factor in the demise of Noble combing was probably the modern trend towards machines which were not fibre specific. The ability to comb only long fibres using the Noble comb obviously provides a positive disincentive to improve the process, since this represents only a limited market to the machine maker. On the other hand, the rectilinear comb is more versatile and hence the incentive for development is high. More recently, Gore and Lee [14] forecast that "rectilinear combing will remain the most common method of removing short fibres and impurities for carded wool. The action will remain the same, but some mechanical parts may in the distant future be replaced by electronics". Because of these considerations, only the combing action of rectilinear combs will be considered in the present study.

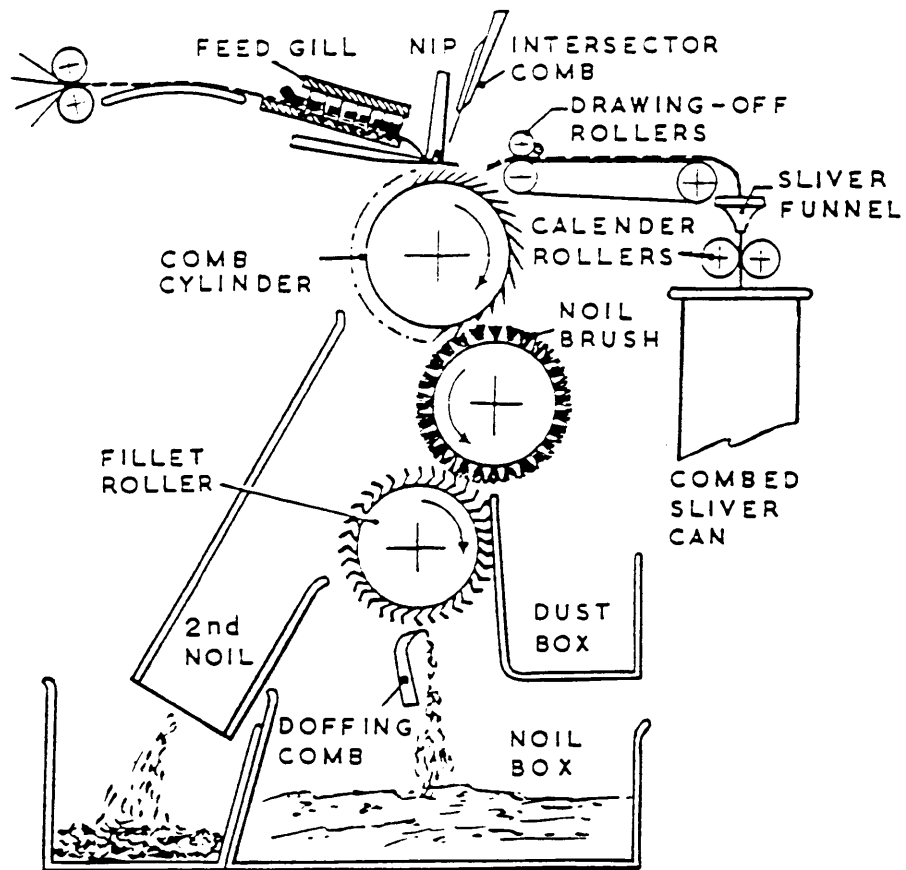


Figure 1.1: Diagram of the rectilinear comb [2]



Detailed descriptions of the working principle of the rectilinear comb have been given by several authors [15, 16, 17], so only a brief review of its operation with relevant emphasis on features which may relate to fibre breakage will be given here. Figure 1.1 is a simple diagram which shows the important parts of the machine [2].

The rectilinear comb functions in an intermittent way. The basic cycle of its operation consists of the following major steps:

- 1). Feeding the carded and gilled slivers into the comb through a pair of intermittently rotating rollers and the feed gill.
- 2). Holding of the leading ends of the slivers in the nipper jaws and initial combing of the fringe protruding from the front of the jaws by the comb cylinder.
- 3). Drawing of the combed fringe from the sliver by the drawing-off rollers and at the same time, final combing of the trailing ends by the intersector comb (top comb).
- 4). Assembling of the fully combed fringes on the leather apron and passing through the sliver funnel and the calender rollers to form a continuous combed sliver.

The short fibres, neps and foreign matters, known as noils and waste materials, are taken by the pins of the comb cylinder during combing and are later removed by a brush roller, which in turn is cleared by a card-clothed roller with an oscillating comb.

Some important factors regarding the machine are:

Gauge setting: the closest distance between the nipper jaws and the nip of the withdrawal rollers. It is also referred to as the noil setting, or the detachment setting, etc.

Comb speed: the rate at which the comb completes a full operation cycle, it is also the rotational speed of the comb cylinder and is normally expressed as nips/min.

Pin density: the density of the pins of the top comb and of the comb cylinder.

Pin type: pins of different size and shape.

It is worth noting that there are two combing actions on the machine to comb the two ends of the fibres, the initial combing by the comb cylinder and the final combing by the top comb and the feed gill. Both can contribute to fibre breakage in the combing process. In order to distinguish between the extent of fibre breakage due to these two different components of the comb's operation, and to gain a greater understanding of the machine, a review of available studies on rectilinear combing follows.

### **1.1.3 Investigations of Rectilinear Combing**

Although the rectilinear and Noble combing machines were invented in the mid 19th century and have played an important role in the textile industry since then, extensive research work on these machines was not reported until 1955. Those research works will be briefly reviewed here in two major categories: theoretical and experimental.

### 1.1.3.1 Theoretical works

The theoretical works on combing include some fundamental studies of the worsted rectilinear comb, and theories of predicting fibre breakage during rectilinear combing.

Ideally, a combing machine is supposed to remove all the short fibres into the noil and reserve the long fibres in the combed sliver. In a qualitative description of the operation of the worsted rectilinear comb, Belin and Walls [18] presented a simplified geometrical theory for the selection of fibres on a length basis into the top and noil during rectilinear combing. The following assumptions (as later summarized by Aldrich [9]) were used in their derivation of the theory:

- 1). no fibre breakage occurs during combing;
- 2). there is no interaction between individual fibres;
- 3). the selection of fibres for the top and noil is made on length basis only and is not influenced by fibre diameter; and
- 4). the combing action of the comb cylinder and top comb is perfect.

This theory qualitatively agrees with the authors' experimental results, but there are quantitative differences. The authors found that their calculated values for percentage noil and mean fibre length of the top were respectively lower and higher than the measured values, and they ascribed the differences partly to fibre breakage which occurred during combing. Further extension of the theory by Belin and Verhagen [19] concluded that ineffective gripping of the fibres in the nipper jaws could also contribute to the discrepancies. Detailed verification by Aldrich [9] of those

conclusions drawn from this simplified geometrical theory established that the assumptions of no fibre breakage and no interaction between fibres were indeed not valid under practical combing conditions.

The importance of the intricate phenomenon of fibre breakage in rectilinear combing was soon realized by many researchers. Theoretical derivations of various formulae to calculate fibre breakage are based on the increase in the number of fibres relative to the original number entering the comb, together with some additional assumptions. Dyson and Happey [4] investigated fibre breakage in Noble combing mathematically on the basis of two alternative hypotheses: that the probability of breakage was equally likely in fibres of all lengths, or, that the probability of breakage was proportional to fibre length. They indicated that the comb made its own noil by breaking many fibres. According to the formula they derived, the calculated percentage fibre breakage values varied from 6.6 to 14.5%. In a study of rectilinear combing of mohair, Kruger [20] derived a formula to calculate the fibre breakage for a blend of different fibres. His formula was later modified by Kruger and Aldrich [21] to investigate wool fibre breakage during rectilinear combing, and the calculated percentage breakage level went up to 31% in certain cases. Godawa et al [22] stated that even under optimum conditions, fibre breakage in rectilinear combing could still be of the order of 15 to 25%.

### **1.1.3.2 Empirical works**

In addition to the empirical work carried out for verification of the various theories mentioned above, numerous other experiments have also been carried out to investigate various aspects of combing performance.

Experiments closely related to fibre breakage were carried out by Aldrich and Kruger respectively [9, 23, 24, 25]. They examined the forces involved in withdrawing a tuft of fibres from a sliver inserted in a pin bed containing combs of variable pin density, at both low and high speeds. Special sets of apparatus were constructed, using strain gauge and pen recording techniques to get the withdrawal forces during combing. A significant increase in withdrawal forces was observed with increased pin density and increased fibre entanglement. However, both of them finally came to the conclusion that the withdrawal forces per fibre were well below the breaking strength of the weakest fibres present in the tuft. Aldrich's results showed that the average withdrawal force per fibre was of the order of 0.45 to 0.65 gf [9], being only 5 to 10% of typical merino wool fibre breaking strengths.

Many experiments have also been carried out to investigate the effects of lubricants in wool combing. Belin [26] investigated the influence of residual grease on gilling and combing performance. The author reported an optimum level of residual grease of approximately 0.8% as giving the lowest percentage noil and longest mean fibre length. Belin [27] also investigated the influence of the viscosity of mineral lubricants on the carding, gilling and rectilinear combing of wool. An extensive investigation of the influence of lubricants in rectilinear combing was made by Kruger [28]. All these investigations generally agree that an improvement in combing performance can be achieved through the addition of a certain amount of lubricant; levels of 1 to 2% were reported, depending on the type of lubricant and the amount of residual grease left on the wool after scouring.

The effect of comb speed has been examined by several researchers. Aldrich [9] reported that, with three different comb speeds of 130, 150 and 165 nips per minute, no significant effect could be detected as far as percentage noil and top cleanliness



were concerned. Turpie and Klazar [29] expanded the speed range from as low as 7 to as high as 165 nips per minute, but no change in the fibre breakage pattern with speed increase was found. They concluded that over the range of speeds from 50 to 165 nips/min, no detectable change in the combing performance of the rectilinear comb could be observed when combing the particular 64's wool investigated.

Belin and Taylor [30] investigated the directional effects of fibre hooks present in slivers subjected to rectilinear combing. They found that when fibres were combed with hooks leading, both ends could be gripped by the nipper and the hook broken by the circular comb, whereas when the hooks were trailing there was evidence that fibre breakage was low.

Investigations into various other aspects regarding combing performance, such as removal of neps and vegetable matters, effect of some precarding conditions, effect of different types of comb cylinders, etc., can also be found in the literature [31, 32, 33, 34, 35].

#### **1.1.4 Scope of the Present Work**

Since 1971, very little research work on woolcombing has appeared in the literature. Many crucial questions regarding combing performance remain unanswered. About a decade ago, Chaikin and Collins [13] pointed out that production rates of combs were still well below that of gill-boxes and hence combs may be regarded as a bottle-neck in the processing sequence. This problem becomes much more serious today, with recent investigations indicating that the production rates in wool carding may be doubled in the near future [36]. Although several experimental works showed no detectable deterioration in combing performance with increased comb speed (over

the range examined), the upper speed limit on the existing combs can not just be simply increased further because of their complex structure and the presence of mechanical shocks on those machines at high speed. No theoretical work has ever attempted to ascertain whether there exists a threshold value for combing speed above which combing performance would deteriorate.

Fibre breakage is another major concern. Existing theories on percentage fibre breakage only provide a "summarizing picture of the combing process as a whole" [9]. Many important parameters, such as combing speed and mechanical properties of the fibres, have not been considered in almost all the available theories on combing. The average withdrawal force (through the top comb and the feed gill) was measured on simulated devices and found to be well below the breaking strength of the weakest fibres present in the fringe, yet the forces involved in the combing action of the comb cylinder (the only other combing element) are unknown. With these considerations, the present study aimed to investigate the role of the comb cylinder in causing fibre breakage, by:

- 1). measuring and studying the forces involved in the combing action of the comb cylinder, using specially constructed simulators. These forces include the force (or tension) experienced by individual wool fibres lying in the fringe during combing, and the forces acting on a single clothing element as it combs through different wool fringes.
- 2). investigating individually, the fundamental mechanisms of fibre breakage with reference to the mechanical properties of wool fibres and the interaction between clothing elements and wool fibres of different configurations.

- 3). exploring theoretically the maximum possible speed of the clothing element without fibre breakage, based on its disentangling of different forms of fibre entanglement present in pre-combed slivers.

It is hoped that these relatively fundamental studies could add to the knowledge of the nature, as well as the cause, of fibre breakage in combing and other similar opening actions. More importantly, it is hoped that these studies could shed some light on the possibility of increasing the production rate in woolcombing without causing excessive fibre breakage.

Since the mechanical properties of wool fibres are closely associated with their breakage behaviour, a brief review of some of the relevant mechanical properties of wool fibres follows.

## **1.2 MECHANICAL PROPERTIES OF WOOL FIBRES**

In various mechanical processes (including combing), wool fibres are very frequently subjected to different kinds of stretching, change of direction, twisting and relative movement against themselves and other surfaces. These activities are closely associated with certain mechanical properties of the fibres, such as tensile, bending, torsional and frictional properties. To a certain extent, these properties determine whether the wool fibres can survive a particular stage of mechanical processing, and whether they can be satisfactorily transferred from one processing stage to another. As far as combing is concerned, while it was realized that "the fibres themselves rather than the mechanism should provide the factor limiting the ultimate combing speed" [37], early research work (both theoretical and empirical) on fibre breakage in woolcombing was mainly concerned with the influence of the machine settings

and the length of the wool fibres, without much concern for the mechanical properties of the wool fibres themselves. Since the internal structure of wool fibres has been described extensively elsewhere [38, 39, 40, 41], it would be redundant to describe it here; rather, some of the relevant mechanical properties of wool fibres are briefly reviewed.

## 1.2.1 Tensile Properties of Wool Fibres

### 1.2.1.1 General introduction

Wool fibre is viscoelastic, i.e. its mechanical response, as can be shown from stress-strain curves, recovery behaviour, creep and stress relaxation, etc., is time dependent. This particular nature of wool fibre means that the stress-strain relationship, and its time dependence can not simply be dealt with by classical theories of elasticity and hydrodynamics; instead, a "constitutive equation" or "rheological equation of state" is normally used [42]. The classical theory of elasticity deals with mechanical properties of solids, for which stress ( $\sigma$ ) is always directly proportional to strain ( $\epsilon$ ) in small deformations, but is independent of the rate of strain ( $d\epsilon/dt$ ), in accordance with the Hooke's law:  $\sigma = E \epsilon$ , where  $E$  is a constant known as the tensile Young's modulus. The classical theory of hydrodynamics, on the other hand, deals with properties of viscous liquids, for which the stress ( $\sigma$ ) is always proportional to the rate of strain ( $d\epsilon/dt$ ) but independent of the strain ( $\epsilon$ ) itself, in accordance with Newton's law:  $\sigma = \eta(d\epsilon/dt)$ , where  $\eta$  is a constant known as the viscous coefficient. Normally the "constitutive equation" for viscoelastic material is much more complicated. As for wool fibre, under standard conditions, only in the

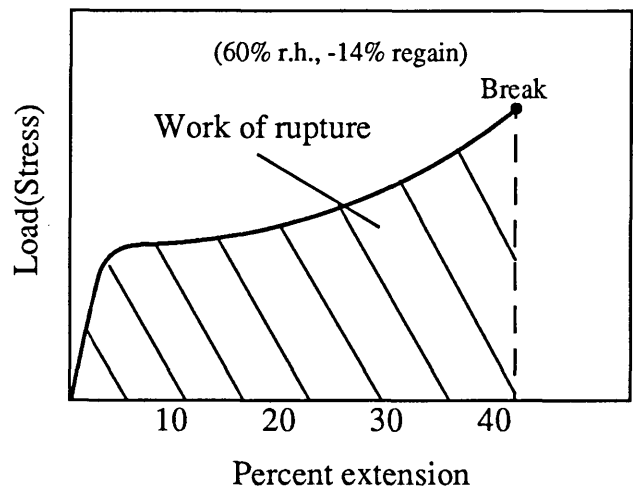


Figure 1.2: Typical load elongation curve for the wool fibre [43, 44, 45]

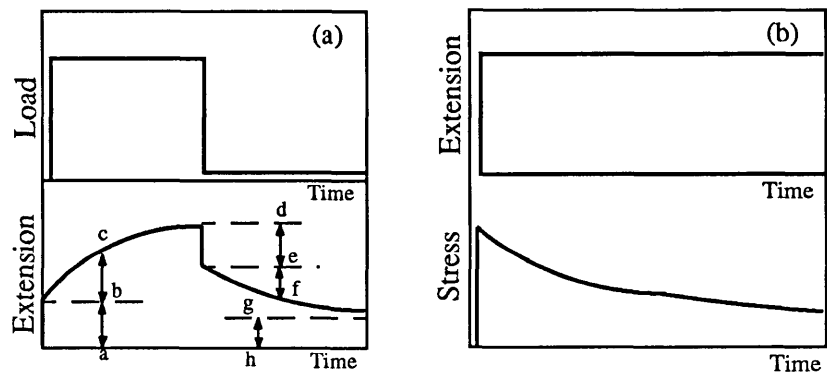


Figure 1.3: (a) Creep under constant load and recovery under zero load, showing instantaneous extension, a-b and d-e; total creep, b-c; primary creep, e-f; and secondary creep, g-h. (b) Relaxation of stress under constant extension [44]

case of very small strains (less than 2% strain, as stated later), does it show some linear viscoelastic behaviour which can be approximately represented with the simple Hooke's law.

### **1.2.1.2 Stress-strain behaviour**

The stress-strain behaviour of the wool fibre has been investigated thoroughly under standard conditions. A typical stress-strain curve of a single wool fibre is shown in Figure 1.2, combining information from several sources [43, 44, 45]. This curve has three distinct and approximately linear regions:

#### 1) The pre-yield region

This region covers the extension range between 0 and 2% strain. In this region, the stress in the fibre is approximately proportional to the strain. This region is also known as the 'Hookean' region and the linearly viscoelastic region. Recovery in this region is good.

#### 2) The yield region

This region extends from about 2 to 30% strain. It is a region of easier extension in which recovery is incomplete.

#### 3) The post-yield region

This region ranges from 30% strain to the breaking point with increasing slope. Permanent damage to the fibre occurs in this region.



In practical tensile testing, what is normally obtained is the load-elongation curve, which becomes the stress-strain curve by a change of units, without affecting the shape of the curve [44], as indicated in Figure 1.2. Two pieces of useful information regarding the breakage of wool fibre which can be obtained from the load-elongation curve are the strength and the work of rupture. The strength, which is given by the breaking load, is a measure of the steady force necessary to break the fibre; while the work of rupture, which is the area under the load-elongation curve, is defined as the energy needed to break the fibre; it gives a measure of the ability of the wool fibre to withstand sudden shocks of given energy. Because of the viscoelastic nature of the wool fibre, its breaking load and work of rupture will depend on the rate at which the load is given. Before any further examination of the loading rate, a brief review of the time effects on the extension caused by a given load, or stress resulting from a given strain in the wool fibre, is necessary.

### 1.2.1.3 Time effects

Figure 1.3 [44] illustrates the time effects on the tensile behaviour of a wool fibre. On the application of a load to the fibre for a given time, the fibre undergoes an instantaneous extension followed by creep; and, on removal of the load, it shows an instantaneous recovery followed by a further partial recovery with time, but some unrecovered extension remains permanently (Figure 1.3(a)).

The stress relaxation behaviour of a wool fibre is illustrated in Figure 1.3(b): when the fibre is stretched to a given extension and maintained at that extension, an instantaneous stress is set up, but this gradually decreases as time passes.

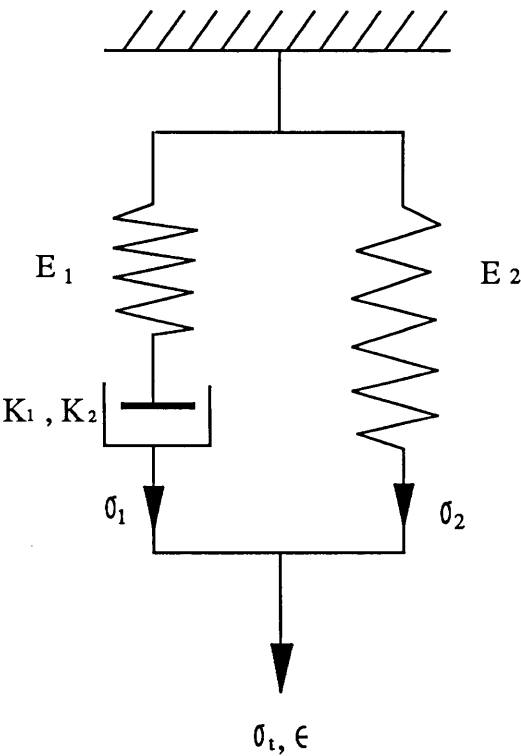


Figure 1.4: Eyring's three element model [47]

The recovery properties of fibres after extension are very important to the preservation of fibre length in certain fibre separation processes (such as carding [45]), where the fibres may be stretched rapidly a number of times; if the fibres can recover quickly from one extension, they will be more able to withstand the next extension.

There are a few models of time-dependent behaviour. The simple ones employ a combination of ideal elastic springs and ideal viscous dashpots, which follow Hooke's law and Newton's law respectively. These simple models have their limitations. First of all, it would require a very complicated arrangement of elements to give a complete representation of the behaviour of fibres; secondly, they can only represent the theory of linear viscoelasticity. By modifying the properties of the ideal viscous dashpot, Eyring and his colleagues [46, 47] put forward the famous three-element model (Figure 1.4). In this model, the springs follow Hooke's law, but the dashpot shows non-Newtonian viscosity, its behaviour being represented by a hyperbolic-sine law of viscous flow:  $d\varepsilon/dt = K_1 \sinh K_2 \sigma$ , where  $K_1$  and  $K_2$  are constants. The total stress, strain, and some other constants as shown in Figure 1.4, are related through the following formula:

$$\frac{d}{dt} \{ (E_1 + E_2) \varepsilon - \sigma \} = E_1 K_1 \sinh K_2 (\sigma - E_2 \varepsilon)$$

This formula, given certain initial conditions, has been found to give good agreement with some experimental results for stress-strain, creep, and stress relaxation behaviour of several fibres [47, 48, 49].

#### 1.2.1.4 Effects of loading rate on breakage

The standard tensile testing methods for textile materials are also referred to as "static" tensile testing. The straining rate is normally between about 1 and 100% per minute in such testing. However, in mechanical processing, fibres are usually subjected to much higher straining rates. Information on the tensile behaviour of the fibres at higher straining rates is therefore very useful. Work on the stress-strain behaviour of some textile materials at straining rates between 10,000 to 200,000% per minute has been published [50, 51]. It is generally agreed that higher straining rate results in higher stress (load) for a given strain (extension), i.e. a higher tensile modulus. Meredith [51] has also obtained evidence that at high rates of straining, the load-extension curves of some materials become more Hookean.

In a theoretical investigation of the stress-strain relationships in yarns subjected to rapid longitudinal impact loading (high straining rate), McCrackin et al [52] developed a formula for "limiting breaking velocity" as below:

$$v_b = \sqrt{\frac{2}{\rho} \int_0^{\epsilon_r} \sigma d\epsilon}$$

where

$v_b$  = limiting breaking velocity,

$\rho$  = density of the material,

$\epsilon_r$  = rupture strain, and

$\sigma$  = stress.

This formula indicates theoretically that a material impacted at a longitudinal velocity greater than its limiting breaking velocity will always be broken, because the material

is unable to accommodate the rapid displacement due to the impact by propagating the strain along it. In the case of material obeying Hooke's law, with initial Young's modulus  $E$ , its limiting breaking velocity becomes:

$$v_b = \epsilon_r \sqrt{\frac{E}{\rho}}$$

It should be noted that the foregoing statements on the stress-strain behaviour, including the analysis of limiting breaking velocity, are mainly based on the assumption that stresses and strains in the material are uniformly distributed at any time, without concern for possible tension wave propagation along the material. This assumption is no longer valid when the loading speed is very high, especially when it approaches (in order of magnitude) the velocity of propagation of a tension wave along the material [53]. In this case, the strain at one instant may be very great at one point along the material, and nonexistent at another point [54]. Smith et al [53] have studied the propagation of strain waves along yarns. They concluded that "when the stress-strain characteristics of a textile fibre are measured at longitudinal impact rates exceeding 10 m/sec, the effects of tension-wave propagation along the fibre must be considered. ...". Based on this conclusion, it should be reasonable to assume uniform stress-strain behaviour when considering wool fibres with one end anchored and the other struck by clothing elements, in worsted combing (maximum clothing element speed below 3 m/sec) and probably in worsted carding as well (maximum speed at present about 9 m/sec), but not in OE rotor spinning (speed up to 30 m/sec).

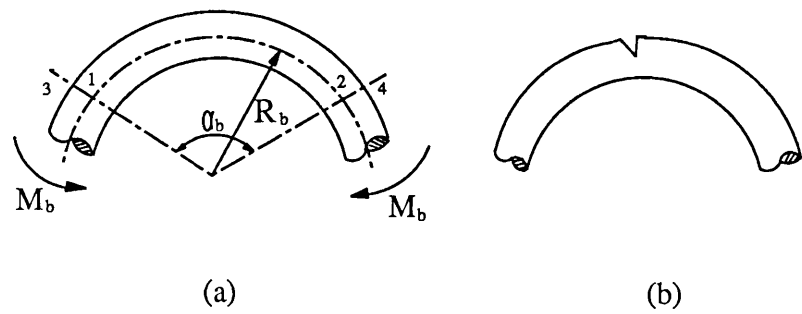


Figure 1.5: Bending deformation

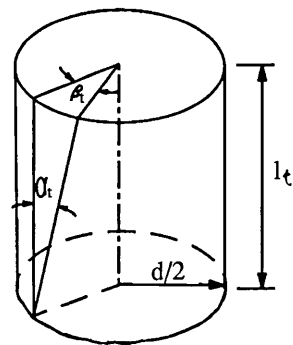


Figure 1.6: Torsional deformation

### 1.2.2 Bending Properties

From classical mechanics of materials [55], when a linearly elastic solid beam with circular cross-section is bent through two bending moments  $M_b$  at each end, the beam takes the form of a circular arc (Figure 1.5(a)). Each cross-section of the beam, originally plane, can be assumed to remain plane and normal to the neutral axis of the beam. The tensile or compressive strains at points in a direction tangential to the neutral axis vary linearly with the distance from it, and the radius of curvature of the neutral surface of the beam  $R_b$  is related to the bending moment  $M_b$  through the formula:

$$\frac{1}{R_b} = \frac{M_b}{EI}$$

where  $E$  is Young's modulus and  $I$  is the moment of inertia and  $B = EI$  is referred to as the flexural rigidity of the beam. For a circular rod of diameter  $d$  [55],

$$I = \frac{\pi d^4}{64}$$

This linear elastic theory of pure bending of a circular rod could be applied to the bending of a single wool fibre [43]. It should be noted that the cross-section of wool fibres is usually elliptical, with the ellipticity varying from 1 to 2 (about 1.3 for merino wool). When a fibre of such ellipticity is bent about the longer axis (the easiest direction), its bending rigidity is about 20% less than that of a circular fibre with the same cross-sectional area [43].

Wool fibres often fail due to compressive failure on the inside of the curve in bending [99]. They can also fail due to crack on the outside of the curve. For a wool fibre of radius  $r$ , the tensile strain  $\epsilon$  of the outmost layer is (Figure 1.5(a)):



$$\varepsilon = \frac{\hat{34} - \hat{12}}{\hat{12}} \times 100\% = \frac{(R_b + r)\alpha_b - R_b\alpha_b}{R_b\alpha_b} \times 100\% = \frac{r}{R_b} \times 100\%$$

where

$\hat{34}$  = length of the outmost layer after bending,

$\hat{12}$  = length of the neutral layer.

When  $R_b$  reduces,  $\varepsilon$  increases. If  $\varepsilon$  goes up to the rupture strain  $\varepsilon_r$ , the outmost layer starts to crack (Figure 1.5(b)), and subsequently the fibre breaks. So, to prevent fibre breakage, the minimum radius of curvature should satisfy:

$$R_b \geq \frac{r}{\varepsilon_r} \times 100\%$$

### 1.2.3 Torsional Properties

When twisting is involved, fibre torsional properties become important. If a linearly elastic rod with circular cross-section is acted upon by a torque  $M_t$  at one end, an angular deformation  $\beta_t$  occurs between two surfaces perpendicular to the axis, a distance  $l_t$  apart along the axis of the rod (Figure 1.6), such that [55]:

$$\beta_t = \frac{M_t l_t}{G I_p}$$

where  $G$  and  $I_p$  are modulus of rigidity and polar moment of inertia respectively. For a circular rod of diameter  $d$  [55],

$$I_p = \frac{\pi d^4}{32}$$

One practical application of the theory to wool fibre during twisting is the concept of "breaking-twist angle". If a fibre is twisted far enough, it will eventually rupture [44]. The twist at which this occurs is called the breaking twist  $\tau_b$ . The breaking-twist angle  $\alpha_t$  is indicated in Figure 1.6, this is the angle through which the outer layers are sheared and is given by:

$$\tan \alpha_t = \pi d \tau_b$$

Typical values of breaking-twist angle found by Koch [56] for wool fibre range from 38.5 to 41.5°, with the test conditions being: 65% r.h.; room temperature; 1 cm gauge lengths; tensile stress of 10 N/mm<sup>2</sup>; twisting rate 240 turns/min.

### 1.2.4 Frictional Properties

Wool fibres, like most others of animal origin, exhibit unusual frictional properties in that the frictional force for motion along the fibre from tip to root is greater than that for motion from root to tip, under an equal load [57]. This effect has long been attributed to the scale-like surface structure of the fibres, and the accepted explanation is that the scales form essentially a ratchet in which motion against the scale edges is possible only if they are subjected to forces sufficiently large to produce local deformation or rupture of the interlocking edges. The directional frictional effect (DFE) has been discussed, in terms of the ratchet theory, by Mercer and Makinson [58], Makinson [59] and Lindberg and Gralen [60]. Experiments have also shown that the adhesion theory of friction developed for metals, may, with little modification, be applied to the frictional behaviour of fibres and other long-chain polymers [61]. In a study of the surface characteristics of fibres and textiles,

Makinson [62] stated that the friction force was due to adhesion and deformation when a wool fibre rubbed against another surface. The asymmetry of the scales may cause deformation processes to differ considerably in with-scale sliding compared to against-scale sliding. Young and Johnson [63] examined the interaction between single wool fibres and the surfaces of different opening rollers in their study of wool fibre damage in feeding devices for OE spinning; they found that the standard deviation of time to break a single wool fibre abraded against-scale was usually much greater than that abraded with-scale, although there was little difference observed in the mean values. Dedicated work on fibre friction was also carried out by Howell, Mieszkis, and Tabor [64].

In fibre separation processes, the frictional forces on a fibre in a fringe may arise from either its interaction with the wires and the base surface of a clothed surface (fibre-metal friction), or its contacts with the surrounding fibres in the fringe (fibre-fibre friction). For fibre-fibre friction, Taylor [65] observed a linear increase in the number of fibre contact points with fringe density over the examined range. Grosberg [66] also found a linear relationship between the force needed to pull a single fibre from a sliver (the withdrawal force) and the length of the fibre tail held by the sliver. When fibre-metal friction was also involved, an exponential relationship was found to exist between the withdrawal force and the length of the fibre that was trapped in the sliver [67, 68]. This exponential relationship was employed by Carnaby [69] in his successful modelling of fibre breakage during carding.

Reduction in fibre friction normally results in less fibre breakage during any opening process. It is well known that this can be partly achieved by reducing the pressure

on the fibres. Effective lubrication can also reduce the fibre friction, but mainly the fibre-metal friction [70, 71]; the fibre-fibre friction was found to be very hard to reduce [45].

## **1.3 THEORETICAL ANALYSES OF FIBRE BREAKAGE**

### **1.3.1 Introduction**

Very little research work has been carried out on the fundamental mechanisms of fibre breakage in woolcombing. These mechanisms are important in that they not only promulgate the real reasons for fibre breakage, but also give theoretical indications of how the combing performance might be maximized.

The comb cylinder is a clothed roller. Its combing action is very similar to the opening actions in carding and open-end rotor spinning. Although OE rotor spinning has a much shorter history than woolcombing, and it has not proved particularly suitable for processing wool fibres, its tremendous success in processing cotton and short staple synthetic fibres has aroused research interest aimed at overcoming the problems of spinning wool fibres on a rotor machine. These problems are associated with the special characteristics of the wool fibres [72]. The longer staple length of wool and the presence of wool crimps normally result in higher fibre breakage during processing, because of the severe interaction between the wool fibres and the teeth of the opening roller on the rotor machine. Research on fibre breakage in OE spinning of wool fibres, together with recent studies on fibre breakage in carding of wool fibres, will certainly aid the understanding of how wool fibres might break during rectilinear combing, and vice versa. It is intended here to integrate and summarize relevant theoretical works on clothed roller related fibre breakage.

Entanglement Type	Description	Schematic Diagram
A	Parallel Fibres as in Top or in Staples in greasy wool	
B	Fibre axes disoriented with respect to one another and to the sliver axis (where appropriate)	
C	Fibres disoriented within themselves. They may be hooked or looped as in card sliver	
D	Fibres are twisted or wrapped around each other	
E	Neps	

Figure 1.7: Entanglement types which may be found in wool stock [73]

### 1.3.2 Different Forms of Fibre--Combing Element Interaction

No matter what kind of opening action (carding, combing or OE spinning) a wool assembly is to be subjected to, the configuration of those wool fibres in the assembly is very important. It is generally accepted that parallel fibre configurations give much less fibre breakage during any opening action, while entangled fibre configurations are normally blamed for the fibre breakage.

There are different forms of fibre entanglement. In a study of the removal of entanglement in carding, Harrowfield et al [73] presented a stylized attempt to classify the forms of fibre entanglement (Figure 1.7). Although their purpose in attempting to classify entanglements in this way was to try to describe the state of the wool stock as it proceeds through the conversion processes, the classification of entanglement types also indicates different possible forms of interaction between wool fibres and the combing elements.

It should be noted that in practical carding, combing, or OE spinning, the fibres are subjected to dynamic processes, that new forms of fibre entanglement may be generated, and that one form of entanglement may be transformed into another during such dynamic processes. Nonetheless, this situation does not necessarily obscure the importance of fundamental studies on the breakage of fibres in those basic configurations listed in Figure 1.7.

### 1.3.3 Theoretical Analysis of Individual Cases

#### 1.3.3.1 Fibre loops

A fibre forms a loop if the two ends of the fibre are both held by the feeding device or nippers, and it is almost impossible for such looped fibres to survive without breakage when engaged in an opening action. Theoretical analyses on fibre loops have been directed towards examination of the maximum load a fibre could sustain without breaking when subjected to the opening action of metal teeth with different shapes. In a study of fibre breakage during carding, Wood, Boden and Carnaby [68] used two types of tooth, saw-tooth wire and round pin, to break looped fibres. The maximum load and the position of break were recorded for fibres broken over both types of tooth. The mean breaking load for the saw-tooth wire was found to be significantly lower than that for the round pin. The same authors also found that the points of breakage when the round pins were used were distributed more or less randomly along the fibres; while with saw-tooth wire, the majority of breakages occurred at the tooth. The authors suggested that the cutting action of the sharp edges of the saw teeth reduced the breaking load required. Xu and Zhou [74] obtained similar results in their study of fibre breakage in the taker-in part of a carding machine. They claimed that the stress in a fibre due to its bending around the surface of a tooth could be used to explain the different behaviour of different teeth. This concept is briefly summarized below.

For a radius of the fibre  $r(\mu\text{m})$ , and its rupture strain  $\epsilon_r$ , the safe radius of bending curvature of the fibre was given in section 1.2.2 as:

$$R_b \geq \frac{r}{\epsilon_r} \times 100\%$$

If  $r = 10(\mu m)$ ,  $\epsilon_r = 35\%$ , then

$$R_b \geq 30(\mu m)$$

Since the radius of the round pin is much greater than  $30(\mu m)$ , the bending deformation it causes is very small. But the cross section of the saw-tooth is rectangular, and the fibre bends sharply at the edges. The radius of bending curvature of the fibre is therefore very small and the deformation and stress are very great. So the fibre breaks more easily.

More recently, this argument was employed by Yan [75] to explain similar breakage behaviour of looped fibres engaged by a saw-tooth, but at much higher opening speed. Yan [75] also mentioned that the contact stress or Herzian stress caused by the tooth might have lowered the breaking strength of the fibre at the tooth, and that this could be another reason why the majority of breakages occurred at the tooth.

### **1.3.3.2 Fibre hooks**

Fibre hooks can contribute to the extent of fibre breakage in several ways, depending upon the conditions associated with both the hooked and unhooked ends of those fibres. Salhotra and Chattopadhyay [76] investigated the incidence and mechanism of fibre breakage in rotor spinning and proposed that a hooked fibre, engaged by a clothing element with both of its ends free, would come out of its surrounding fibres unbroken; while in the event that the unhooked end of an engaged fibre was somehow firmly gripped, either the hooked portion might slip out from the clothing element if it was short and not strongly engaged with the clothing element, or otherwise the fibre might break at the apex of the clothing element.



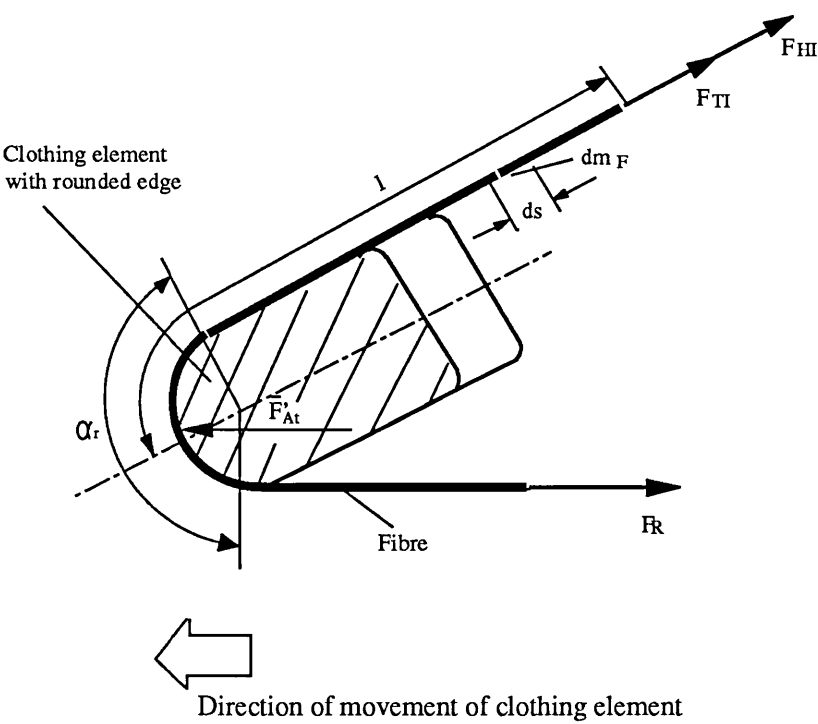


Figure 1.8: Forces acting on a fibre wrapped around a clothing element [77]

In a study of the directional effects in worsted rectilinear combing, Belin and Taylor [30] found that, when fibres were combed with hooks leading, both ends could be gripped by the nipper and the hook broken by the circular comb. This is much like the breakage of looped fibres mentioned earlier. A hooked fibre with the end of the hook not directly held by the nipper, but by entanglements with other fibres, could break in a similar manner.

Generally, for a hooked fibre to survive an opening action without breaking, one end of the fibre must be able to sustain the tension (or the restraining force) caused by the passage of the other end around the clothing element(s). In this sense, fibres with 'free' hooks engaged by clothing elements might have a good chance to get straightened instead of break. A detailed mathematical analysis of such a fibre hooked around a single clothing element was carried out by Siersch [77]. The author assumed a rounded front edge for the clothing element (Figure 1.8).

The restraining force  $F_R$ , used as a measure of the fibre strain, was obtained according to the simple Capstan formula:

$$F_R = (F_{Ti} + F_{Hi})e^{\mu_{F/S}\alpha_r}$$

where

$F_{Ti}$  = inertia of the free fibre length  $l$ ,

$F_{Hi}$  = static friction of the free fibre length  $l$ ,

$\alpha_r$  = wrapping angle,

$\mu_{F/S}$  = coefficient of friction fibre/steel.

The necessary condition for fibre sliding must be:

$$F_R < F_{\max}$$

where  $F_{\max}$  is the maximum fibre tension before breakage.

Setting  $Tt_F$  as the fibre fineness,  $V_A$  the surface speed of the clothing element, and  $V_E$  the feeding speed, the inertia of the free fibre length  $l$  was calculated by considering a small element of length  $ds$  and mass  $dm_F = Tt_F ds$ :

$$dF_{Tl} = dm_F \frac{dV}{dt} = Tt_F ds \left( \frac{\partial V}{\partial t} + \frac{\partial V}{\partial s} \frac{ds}{dt} \right)$$

By assuming constant sliding motion, then

$$\frac{\partial V}{\partial t} = 0$$

$$\frac{\partial V}{\partial s} = \frac{dV}{ds}$$

$$\frac{ds}{dt} = V$$

therefore

$$dF_{Tl} = Tt_F V dV$$

$$F_{Tl} = Tt_F \int_{V_E}^{V_A} V dV$$

$$F_{Tl} = \frac{Tt_F}{2} V_A^2 \left( 1 - \frac{V_E^2}{V_A^2} \right)$$

Since  $V_E \ll V_A$ , then

$$F_{Ti} \approx \frac{T_{tF}}{2} V_A^2$$

i.e. the tension due to inertia of free length  $l$  is proportional to the fibre fineness and the square of the clothing speed.

The additional static friction force was assumed by the author to be of the same magnitude as the inertia, with the consideration that the fibres were accelerated only to about 60% of the surface speed of the roller.

The average tension  $F_R$  acting on the fibre during the opening process was thus calculated to be about  $10^3$  to  $10^4$  smaller than the maximum tensile strength of an individual fibre, even at the high clothing speeds used in open-end spinning. Therefore, fibre breakage is unlikely to occur in this case.

### 1.3.3.3 Parallel fibres

Although it is well known that a fringe with more parallel constituent fibres will normally result in much less fibre breakage when subjected to any opening action, such fringe also gives more freedom to fibre end movement if the fibre is acted upon by fast moving clothing elements. The free fibre ends may wrap around the clothing elements more easily. A theoretical analysis of the wrapping action was conducted by Yan and Johnson [78] in their study of fibre breakage during OE rotor spinning. The following is a brief summary of their analysis.

Imagine a straight single fibre of length  $L$  with one end fixed and the other end hanging free to be struck at an angle  $\alpha$  by a round pin moving at a constant speed

V. The fibre is assumed to be perfectly flexible. If the pin speed is very high, as is true in OE rotor spinning, the strain wave propagation within the fibre should be considered. Immediately after the initial pin impact on the fibre, the longitudinal strain generated in the fibre at the point of impact propagates along the fibre towards both ends. The fundamental equation connecting Young's modulus of the fibre and the velocity of strain wave propagation is [79]:

$$V_l = \sqrt{\frac{E}{\rho}}$$

where  $V_l$  is the propagation velocity of the longitudinal strain,  $\rho$  is the density of the fibre, and  $E$  is the Young's modulus.

The motion of the pin also causes a transverse wave spreading towards both fibre ends with a velocity dependent on the tension (or stress) in the fibre. If the amplitude of the transverse wave is relatively small, the equation generally used for the velocity of transverse propagation  $V_t$  has the form [80]:

$$V_t = \sqrt{\frac{\sigma}{\rho}}$$

where  $\sigma$  is the fibre stress. The above two equations were combined, noting  $\sigma = \epsilon E$ , to give:

$$\frac{V_t}{V_l} = \frac{\sqrt{\frac{E}{\rho}}}{\sqrt{\frac{\sigma}{\rho}}} = \sqrt{\frac{E}{\sigma}} = \frac{1}{\sqrt{\epsilon}}$$

i.e. the propagation velocity of the transverse wave is lower than that of the longitudinal wave by a factor of  $\epsilon^{1/2}$ .

By assuming no friction between the pin and the fibre, Yan and Johnson [78] then derived an equation for the velocity of the transverse wave on both sides of the pin as:

$$V_t = \sqrt{\sqrt{\left(\frac{\sigma^2}{\rho^2} - V^4 \sin^2 2\alpha\right)} + V^2 \cos 2\alpha}$$

Solutions incorporating friction between pin and fibre were obtained using an iterative computation method.

Once the strain front in the fibre reaches the free fibre end, the tension due to this initial strain provides a lifting force which will move the free fibre end upward towards the point of initial impact with an increasing velocity. At the same time, the transverse wave causes some transverse displacement, but only in the elements of the fibre behind the wave front. The section of the fibre length ahead of the transverse wave front is not affected and hence remains vertical. When the transverse wave front reaches the free fibre end, this vertical length becomes zero, and the free fibre end has some velocity  $v$  upwards in the vertical direction. This velocity can be divided into two components:  $v_p$  in the direction along the fibre (but probably away from the pin), and  $v_n$  normal to the fibre. The tension in the fibre will decelerate the velocity  $v_p$  and eventually force it to move in the opposite direction, i.e. towards the pin, but this tension cannot stop the velocity  $v_n$ , it can only change its direction, making it move around the pin. Such movement actually forms a fibre hook around the pin, and sometimes makes the fibre wrap around the pin so that the section of fibre above the pin might be easily broken because of the large capstan frictional force.

## 1.4 SUMMARY

In this chapter, the importance of the worsted combing process has been highlighted, followed by a brief introduction to the working principle of the rectilinear comb. The existing theoretical analyses and empirical works on woolcombing have been reviewed and discussed. The important information thus obtained regarding combing performance can be outlined as follows:

- 1). Combing speed, over the range currently used in the industry, does not have a detectable effect on the combing performance, but the upper speed limit on the existing combs can not be further increased because of their complex structure and the presence of mechanical shocks on those machines at higher speed.
- 2). Existing theories on fibre breakage in the combing process are confined to examination of the effects of machine settings and fibre length variations, without much consideration of the mechanical properties of the fibres and their interaction with the clothing elements; thus they can only provide an external, "black-box" picture of the combing process as a whole.
- 3). The different forces involved in combing are closely associated with fibre breakage. Measurement of the tensile forces created in the fibre during drawing-off has indicated that they do not make a significant contribution to the total fibre breakage occurring in the combing process; while the tension experienced by individual fibres due to the combing action of the comb cylinder and the forces acting on the clothing elements of the comb cylinder are still unknown.

- 4). It has been proposed that the fibres themselves, i.e. their physical properties, rather than the mechanics of the combing machine should provide the factor limiting the ultimate combing speed, but there are no reports of theoretical work to ascertain whether there exists a threshold value for combing speed above which combing would be impractical.

The information provided in this chapter clearly indicates that the physical or mechanical properties of the fibres, and the interaction between individual fibres and the clothing elements, should be considered in examining the combing performance.

A brief review of the relevant mechanical properties of wool fibres has also been given in this chapter, followed by a schematic presentation of individual fibre entanglement forms that may be found in a pre-combed sliver. A few of the fundamental mechanisms of fibre breakage which occur in opening processes, due to the interaction between the clothing elements and fibres of very simple forms of entanglement (loops and free hooks), have been theoretically analysed. Two important and more complex entanglement forms, namely the twisted fibres and the neps, have not yet been investigated.

The following two chapters investigate the different forces involved in the combing action of the comb cylinder. In chapter four, a theoretical approach to study the disentangling of two twisted fibres is presented.



## CHAPTER 2

# STUDY OF FIBRE TENSION IN COMBING

---

## 2.1 INTRODUCTION

The different forces involved in the rectilinear combing process can be generally classified as being: 1) the force or tension experienced by individual fibres in a sliver subjected to combing; 2) the forces acting on the clothing elements during combing by the comb cylinder; and 3) the forces acting on the pins of the top comb and feed gill during drawing-off. It is very likely that much of the fibre breakage occurring in rectilinear combing is more directly related to the first one.

Previous investigations indicate that the extent of breakage can be from about 17% up to 31% [21], depending upon the conditions of the pre-combed sliver and the setting of the comb. Two combing actions can contribute to this fibre breakage, the initial combing by the comb cylinder, and the final combing by top comb and feed gill. The forces relating to these two combing actions will be called "combing force" and "withdrawal force" respectively in this chapter.

Under practical combing conditions, it is extremely difficult to measure the combing forces directly on the comb, because of its complex structure and the presence of mechanical shocks and vibrations. Early attempts were confined to the study of withdrawal forces through the top comb and feed gill. Kruger [23] and Aldrich [9] constructed special apparatus to simulate the combing action of the top comb and feed gill; they measured the forces required to withdraw a tuft of fibres from a sliver

inserted in a pin bed containing combs of variable pin density. Their important conclusion was that the contribution of withdrawal forces to total fibre breakage was not significant, because the measured withdrawal forces (average only) per fibre were well below the breaking strength of the weakest fibres present in the tuft. Therefore it is natural to consider the comb cylinder as the major cause of fibre breakage during combing, because it is the only other combing element. The study and measurement of fibre tension generated by the comb cylinder in its combing action are the objects of this chapter.

A comb cylinder is simply a clothed roller, so studies on other machines with clothed rollers are also relevant. Siersch [77] in Germany used a torque transducer to measure the torque on opening rollers to study the opening forces in OE rotor spinning. A similar technique was also used by Harrowfield et al [73] to measure the torque in the drive shaft to the worker on a carding machine to calculate the specific opening energy. While this technique was quite practical and successful for their specific purposes, it only gives an average value of combing forces. In order to get a more complete picture about the forces experienced by individual wool fibres in the fringe, a special device simulating the combing action of a comb cylinder was constructed, which made possible the direct real time force measurement on a single wool fibre in the fringe during combing.

It is intended in this chapter to first of all elaborate a qualitative theory for the generation of fibre tension in combing, and then to investigate empirically the effect on fibre tension of different parameters like fibre length, combing speed, and fringe density, etc.

## 2.2 QUALITATIVE THEORY

When a wool fringe is subjected to the combing action of a comb cylinder, one end of the fringe is firmly held by the nipper jaws. The only forces which can act on the free end of a fibre (in the fringe) projecting from the nippers arise through:

- \* contacts with neighbouring fibres in the fringe,
- \* direct contact with the pins of the comb cylinder,
- \* direct contact with the surface of the comb cylinder,
- \* gravity and air drag (assumed to be negligible in most cases).

Because of the fibre crimp and imperfect alignment of a fringe of wool fibres, when the pins of the comb cylinder pass through the fringe, the resultant 'combing force' can extend the fringe as a whole. If the fringe is longer or denser, a greater total force will be applied to it by its contacts with the comb cylinder, and so the tension in the fringe, and therefore its extension, will be greater. An individual fibre not in direct contact with a pin will still be extended through its frictional contacts with other fibres. The tension will build up in the fibre in much the same way as in a fibre being withdrawn from a fringe. Theoretical derivations for withdrawal force are well established [81] and it is not necessary to pursue a similar theory here, other than to borrow some assumptions and conclusions. The tension that will develop in the fibre is assumed to be proportional to the number of contacts with other fibres; if it is also assumed that the number of contacts will be proportional to both the length of fibre in the fringe and the density of the fringe, then it is expected that the fibre tension will increase with fibre length in the fringe (for a uniform fringe density) and increase with fringe density. Furthermore, it will also increase with fringe tension, which itself is a function of fringe length and fringe density.

When a fibre comes into direct contact with a pin, an additional force will be generated. This will be an occasional event, with the magnitude of this additional force depending on the fringe density, as a denser fringe increases the normal force between fibre and pin. Furthermore, longer fibres have a greater probability of being in contact with two pins at the same time.

If a fibre is in direct contact with the surface of the comb cylinder, tension will develop in the fibre through friction arising from normal force between fibre and roller surface. There are two sources for this normal force. Because the surface of the cylinder is curved, any tension in the fibre has a component normal to the surface and similarly, fringe tension creates a pressure pushing the fibre down onto the surface. It can be reasoned that the tension in the fibre due to its frictional contact with the roller surface will increase with fringe length, fringe density and with fibre length.

It is also expected that the tension in the fibre would increase with the speed of the combing cylinder through the above-mentioned frictional contacts [64].

When a pin tries to disentangle a fibre from its neighbours, a combination of direct pin contact and strong fibre contacts occurs. This combination can lead to very large tension peaks, which could break the fibre.

Yan and Johnson [82] have described how a round pin striking a fibre at high speed can cause the fibre to wrap around the pin and be broken. A similar behaviour could occur at the slower speeds encountered in combing, and even though this action may not break the fibre, it may cause the fibre to flail around sufficiently to become seriously entangled with other fibres.

Table 2.1: Details of the beater (STB)

Diameter (mm) (to surface)	Wire Dimensions (mm)				Carding angle	Tooth apex angle	Point density (1000/m <sup>2</sup> )
	Height of base	Overall height	Base width	Pitch			
58	0.5	3	1.4	2	19 <sup>0</sup>	15 <sup>0</sup>	234

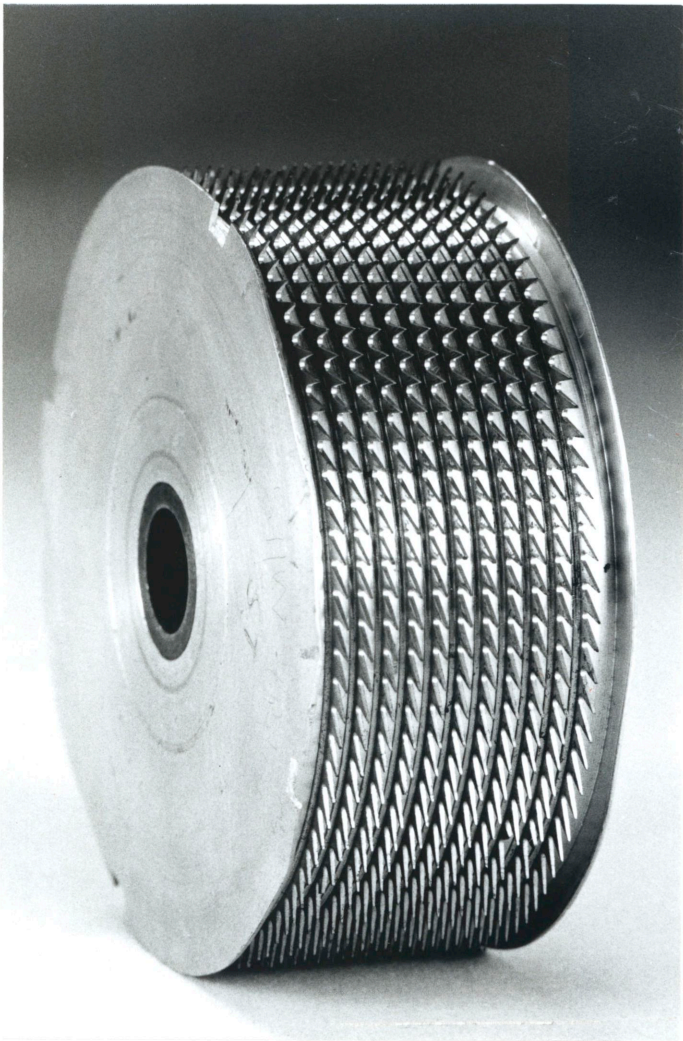


Figure 2.1: General view of the beater

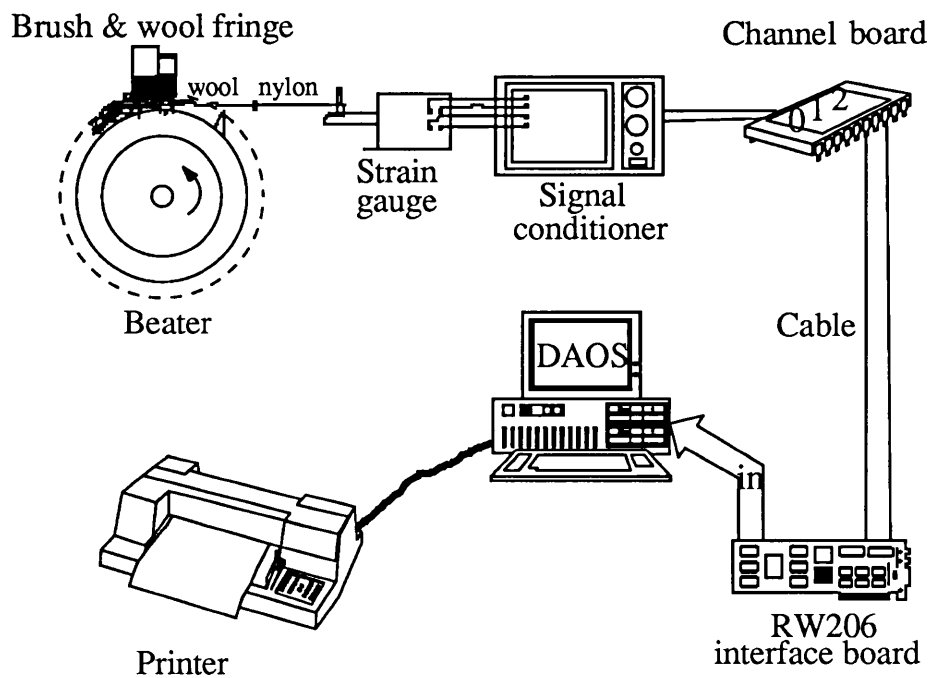


Figure 2.2: Diagram of the experimental set-up for fibre tension measurement



Figure 2.3: General view of the experimental set-up for fibre tension measurement

Young and Johnson [83] have observed rare tension peaks in tensioned single fibres being abraded by a pinned surface. This may be due, for instance, to the fibre surface snagging on a minute asperity on the pin surface, and the same peaks are likely when the fibre is in a fringe.

## 2.3 EXPERIMENTAL

### 2.3.1 Apparatus

To simulate the combing action of the comb cylinder, a small sawtooth beater was used to comb a prepared wool fringe. The same beater (designated STB) was also used by Young and Johnson [63] in their study of fibre damage in feeding devices for OE spinning. Details of the beater are listed in Table 2.1. A photograph of this beater is also shown in Figure 2.1.

A pig bristle brush was used to push the fringe slightly into the beater teeth. The tip end of a clean untreated wool fibre (the test fibre) was carefully put into the fringe by slowly rotating the beater, and its root end was attached to a strain gauge via a short length of nylon filament. Figure 2.2 is a schematic diagram of the apparatus. A photograph of this apparatus is given in Figure 2.3. The beater was driven by a speed adjustable motor at surface speeds typical of worsted comb cylinders.

While the wool fringe was being combed by the beater, the tension in the test wool fibre was detected by the attached strain gauge (with sensitivity of 50 g/1655 micro-strain and natural frequency of 320 Hz). The output signal of the strain gauge was amplified through a signal conditioner and then sent to a computer via an interface board. The central unit of this apparatus is the Data Acquisition Operating



System (DAOS) [84], which can acquire external real time signals at very fast speed and analyse the signals statistically and graphically. According to Shannon's sampling theory [85], the selected sampling rate for this system to faithfully reproduce a real time signal has to be at least twice the frequency of the highest frequency component in that signal.

### 2.3.2 Preparations

System calibration: Before any experiment, the whole system was calibrated by applying a series of weights to the strain gauge and checking the DAOS output. A calibration function was obtained as below:

$$\text{TENSION}_{\text{in test fibre (cN)}} = \text{DAOS}_{\text{output (mv)}} * 0.0102$$

Single test fibres: Long staples of greasy merino wool (24  $\mu\text{m}$  in diameter) were solvent de-greased using dichloromethane in a soxhlet apparatus. Their mean breaking strength was determined on the WIRA single fibre strength meter to be 9.7 cN with a standard deviation of 2.5 cN.

Fibre fringe: Wool tops of 23.3  $\mu\text{m}$  fibre diameter were end-aligned on an Almeter Preparer. A hand comb was used to remove short fibres from the fringe, which was then cut to the required lengths and divided into widths of about 12 mm. Fringes were thus 'square' and of uniform linear density. An accurate balance was used to weigh the fringe to determine its density. The fringe was carefully arranged on the roller surface with the help of the brush and some slow rotation of the beater. The fringe was then firmly held with the brush by a nip above the roller.

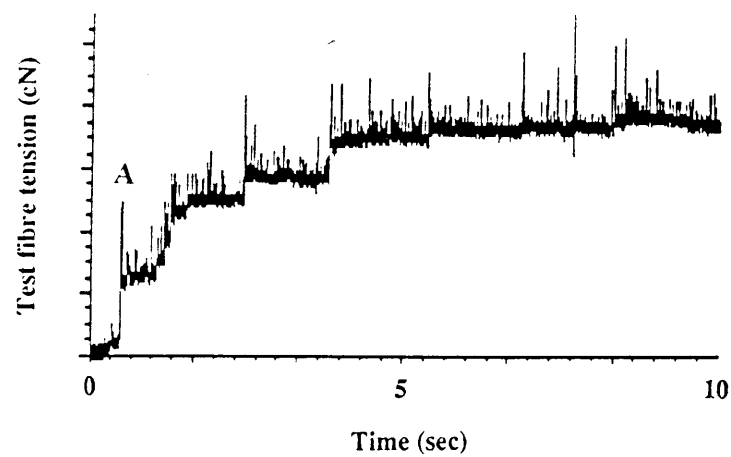


Figure 2.4: Typical tension signal

### 2.3.3 Testing Procedure

For each set of experiments, several almost identical fringes and many test fibres were prepared. A separate test fibre was used for each individual test, but one fringe was used for 3 to 5 individual tests. The fringe was pushed into the beater teeth first with the help of the brush above the beater, then the test fibre was carefully buried in the fringe by slowly rotating the beater. For each individual test, the motor and the data acquisition program were started at the same time and run for a period of 10 seconds. The computer acquired the tension signal at a pre-determined sampling rate of 3,000 Hz, giving 30,000 digitized data points representing the analog tension signal in each test. These were stored in the computer and graphically displayed on the screen. A typical tension signal is shown in Figure 2.4.

There is a gradual increase in tension at the beginning as the motor increases its speed from zero (at start-up) to the set level. Although the motor would have taken about 2 seconds to reach the set speed level, to ensure that it had reached the set speed, only the average value of those data acquired in the last five seconds was recorded as an individual average tension value. The mean and 95% confidence interval of 10 to 15 such individual average fibre tension values were used for each data point.

The tension increase appears as a series of steps, and the beginning of each step appears to always coincide with a small tension peak. This pattern is indicative of stick-slip behaviour. By applying a range of increasing and decreasing loads to the measuring system, it was found that the measuring system itself was not prone to stick-slip behaviour. A likely explanation for these steps is that when the fibre is rapidly extended (as marked by a tension peak), it does not fully recover because of its frictional contacts with other fibres in the fringe. The magnitude of this effect

diminishes as the whole fringe approaches its maximum tension and extension levels. That this stepping effect seems more prominent at higher fringe densities (see Figure 2.16(b)) is also consistent with this explanation.

If the test fibre broke, the relevant tension signals were recorded. The length of test fibre was measured before and after breakage, in order to determine where the breakage occurred.

Experiments were carried out in conditions of  $(65 \pm 5)\%$  r.h.,  $20 \pm 5$  °C. Test fibres were combed in the with-scale direction.

### 2.3.4 Parameters Investigated

Test fibre length: This refers to the length within the "combing zone"<sup>1</sup>, of a test fibre. Results were obtained for both cases of the test fibre length longer than the fringe, and shorter than the fringe.

Combing speed: Three different combing speeds, with the lowest one close to the speed on a modern commercial comb, were used with four different test fibre lengths. The rotational speeds of 800, 1000, & 1200 rpm correspond to roller surface speeds of 145.8, 182.2, & 218.7 m/min.

Fringe density & fringe length: Fringes of different density and length (in the combing zone) were prepared. They were carefully put on the roller surface with the single test fibres.

---

<sup>1</sup> that region of the fringe which is actually combed by the comb cylinder.

---

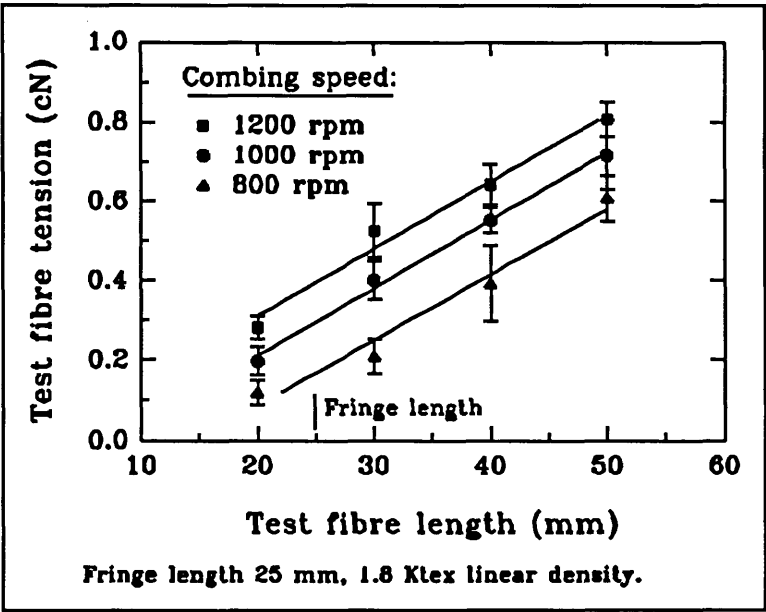


Figure 2.5: Tension in test fibre vs test fibre length (test fibre protruding beyond fringe)

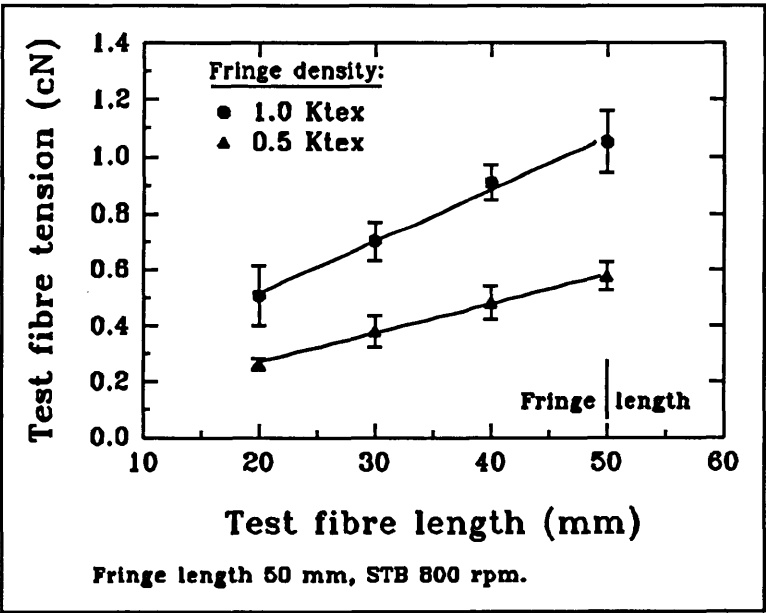


Figure 2.6: Tension in test fibre vs test fibre length (test fibre within fringe)

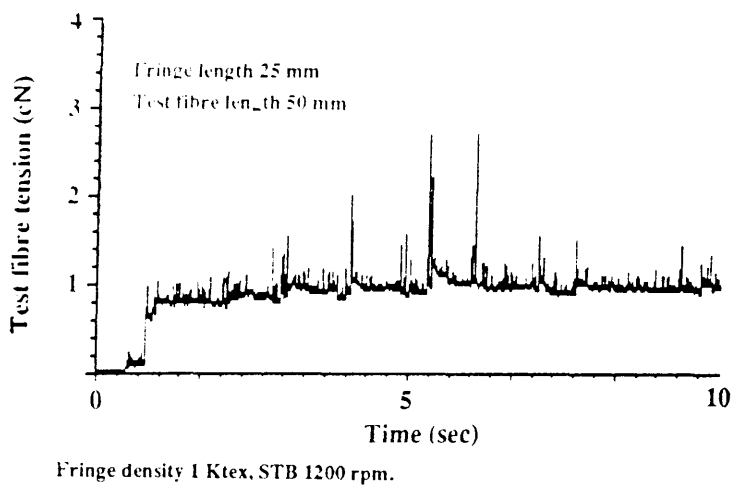


Figure 2.7: Tension signal (fibre protruding beyond fringe)

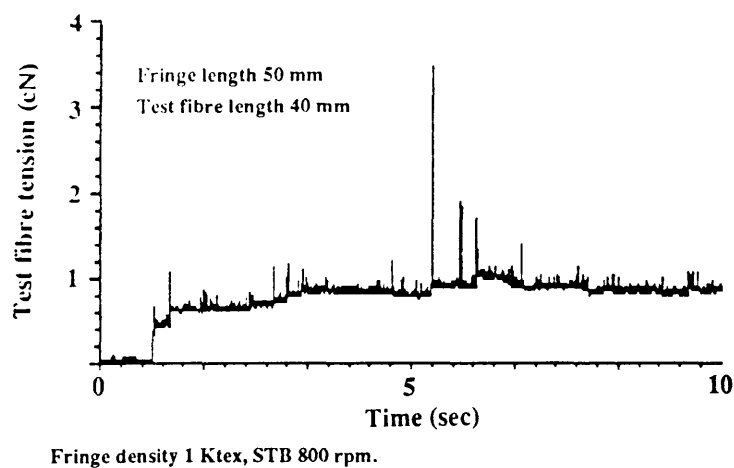


Figure 2.8: Tension signal (fibre within fringe)

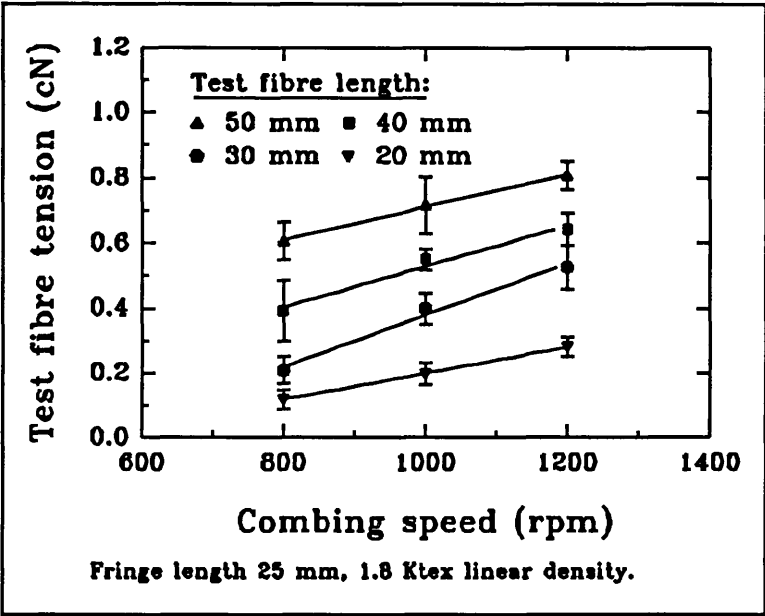


Figure 2.9: Tension in test fibre vs combing speed

## 2.4 RESULTS AND DISCUSSION

### 2.4.1 Mean Tension Levels

The mean tension levels were plotted using the mean and 95% confidence interval of 10 to 15 individual average fibre tension values.

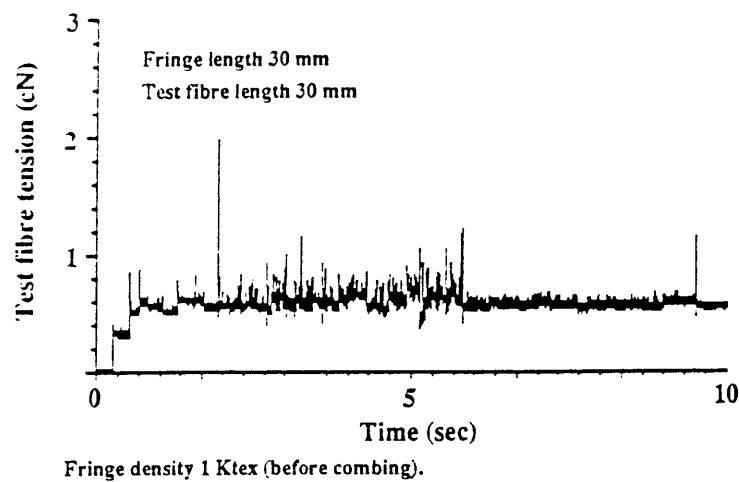
#### 2.4.1.1 Effect of test fibre length

Figure 2.5 and Figure 2.6 show the effect of the test fibre length on the average tension experienced by the test fibres. Fibre tension increased linearly with the test fibre length in both cases of test fibre length longer (Figure 2.5) and shorter (Figure 2.6) than the fringe. While the simple hypothesis described in section 2.2 predicts this result for the case of the test fibre being fully within the fringe, it is interesting that the tension also increases linearly when the test fibre extends beyond the fringe. This may be a function of the total number of pins acting on the fibre at any time. The average tension values in the test fibres were well below their average breaking strength, which is a reasonable outcome, because fibres in the fringe are relatively straight and free from heavy fibre entanglements. If the average fibre tension was near the fibre breaking strength, then all fibres in the fringe would be likely to break. Typical individual results are shown in Figure 2.7 and Figure 2.8.

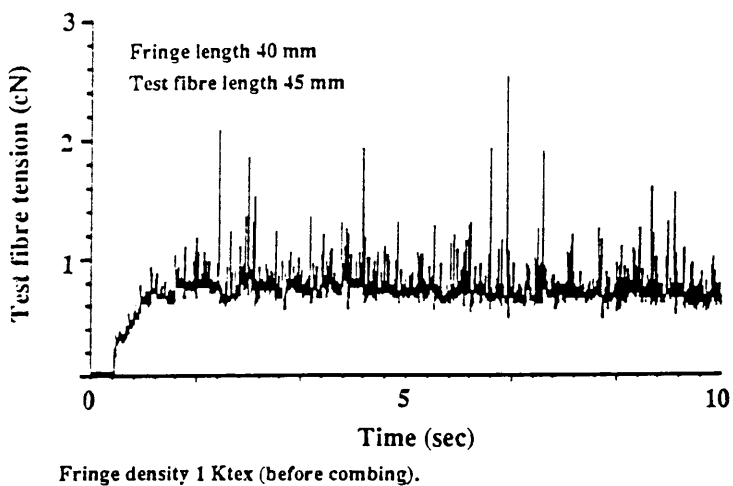
#### 2.4.1.2 Effect of combing speed

There is not a huge absolute increase in fibre tension with speed within the range of 800 rpm to 1200 rpm (Figure 2.9) in comparison to the fibre breaking strength. This result is in agreement with some previous works on combing speed. Aldrich [9] carried out some studies on different wools





(a)



(b)

Figure 2.10: Tension signal within combing speed range of 0 to 10800 rpm

using a Schlumberger PB 26 comb and reported that at three different speeds which could be selected on the comb, namely 130, 150 and 165 nips per minute, no significant effect could be detected as far as percentage noil and top cleanliness were concerned. Turpie and Klazar [29] expanded the speed range from as low as 7 to as high as 165 nips/min., and still no change in the fibre breakage pattern with increase in comb speed was found. Since fibre breakage is very likely to be closely related to the tension experienced by the fibre during combing, it is quite reasonable to predict that the slight increase in fibre tension with comb speed observed here would not be enough to produce detectable changes in fibre breakage patterns.

However, in high speed opening processes, it could be another picture. In a study of OE rotor spinning, Siersch [77] obtained a set of curves showing the effect of opening roller speed on the opening force for acrylic slivers. There was little effect of speed for short fibre sliver, but for longer fibres, the opening force increased with speed, and the slope of the curves of force vs speed increased with speed as well. This differs from the relatively straight relationship obtained for single fibre tension over a much slower speed range in the present work. The increasing slope found by Siersch [77] for longer fibres at very high speeds could be due to the onset of fibre impact effects, such as that described by Yan and Johnson [82].

In an attempt to reconcile these various results, the present test was operated at similar high speeds, and the tension signals in Figure 2.10 were obtained within the speed range of zero at start-up to the set level of 10800 rpm, which is the maximum speed range available on the device used. The increase in tension with roller speed at the start-up is similar to that seen in Figure 2.4; however, as the speed continues to rise, the average tension levels off or may even decrease. This occurs because the beater at high speed rapidly removes fibres from the fibre fringe and reduces its density.

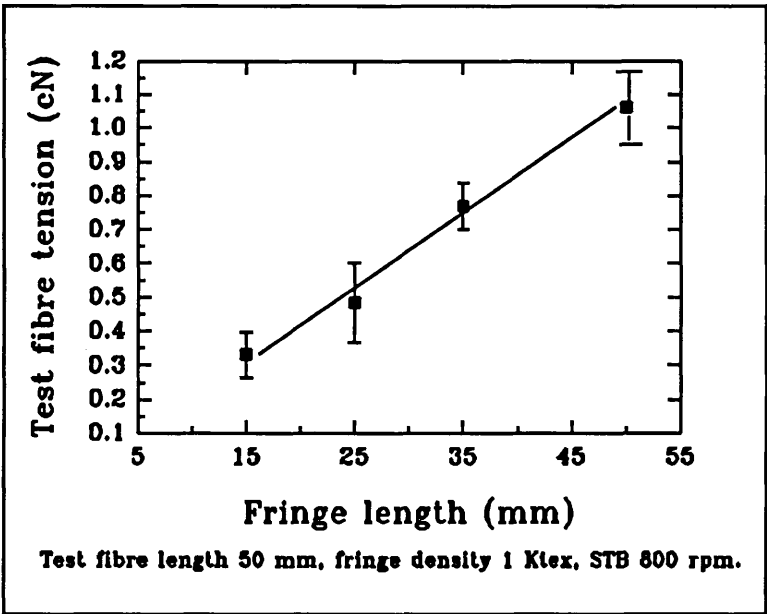


Figure 2.11: Tension in test fibre vs fringe length

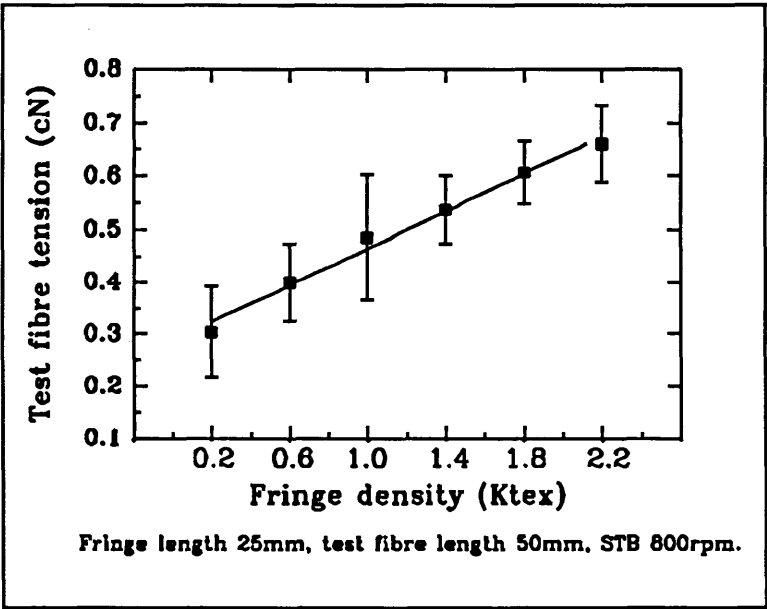


Figure 2.12: Tension in test fibre vs fringe density

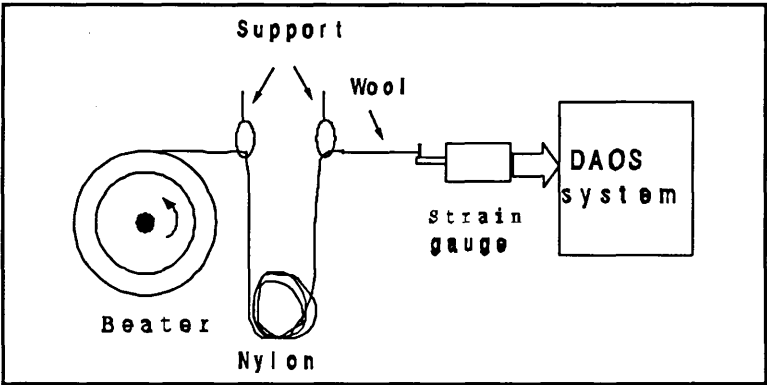


Figure 2.13: Diagram of the experimental set-up for checking system response time

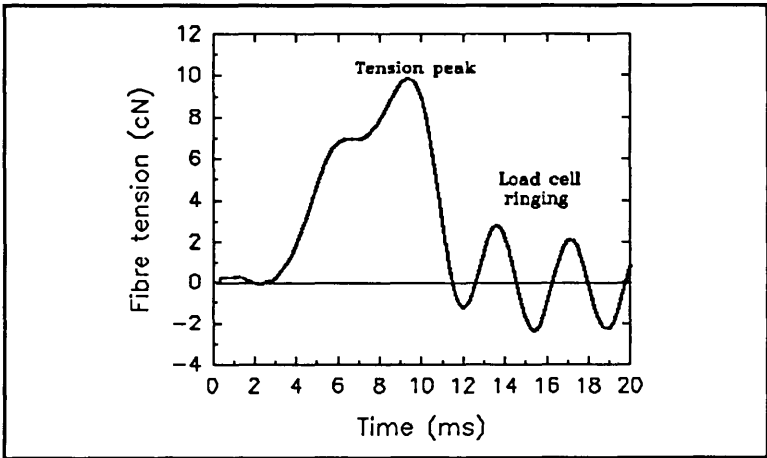


Figure 2.14: Typical tension signal recorded

The air flow generated by the roller surface at high speed might have contributed as well, by blowing the test fibre and fibre fringe up from the beater surface. The relatively smoother tension at the end in Figure 2.10(a) was due to the tip end of the test fibre (about 5 mm long) breaking off during the test. It is thus not possible to accurately measure the effect of very high combing speeds on single fibre tension with the present apparatus, other than to note that fibre breakage levels increase dramatically.

#### **2.4.1.3 Effects of fringe length and fringe density**

The effects of fringe length and fringe density are quite linear within the tested range, as shown in Figure 2.11 and Figure 2.12. These results agree with the prediction of the hypothesis put forward in section 2.2.

#### **2.4.2 Peak Tensions**

While average tension values are of interest in confirming the basic predictions of the hypothesis, it is the tension peaks that will be responsible for fibre breakage.

To confirm that the measuring system could respond quickly enough to accurately record tension peaks, one end of a 50 mm wool fibre was attached to the beater surface via a nylon filament and the other end to the strain gauge (Figure 2.13). The filament was sufficiently long to allow the beater to reach operating speeds of 800 rpm and 1200 rpm before the wool was rapidly extended to break. This represents the maximum rate of tension rise that could occur over a 50 mm fibre length in experiments at beater speeds of 800 rpm and 1200 rpm. The measuring system

recorded peak tension values of 9.9, 9.2, and 8.2 cN for three different fibres at the speed of 800 rpm. It also recorded a tension value of 9.9 cN for the only fibre used at the speed of 1200 rpm. All these tension values are within one standard deviation of the mean single fibre strength. Figure 2.14 shows a typical individual tension signal recorded at the beater speed of 800 rpm.

The fall in recorded tension signal (Figure 2.14) after breakage takes place in about 2.5 ms. At 800 rpm, the surface speed of the beater is about 250 cm/sec. Approximately, a 50 mm fibre will break if extended 2 cm. This extension would take place in 8 ms at 250 cm/sec, which is much longer than 2.5 ms. This indicates sufficient response rate for the present circumstance.

### **(i) The first peak**

It is worth noting the first peak (denoted by A) on the curve in Figure 2.4. The magnitude of this first peak changes with two factors: the static frictional force involved (influenced by fringe density, etc.) and the presence of a leading hook on the test fibre. When the test fibre was laid straight in the fringe and combing started, the peak was quite small. But if the test fibre was laid with a leading hook in the fringe and combing started, the peak was much bigger, occasionally big enough to cause fibre breakage, as can be seen later.

### **(ii) Random peaks**

Figures 2.7 and 2.8 illustrate the randomly occurring tension peaks which arise in test fibres which protrude beyond, and lie within, the fringe respectively. In general,

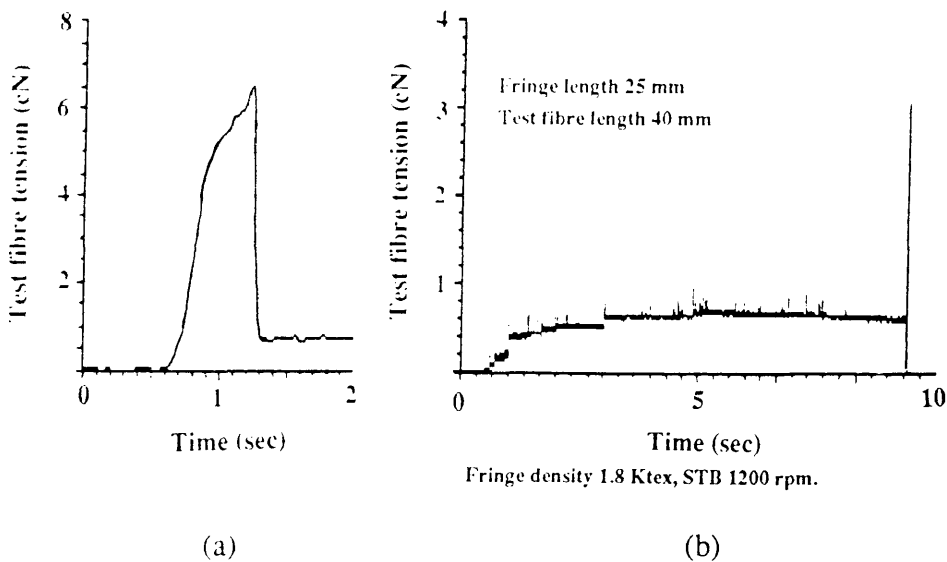


Figure 2.15: Patterns of fibre breakage behind the combing zone

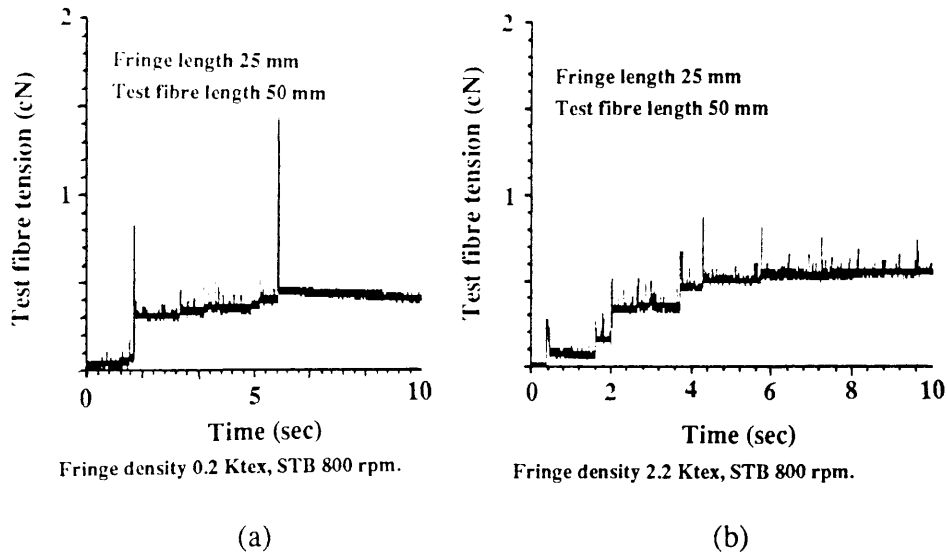


Figure 2.16: Patterns of fibre breakage near the end of combing zone

the smaller tension peaks are more frequent when the fibre extends beyond the fringe. This is consistent with a flailing action of the free end frequently wrapping it around the pins and generating a small tension peak. When the fibre end lies within the fringe, it will be constrained and the level of fibre movement will be less.

Both curves also display some relatively major peaks. These may be due to entanglements induced during combing or due to the test fibre catching on, or wrapping around, a pin. These major peaks are of particular interest as a possible source of fibre breakage.

### 2.4.3 Fibre Breakage

There were a few cases of test fibre breakage throughout the experiments. The occurrence and position of a break, or of the last break in the case of multiple breakages, were determined by measuring the test fibre length after the test. In most cases, fibre breakage happened in one of the following two places:

i). Behind the combing zone. In this case, test fibres broke in the region between the strain gauge and the combing start point. This occurred occasionally for all test fibre lengths and there were always tension peaks corresponding to fibre breakage. The breakage could be generated by putting a leading hook on the test fibre, so that, once combing started, the tension built up rapidly because of the hook, and the fibre broke at a very low speed (Figure 2.15(a)). However, in other cases there was no leading hook on the test fibre, and the fibre broke long after the combing speed had reached the set level (Figure 2.15(b)). Such random peaks must be due to one of the mechanisms described earlier.



ii). Near the end of combing zone. For test fibres protruding beyond the fringe, it was more common for the test fibre to break near the end of the fringe. This position of breakage was found especially at higher combing speeds. Furthermore, there was not always a high tension peak to account for the breakage. Figure 2.16 shows two different breakage patterns. Although the tension peak in Figure 2.16(a) is much higher than the mean tension value and was probably responsible for shortening the fibre, it is still much lower than the average fibre breaking strength, suggesting either a cutting of the protruding free end by the sawteeth or a defect in the test fibre. Unlike the breakage behind the combing zone which showed a sudden tension drop after break (Figure 2.15(b)), here the tension remained because only the tip end of the test fibre was chopped off. While there is no obvious tension peak in Figure 2.16(b) which could have broken the fibre (it was shorter after the test), the small tension peaks may be associated with repeated breakages of short lengths of the test fibre tip due to a wrapping action, as found in OE spinning by Yan and Johnson [82].

Test fibres could also be broken within the fringe. This case was rare, and among the very few such cases encountered throughout the experiments, none gave any tension peaks corresponding to the fibre breakage. One possibility is that the test fibres were simply worn away gradually because of their relatively heavier contact with the beater in that region.

The tension trace in Figure 2.10(a) is an interesting case, with the test fibre length initially the same length as the fringe. As the combing speed increased, the magnitude of frequent peaks increased, due to either the increasing speed, or the thinning out of the end of the fringe allowing the fibre to flail about more wildly. These peaks suddenly disappear, suggesting that the shorter fibre is no longer flailing about, but still long enough to maintain the same base tension.

## 2.5 CONCLUSION

A device capable of measuring fibre tension during simulated combing has been developed, using computer data acquisition and strain gauge techniques. Detailed measurements were made of the tension generated in a single wool fibre (the test fibre) in a fringe by the combing action. Variables such as how far the test fibre protrudes into or beyond the fringe, and the length and density of the fibre fringe, had the expected linear effects on the average tension experienced by single fibres. The effect of the combing speed was relatively small.

It was also found in this study that, initially, even when the test fibre did not have leading hooks, and even though the fibre fringes were free of short fibres and fibre entanglements, test fibres could still be broken during combing. While the measured average tension levels were normally far too small to be blamed for the breakage, peaks in the tension usually coincided with fibre breakage.

Fibre breakage sometimes occurred behind the combing zone, and was always associated with tension peaks. These were sometimes induced by a leading fibre hook, or perhaps by fibre entanglements; the relatively high accumulated tensile stress in that region (the tension built up from all contacts in the combing zone) could also contribute to the forces causing this breakage. Fibres extending beyond the fringe usually broke near the end of the fringe, but there was not always a high tension peak to account for the breakage; breakage here was possibly due to either a cutting of the protruding free fibre end by the saw-teeth, or a defect in the fibre, or abrasion and fatigue due to repeated wrapping of the protruding free fibre end around the

teeth. Such repeated wrapping action could have also been responsible for the excessive breakage of fibres in the fibre fringes when a much higher combing speed was used.

The test fibres rarely broke within the fringe, and no tension peaks were found to be associated with these breakages in this study. Probably the test fibres were simply worn away and weakened gradually because of their relatively heavier contact with the beater in that region.

The information provided in this chapter also suggests that, in terms of determining the extent of fibre breakage, conclusions drawn from average fibre tension levels only may be misleading; detailed examination of fibre breakages requires knowledge of the tension peaks experienced by individual fibres during combing processes. This may apply to the withdrawal process through the top comb and feed gill; it is therefore necessary to investigate fibre tension peaks, instead of average fibre tension only, in the withdrawal process, and to re-evaluate the contribution of this process on the total fibre breakage level in rectilinear combing.

## CHAPTER 3

### STUDY OF PIN FORCES IN COMBING

---

#### 3.1 INTRODUCTION

Chapter two described a system for measuring the tension experienced by individual fibres within initially unentangled wool fringes during simulated combing. The development of tension peaks in fibres and the difference in behaviour between fibres which do, or do not, protrude beyond the fibre fringe were studied.

Another important set of combing forces are those forces experienced by the combing elements. As the combing elements (round pins in the present study) comb through a fibre fringe, the fringe imposes certain forces on them, called "pin forces" in this chapter. They can be quite large, especially if fibres in the fringe are entangled, causing some fibre breakage. The magnitude and pattern of these pin forces can give a good indication of the extent of fibre entanglements in the fringe, and of fibre breakage during combing. The measurement and study of the pin forces are the objects of the work reported in this chapter.

Previous studies of opening force in carding and OE spinning employed torque transducers to measure the torque on opening rollers [77, 73]. However, this approach only gives the average value of the combing forces. In order to obtain more detailed information on the forces experienced by a single pin as it combs through a wool fringe, small strain gauges were attached to a single combing pin, and the forces detected by the strain gauges were recorded and analysed through a computer data

acquisition system.

### 3.2 THEORETICAL CONSIDERATIONS

The forces acting on the pin during combing arise from:

- \* fibres which are in direct contact with the pin,
- \* air resistance (negligible at slow speed),
- \* effects of angular velocity and acceleration (also to be taken as negligible).

If the fibres in the fringe are more or less straight and parallel to the path of the pin, it would be relatively easy for the pin to comb through the fringe, and the forces acting on the pin will simply be the frictional force arising from sliding contacts between the pin and fibres plus the force required to push the fibres sideways to allow room for the pin to pass. The frictional force normally would be quite small and affected by inter-fibre pressure as a result of the density of the fringe. Similarly, the fringe separation force would be largely determined by inter-fibre pressure in the fringe. Note that an additional force arises if the fibre ends tend to wrap around the pin. The mechanism of such wrapping action at high speed was examined in detail by Yan and Johnson [78] in their study of fibre damage in OE spinning.

Consider the progress of a tapered pin combing such an ideal fringe, of constant linear density. As the tapered pin progressively penetrates the fringe, it will contact more and more fibres, leading to greater total frictional resistance. It will also force a wider path through the fringe, creating higher inter-fibre pressure as it pushes the

displaced fibres into the surrounding fringe. This will progressively increase both the frictional resistance and the fringe separation force. Thus, the pin force would be expected to rise steadily from zero.

Once the pin had fully penetrated, the pin force should remain constant until the pin leaves the fringe. However, because of cohesion in the fringe, the fringe separation force will tend to split the fringe ahead of the pin, so that fibre pressure on the pin will reduce as it approaches the end of the fringe.

However, fibres in a fringe before combing are normally not parallel but entangled. It is these entanglements that are blamed by several researchers [21, 23, 45] for most of the fibre breakage occurring during combing and other opening processes, such as carding. In an attempt to describe the state of a wool stock as it proceeds through the conversion processes, Harrowfield et al [73] classified different forms of fibre entanglement that may be found in wool stock. According to this classification, the major forms of fibre entanglement existing in a pre-combed fringe can be: 1) 'parallel' fibres; 2) hooked fibres; 3) twisted fibres; and 4) neps. To this list could be added the special case which arises when both ends of a fibre or of a fibre hook are held by the feeding mechanism, defined here as a 'looped fibre'. These various forms of entanglement offer different forces of resistance to a pin trying to disentangle them. Chapter one described some previous theoretical analyses of the disentanglement of the 'parallel', looped, and hooked fibres. A theoretical examination of a pin disentangling twisted fibres will be presented in the following chapter. For the present, it is sufficient to consider that all these various entanglements will provide additional restraints to the passage of the pin.

Having engaged an entanglement, the pin will initially push the entanglement along with it. If the entanglement is not firmly held by the feeding mechanism or by other fibres in the fringe, it will move with the pin and be dislodged from the fringe. The additional inertia and frictional forces will be very small and have little effect on the pin force. In the simple case of a fibre anchored at the trailing end with a single leading hook, if the end of the hook is free from other entanglements, it will straighten with very little chance of breakage. Siersch [77] calculated the average fibre tension due to the inertial and frictional restraint as a high speed pin with a rounded edge straightened a fibre hook and found it to be  $10^3$  to  $10^4$  times smaller than the tensile strength of the fibre. The pin force required to straighten such a hook would therefore also be quite small, unless the hooked end is firmly held in some way.

For those entanglements which are firmly held in the fringe, the progress of the pin will build up forces on the fibres in the entanglement, either causing them to move in order to disentangle and straighten, or extending them to break. In some cases, the entangled fibres may break away from the fringe and move with the pin. Thus the pin force will rise as the pin engages an entanglement, but will drop back, either gradually if progressive disentanglement occurs, or sharply if fibres break or the entanglement is released.

Depending on the level of entanglement in the fringe, the pin may always be acting on several entanglements simultaneously. Thus, entanglements would not just appear as spikes on the pin force curve, but would combine to raise the overall level of pin force.

Once the pin leaves the fringe, the pin force should drop to zero, except that some fibre entanglements which are still connected to the fringe, may travel with the pin and generate residual force on the pin until they finally break away from the fringe or the pin.

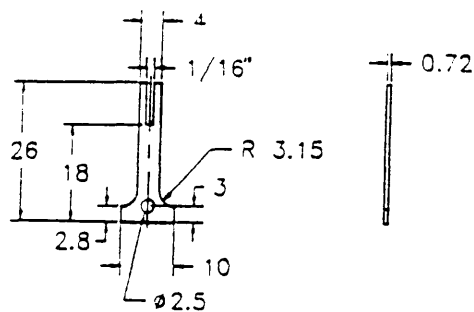
Variations in the density of the fringe are another possible cause of variations in the pin force. Longer term variations will affect the variability between individual pin force measurements, while very short term variations (within an ideal short fringe) are likely to be associated with entanglements.

This qualitative discussion has built up predictions of the pin force profile to be expected as a pin combs a prepared ideal fringe. It also allows some predictions to be made about the effects of various factors on average pin force. Pin force will increase with:

- \* increase in fringe density, because of increased inter-fibre pressure,
- \* increase in fringe length, because of the greater accumulation of entanglements as the pin progresses,
- \* decrease in the number of gillings, because of the greater level of entanglement in un-gilled slivers.

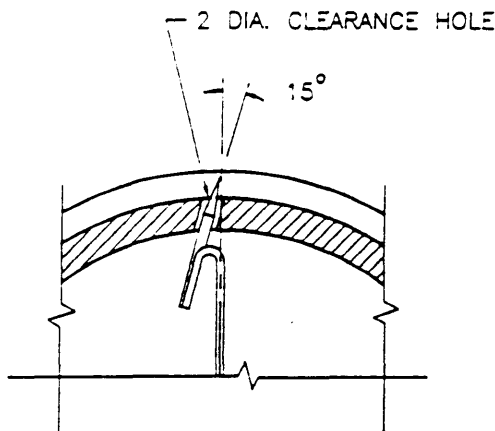
The effect of combing speed has been examined by several researchers. In the previous chapter, it was found that with increasing combing speed, only a slight increase in the tension in individual fibres in a fringe was observed. Aldrich [9] reported that, with three different comb speeds of 130, 150 and 165 nips per minute, no significant effect could be detected as far as percent noil and top cleanliness were concerned. Turpie and Klazar [29] expanded the speed range from as low as 7 to as





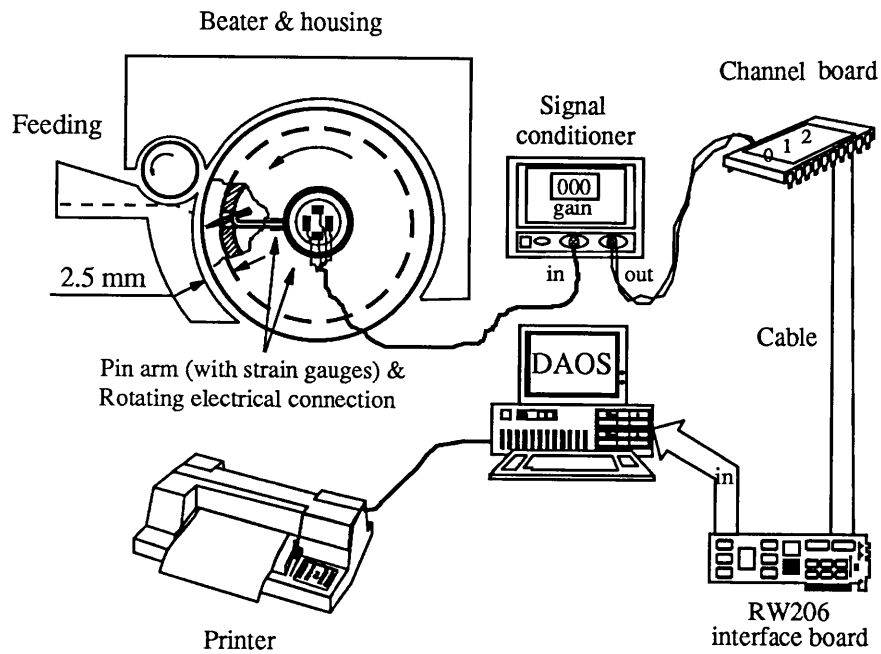
PIN ARM

MATERIAL STAINLESS STEEL SHEET 0.72 THICK



DETAIL OF BEATER AND PIN

**Figure 3.1: Beater--pin--pin arm assembly**



**Figure 3.2: Diagram of the experimental set-up for pin force measurement**

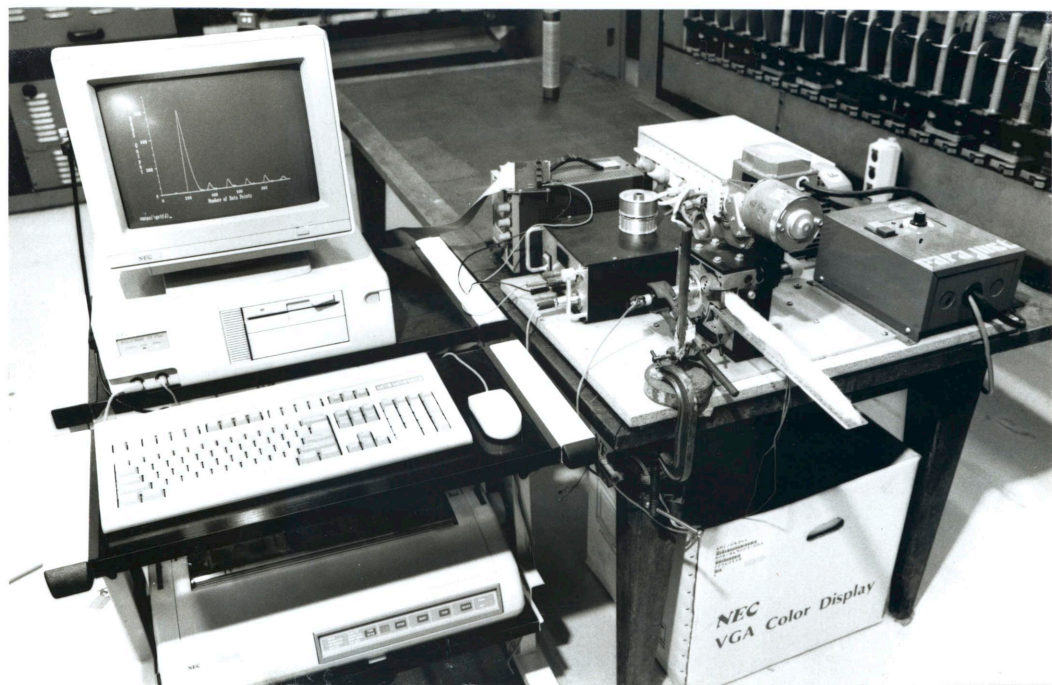


Figure 3.3: General view of the experimental set-up for pin force measurement

high as 165 nips per minute, but no change in the fibre breakage pattern with speed increase was found. If speed over this range has no detectable effect on fibre breakage, it is unlikely to have a significant effect on pin forces. It is therefore reasonable to measure pin force at relatively slow combing speeds, in order to obtain a more detailed profile of pin force. Moreover, other non-fibre effects, such as air resistance and centrifugal forces, may influence the measured pin force at very high combing speeds.

Note that throughout this discussion, only fringes of constant linear density (or 'rectangular' fringes) are considered. This makes fringes of different length and density more definable, and their effects on pin forces more comparable. The various predictions thus built up, on the effect on pin forces of individual parameters defining an ideal fringe, can also be extrapolated to interpret and predict the effect on pin forces of other non-ideal fringes, such as a 'tapered' fringe, which normally requires more parameters to define than that required by an ideal fringe described here.

### **3.3 EXPERIMENTAL**

#### **3.3.1 Apparatus**

A small beater (58 mm in diameter at the surface) with one round pin and a specially designed pin arm (Figure 3.1) was used to comb the fibre fringes, which were fed in through the feeding roller and the beater housing. Details of the pin arm design can be found in Appendix I. The beater and the feeding roller were driven by separate motors. Figure 3.2 is a diagram of the apparatus. A photograph of this apparatus is shown in Figure 3.3. The combing pin was 2 mm in height above the beater surface, tapering gradually from a rounded point to a diameter at the beater surface of 0.8 mm. The designed natural frequency of the pin arm (with the pin) was about 850

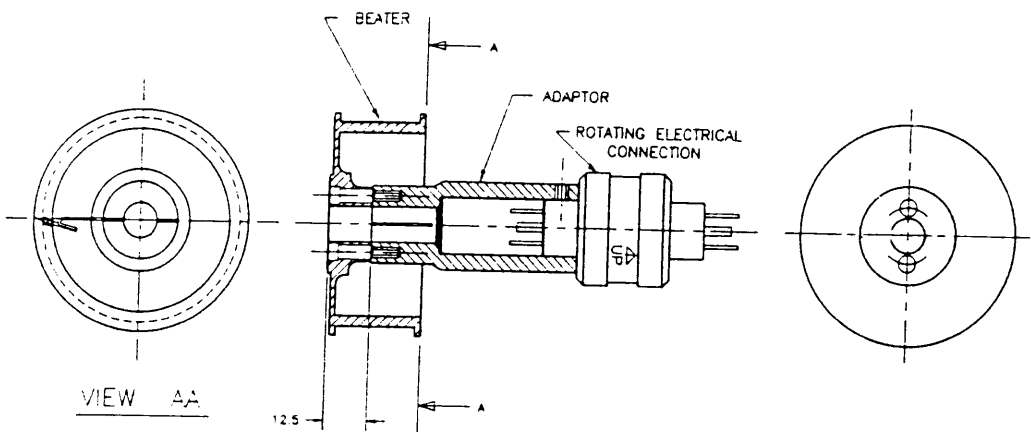


Figure 3.4: Details of the rotating electrical connection

Hz. There were no other pins on the beater surface. Two small strain gauges were mounted on each side of the pin arm to detect its bending deformation during the combing action of the pin. The signals from the strain gauges were sent out through a rotating electrical connection (similar to slip rings) to a signal conditioner, and then recorded and analysed through the Data Acquisition Operating System (DAOS), as was described in the previous chapter. Relevant details of the rotating electrical connection are shown in Figure 3.4.

Before any testing, the whole system was calibrated, by applying a series of weights on the pin near the centre of its length outside the beater surface (with the pin arm horizontally positioned) and checking the DAOS output. Direct readings of pin forces were obtained through the calibration function below:

$$\text{PIN FORCE}_{(\text{cN})} = \text{DAOS OUTPUT}_{(\text{mv})} * 0.22$$

The difference in measured pin force due to applying a known force to the pin either at its tip, or near the beater surface was about 4%.

### 3.3.2 Sample Preparation

Scoured merino wool fibres with an average diameter of 23  $\mu\text{m}$  were carded once on a double swift worsted card with fillet clothing and gilled three times at a draft of 8 in conditions of  $(65 \pm 5)\%$  r.h.,  $20 \pm 5^\circ\text{C}$ . Samples of sliver were taken randomly after each processing stage, cut to be 50 cm long. Since these samples were normally too dense to be used directly on the present combing device, some fibres were then carefully removed along the length of each sample and an accurate balance was used to weigh the remaining sliver sample to determine its linear density. Also in this

process, each sample was arranged to be about 12 mm in width to fit the funnel of the feeding device. Special care was taken to minimise disturbance to the fibre configurations in each sample. Thus, upon combing, each of the prepared samples would be 50 cm long and about 12 mm wide, with a certain determined linear density.

### 3.3.3 Testing Procedure

Each sample was fed into the beater housing in the direction of normal reversal through the feeding roller, which was then stopped once a specified length of the sample was in the combing zone. Since it took a finite time for the motor (hence the beater) to reach a set speed level after its start-up, in order to achieve a constant combing speed during each passage of the pin through the fringe, the combing pin was positioned near the front end of the sample fringe in the beginning, and during the motor start-up, the beater shaft outside the beater housing was firmly held (allowing belt slippage) until the motor speed reached its set value, then the beater shaft was suddenly released; thus, well before the pin approached the combing start point, the beater would have reached its set speed value, because the beater speed was quite slow. Therefore the pin could comb three times through the sample fringe at a constant speed (set at 60 rpm, corresponding to a surface speed of about 19 cm/sec) while the data acquisition system (with a selected sampling rate of 2500 Hz) recorded the signals from the strain gauges mounted on the pin arm. Since both the calculated tensile strain on the pin arm caused by centrifugal force and the effects of air resistance are very small at this relatively slow combing speed, the strain gauges can be regarded as detecting only the bending deformation of the pin arm due to the combing forces on the pin (refer to Appendix I).

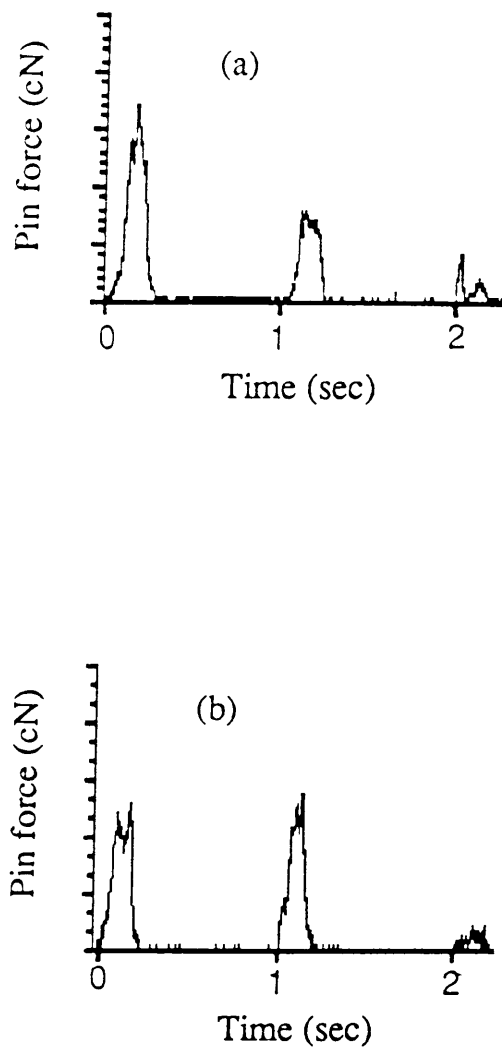


Figure 3.5: Typical individual pin force profiles



After each such test, the feeding roller was rotated in the opposite direction to remove the fringe. The combed end of the sample was then cut off and the same sample was fed into the beater housing again for another similar test. Figure 3.5 shows two typical individual pin force results. The three pin force peaks on each graph correspond to three rotations of the beater. Five such tests were carried out on each sample, and five almost identical samples were used for each set of experiments. In other words, in each set of experiments, 25 individual tests were carried out under the same conditions. The peak pin force for the first beater rotation was recorded and the mean and 95% confidence interval of these 25 individual results were used for each data point.

### 3.3.4 Parameters Investigated

Fringe density: Fringes of different linear densities (0.5, 1.0, 1.5 Ktex) after a certain processing stage were combed to check their effect on the pin forces.

Fringe length: The length of fringe within the combing zone was set variously at 20, 30, and 40 mm.

Processing stages: With other parameters the same, sample fringes obtained after carding, 1 gilling and 3 gillings were tested to examine the effects of gilling on the pin forces.

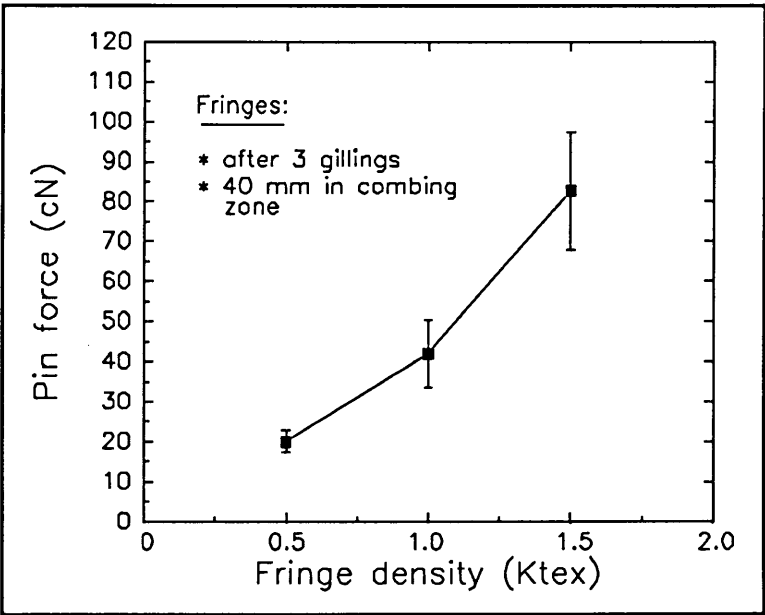


Figure 3.6: Effect of fringe density on pin force

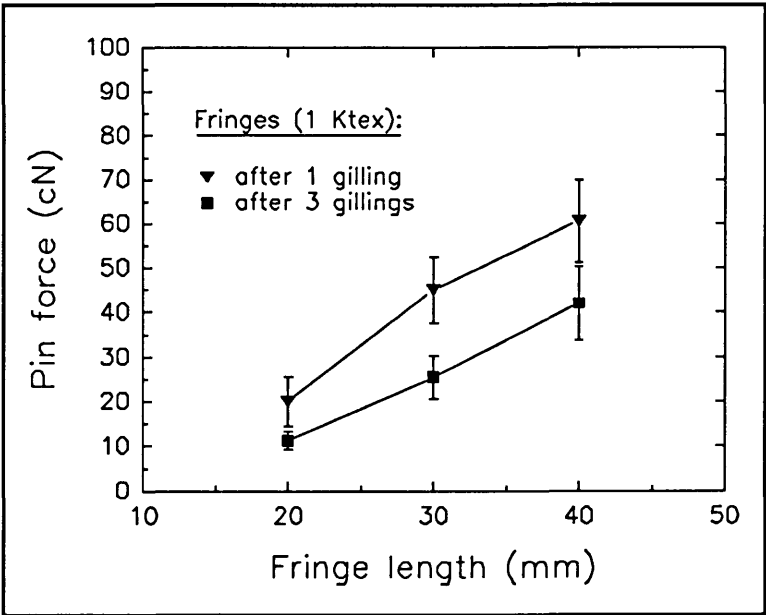


Figure 3.7: Effect of fringe length on pin force

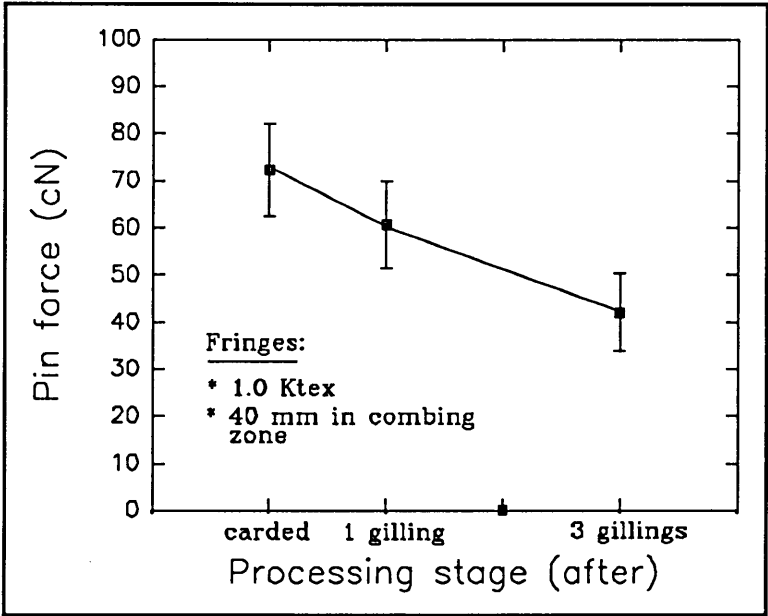


Figure 3.8: Effect of processing stage on pin force

## **3.4 RESULTS AND DISCUSSION**

### **3.4.1 Mean Levels of the Pin Force**

The means and 95% confidence intervals of the 25 individual peak readings were plotted.

#### **3.4.1.1 Effect of fringe density**

The pin force increased with increasing fringe density, as indicated in Figure 3.6. This outcome is consistent with the simple hypothesis, because increases in fringe density would increase the inter-fibre pressure, affecting both the frictional forces between the pin and the fibres, and the difficulty of removing entanglements.

#### **3.4.1.2 Effect of fringe length**

The pin force increased approximately linearly with increasing fringe length (Figure 3.7). While the trend agrees with the simple hypothesis, the apparent linearity of the relationship is noteworthy.

#### **3.4.1.3 Effect of processing stage**

The pin force progressively decreased with additional gilling processes (Figure 3.8). Obviously, fibres in the fringe become more and more parallel as the processing proceeds, thus reducing the degree of fibre entanglement in the fringe and hence the

pin force.

### 3.4.2 Individual Patterns of the Pin Force

While the mean levels of the pin force provide a general view of how certain parameters affect the pin force, which is of interest in confirming the basic predictions of the hypothesis, it is the individual patterns of the pin force that can give more direct indications of whether or not, and how, fibres break during combing.

Certain features are very consistent throughout the experiments: of the three pin force profiles obtained in any individual test, the peak of the first is usually greater than that of the other two (Figure 3.5(a)), except in very rare cases where the peak of the second force profile is the largest, as shown in Figure 3.5(b). This indicates that with repeated combing actions of a single pin on a fringe, the first passage normally removes the major fibre entanglements present at that position in the fringe, leaving only inter-fibre pressure to act on the pin during its second passage. However, there is also some chance for the first combing action to create new fibre entanglements in its wake so that in the subsequent combing action, a greater pin force might be realised. Another possible explanation for the second peak sometimes being larger than the first is that the sample fringe may shift laterally after the first passage of the pin, causing the pin to pass through a previously uncombed region of fringe.

It should also be borne in mind that a fully pinned combing roller may generate additional fibre movements, and a much greater potential for fibre re-entanglement.

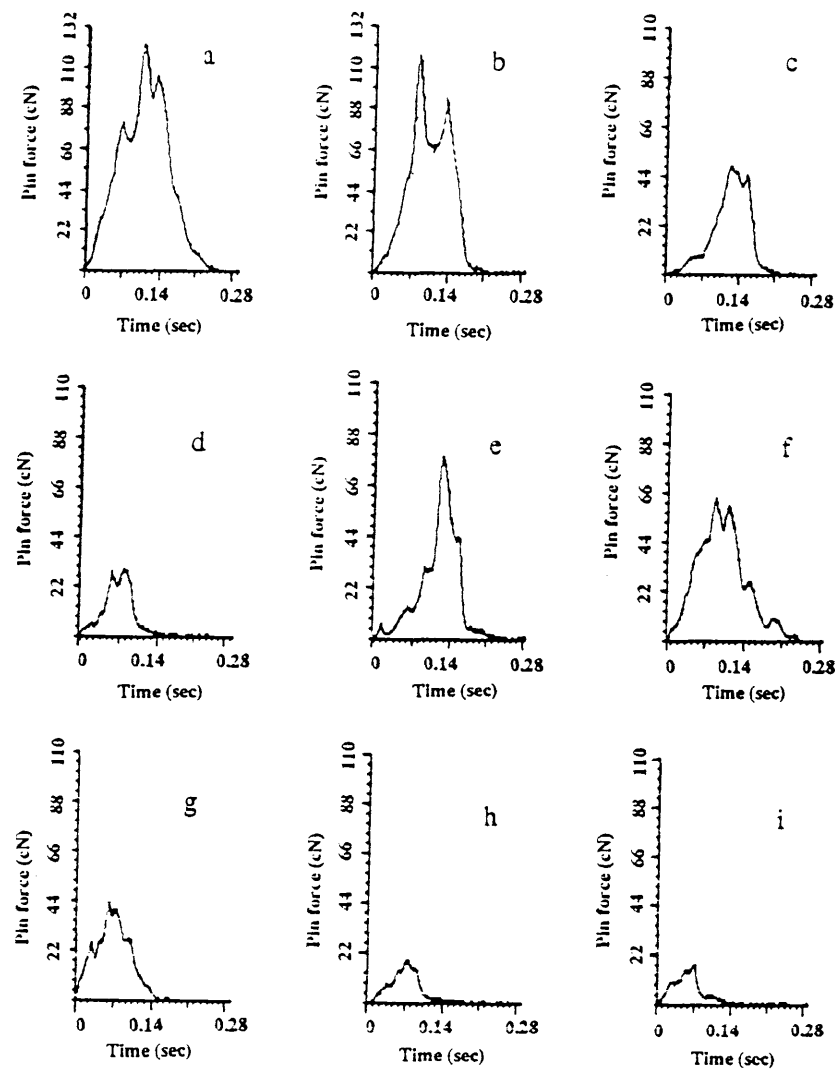


Figure 3.9: Different pin force patterns

Legend

Graph	a,b	c	d	e	f	g	h	i
Fringe density (Ktex)	1.5	1.0	0.5	1.0	1.0	1.0	1.0	1.0
Fringe length (mm)	40	40	40	40	40	30	20	20
No. of gillings after carding	3	3	3	0	1	3	1	3

Since the first combing actions are normally the most important, the pin forces caused by them will be considered in greater detail.

The effects of certain parameters on the mean peak force have already been shown in section 3.4.1, but the actual shapes of individual force profiles are also quite different under the different conditions.

Figures 3.9(a) and 3.9(b) show two individual pin force patterns for combing two fringes (after 3 gillings) of the highest linear density used in this investigation. Fibre breakage is clearly indicated by the peaks and valleys on each graph. The large drop in pin force (about 50 cN) in Figure 3.9(b) indicates possible breakage of several fibres (considering the average single fibre strength is of the order of 10 cN). This could happen, for example, if a nep, anchored in the fringe by several fibres, is being pushed by the pin. Once one of the anchoring fibres breaks, the others may also fail quickly in succession, or the entire nep may then be free to slip around the pin.

As the fringe density decreases, there is less pressure on the pin and more freedom for fibres to move and be disentangled. The resultant pin force patterns are shown in Figures 3.9 (a & b), (c), and (d), where the maximum pin force is progressively lower, and the pin force fluctuations become less obvious. Note also that at the lightest fringe density (0.5 Ktex), the pin force decays much sooner than in other cases, suggesting that either the pin has been able to separate this light fringe ahead of its path, or the fibre resistance to the pin after about 0.14 seconds is too small to be detectable.

Gilling reduces the frequency and severity of fibre entanglements in the sliver after carding. Figures 3.9 (e), (f), and (c) are pin force traces for carded, once and three



times gilled slivers respectively of the same fringe length and density, showing that the traces become smoother and have a lower maximum for the more gilled material. For example, the series of smaller peaks on the card sliver trace suggest the pin has acted on a series of entanglements as it penetrated the fringe, with these obstructions eventually yielding, presumably either through fibre disentangling or fibre breakage.

The particular trace shown for the once-gilled sliver (Figure 3.9(f)) indicates that a series of entanglements were encountered as the fully-penetrated pin tried to push its way through the fringe. Of course, this may have been one large entanglement, being pushed along by the pin and yielding progressively as anchoring fibres were pulled taut and then slipped free or were broken. The entanglement would then be pushed along until other anchoring fibres were tensioned

If the fringe length in the combing zone is shorter, a significant decrease in both the maximum value and variation of the pin force profiles is observed (compare Figures 3.9 (c), (g), & (i) and Figures 3.9(f) & (h)). These results are in good agreement with the previous work by Aldrich [9] on the effect of gauge length on fibre breakage in rectilinear combing.

### 3.5 CONCLUSION

A device capable of measuring the forces experienced by a single pin as it combs through prepared fibre fringes has been developed. The average peak values of the "pin force" recorded by this device increased with increase in fringe density, increase in fringe length and decrease in number of gillings. These results are in general agreement with the findings of other workers.

The individual traces of pin force show how the force builds up as the pin penetrates the fringe, dislodges entanglements, breaks fibres and separates the fringe. These individual pin forces can indicate the degree of fibre entanglements, ease of disentangling, and level of fibre breakage in a fringe. The measurement technique could also be used to evaluate other factors, such as fibre type, pin geometry, and fibre lubricants.

Although the various predictions put forward and the results obtained in this chapter were mainly based on the prepared ideal fringes, they could also be extrapolated to interpret and predict the effect on pin forces of other non-ideal fringes, such as tapered fringes.

## CHAPTER 4

# THE BEHAVIOUR OF A PIN DISENTANGLING TWO TWISTED FIBRES

---

### 4.1 INTRODUCTION

It is generally believed that in various fibre opening processes such as carding, combing and sliver opening for OE spinning etc., the interaction between fibres and clothing elements causes fibre breakage, especially at very high speeds of the clothing element. This breakage has been a major concern for increasing the production rates in those fibre opening processes. In an industrial practice, it would be desirable to achieve high production rates without excessive fibre breakage. This is particularly true in worsted woolcombing.

As has been highlighted in chapter one, the production rates of worsted combs are well below those of gill-boxes and cards, and combing is actually a bottle-neck in worsted topmaking [13]. However, the work reported in chapter two has indicated that an increase in combing speed does not have a significant effect on the tension experienced by individual fibres; previous experimental works on wool combing [9, 29] have also observed no detectable deterioration in combing performance with increased speed over the range currently possible on existing commercial machines. The upper speed limit set on existing combing machines is due to the complex mechanical structure of the machines and the presence of mechanical shocks which occur in these machines at high speeds, but ideally, the fibres themselves, rather than the mechanism, should provide the factor limiting the ultimate combing speed [37].

Existing theories on percentage fibre breakage in combing [18, 20, 21] only provide a "summarized picture of the combing process as a whole" [9], and have not included parameters such as combing speed and many of the physical properties of the fibres. No theoretical work has yet attempted to ascertain whether there exists a fundamental speed limit, or to predict what that speed limit might be, although there are some relevant studies of special cases.

In chapter three, the forces acting on a single combing pin were measured as it combed through different prepared fringes. Some useful information was obtained from the pin force profiles as the pin dislodged various entanglements, broke fibres, and separated fibres in the fringes. However, detailed examination of the mechanism of fibre breakage and its prevention requires additional knowledge about whether or not, and how, an individual entanglement makes its contribution to the forces in combing.

The different forms of fibre configuration possible in a pre-combed fringe have been classified as: a) parallel fibres, b) looped fibres, c) hooked fibres, d) twisted fibres, and e) neps [73].

Of these, parallel fibres are generally believed to cause much less fibre breakage. Yan and Johnson [78] have already considered the effect of the speed of the clothing element for this case, and described how, at very high speeds, the fibre end can wrap around the clothing element to cause excessive fibre breakage. At even higher speeds, the fibre may break instantly due to its inability to propagate strain at a sufficiently high speed [78].

The form of fibre loop, in which both ends of the fibre are somehow firmly held, provides little scope for further theoretical analysis as far as fibre breakage is concerned, because no matter how high or low the combing speed, the looped fibres will simply be stretched to break if engaged by the combing elements; only the position of break has been the subject of some study [68].

Fibres are often in the form of hooks in a sliver. Many of these behave as looped fibres, because there is a great chance for those hooks, especially the leading hooks, to be gripped by the nipper jaws during rectilinear combing, and subsequently broken by the combing elements [30]. The straightening by a clothing element of a fibre hook with only one end firmly gripped and the other end embedded loosely in a fringe has been analysed in detail by Siersch [77], as summarized in chapter one. His analysis showed that, while the speed of the clothing element played an important role, the forces generated were well below fibre breaking strengths.

In this chapter, the twisted fibre form of entanglement is considered. A theoretical study of the interaction between a combing element and two twisted fibres has been attempted. Also examined are the mechanism of fibre breakage which might occur during such interaction, and the maximum speed of the combing element below which fibre breakage could be avoided.

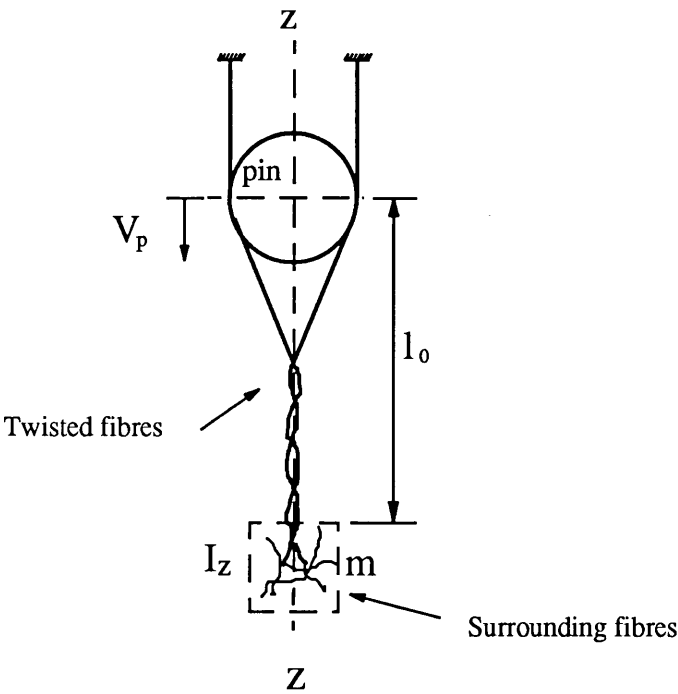


Figure 4.1: Diagram of two twisted fibres engaged by a round pin

## 4.2 THEORY

### 4.2.1 Qualitative Description

Figure 4.1 shows two twisted fibres about to be engaged in the combing action of a clothing element (a round pin in the present study). The bottom ends of the twisted fibres may be in contact with other fibres present in the fringe being subjected to combing. For simplicity of the description, the twisted section of the two fibres will sometimes be referred to as a two-ply cord, and the fibres attached to the end of the cord as a body of mass  $m$  with a moment of inertia  $I_z$  about axis  $z$ . Suppose the initial 'cord' twist number is  $N_0$ . If each fibre in the twisted structure contains no initial torque, the 'cord' twist (twist per unit length) will be stable (balanced) until the pin action changes it. As the pin engages the twisted fibres, the convergence point  $cp$  will be forced towards the bottom end, thereby increasing the 'cord' twist. The consequent increase in the cord twist angle  $\theta$  will develop a certain torque  $M_\theta$  in the 'cord'. The development of such torque is very similar to the torque generation during yarn twisting. The cord twist will keep accumulating until the torque it generates can overcome the 'restraint torque'  $M_{ZR}$  from the surrounding fibres. The resultant torque ( $M_\theta - M_{ZR}$ ) can then act upon the 'body' below the twisted section and will drive this body to rotate, giving rise to some angular acceleration  $\delta$ , and untwisting of the cord.

Suppose the pin, moving at a speed  $V_p$ , must travel a distance  $l_0$  from its initial position of engagement to reach the end of the fibres. For simplicity of explanation, consider for now that the resultant torque is uniform throughout the engagement. If the fibres are to untwist to allow the pin to pass through, rather than to break, then the body attached to the twisted fibre section needs to rotate a total angle of  $2\pi N_0$  in

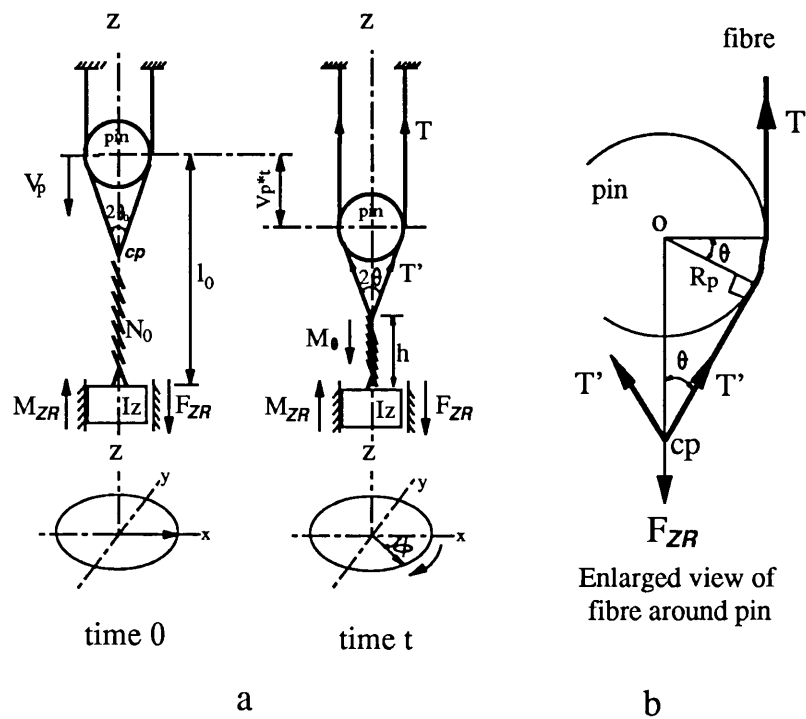


Figure 4.2: Model of two twisted fibres engaged by a round pin



a time of  $l_0/V_p$  or less, requiring an angular acceleration of at least  $\delta_c$  (the 'critical' angular acceleration), corresponding to a torque  $I_z\delta_c$  [86]. It is obvious that the time needed for the body to rotate an angle of  $2\pi N_0$ , will be shorter at a higher pin speed, i.e. the angular acceleration should be higher. If the total torque acting on the 'body' at the end of the twisted section,  $\Sigma M$ , is greater than  $I_z\delta_c$ , then the fibres will be able to untwist to allow the pin to pass through. However, if  $I_z\delta_c > \Sigma M$ , then the cord twist will keep increasing towards its geometrical limit, which might lead to lateral buckling or snarling of the two twisted fibres, so that further pin movement will simply stretch the fibres and subsequently break at least one of them.

In summary, if the pin speed is slow, and if the twisted fibres are not subjected to much restraint, as is true when the density of the surrounding fibres is low, the twisted fibres will untwist and not break, but if either the pin speed or the external resistance to fibre rotation is too high, the twisted fibres will not be able to untwist quickly enough, and will break. It can therefore be predicted from this simplified description that the pin speed  $V_p$ , which influences  $\delta_c$ , might play a very important role in determining whether or not the twisted fibres break.

#### 4.2.2 Physical Modelling

From the foregoing description of the interaction between two twisted fibres and a combing pin, a physical model of this interaction can be represented as in Figure 4.2, where two identical fibres of circular cross section, twisted together and attached to a body with a moment of inertia  $I_z$  about axis  $z$ , are to be engaged by a round pin. The weight of the body,  $F_{ZR}$ , can be regarded as a tensile force applied to the twisted fibres in the direction of axis  $z$ . To be consistent with the nomenclature of textile

cords, the assembly of twisted fibres will be referred to as a 'cord', and individual component fibres as 'plies'. The ultimate goals of such modelling are to investigate the mechanisms of fibre breakage and certain critical parameters associated with the breakage.

As in other theoretical analyses of the physical properties of textile yarns and cords [87], certain basic assumptions must be introduced here regarding the geometrical disposition of the fibres in the twisted structure prior to any lateral buckling or snarling. They are:

- 1). the two plies in the cord form a perfect helical conformation about the cord axis  $z$ .
- 2). the cord helix angle  $\theta$  is the same as the angle made by each ply with the cord axis above the convergence point  $cp$ .
- 3). before the pin acts, no initial torque exists in either ply, hence there is no initial untwisting of the cord.
- 4). once the pin engages the twisted fibres (time 0), a torque develops in the cord with the increase in cord twist level, and the torque transmits instantly.
- 5). only rotation around axis  $z$  is allowed during the pin action, and  $I_z$  is independent of the twist level.
- 6). the tension in the ply lying in the cord is considered to be localized to the ply axis and to have the same value everywhere.

Some other assumptions regarding the physical properties of the ply (fibre) will be introduced later when deriving the torque developed in the cord. It should be noted

that although assumption 2 may be reasonable for the purpose of this study, and experimental evidence has also suggested its validity in the analysis of twist triangle by El-Shiekh [100], it is not strictly true because of the finite flexural rigidity of the fibre [88].

### 4.2.3 Torque in Two Twisted Fibres

The twist level increase in the two twisted fibres due to the pin action creates a certain torque. The development of such torque is quite similar to the torque generation in singles yarns during ply twisting. Assuming idealized yarn geometry and making some additional assumptions such as fibres in the yarn being linearly elastic, etc., Platt et al [89] derived equations for the torque due to fibre bending and fibre torsion during ply twisting. Postle et al [90] analysed the torque contributed by the tensile force applied during twisting, and presented an expression for the total torque in a twisted yarn by summing the components of torque due to fibre tension, fibre torsion, and fibre bending. In the following, their derivations are adapted to derive an expression for the torque developed in the two twisted fibres, as contributed by fibre bending, fibre torsion, and fibre tension, as a function of the cord helix angle  $\theta$  and some other fibre property related parameters. However, in both of the above works, fibre diameters were assumed to be negligibly small compared to the yarn diameter, but this assumption is no longer valid in the present study of torque in two twisted fibres. Nor do these previous works include assumption 3 above; a rigorous approach incorporating this assumption for calculating the torque in the cord requires consideration of changes (with respect to the initial twisted state) in ply torsion and curvature etc. In this study, however, an approximate but simple approach is taken, which follows the previous works. The torque that would have been created by

twisting the two fibres from an untwisted state to the initial cord helix angle is calculated. This is then subtracted from the torque calculated for the new cord helix angle created by the pin action, to approximate the effect of there being no torque in the initial twisted state. Some other assumptions used in the previous works, such as linearly elastic fibre properties, are still used here.

### **a) Torque due to fibre bending**

If the axes of two fibres with radius  $r_f$  form a perfect cylindrical helix about axis  $z$ , and the cord twist level is  $T_c$  (twist per unit length), the following equation stands [91]:

$$\tan \theta = 2\pi r_f T_c \quad \dots(4.1)$$

Each fibre as it lies in the helix configuration, has a definite curvature. This curvature, designated as  $1/R_c$  where  $R_c$  is the corresponding radius of curvature, can be expressed as [89]:

$$\frac{1}{R_c} = \frac{\sin^2 \theta}{r_f}$$

The bending moment ( $M_B$ ) acting in the plane of bending of each fibre is normally calculated from the classical (small-deformation) theory by means of the formula [87]:

$$M_B = \frac{E_f I_f}{R_c} = \frac{E_f I_f \sin^2 \theta}{r_f}$$

where  $E_f$  and  $I_f$  are respectively the modulus of elasticity of the fibre in bending and the moment of inertia of the cross section of the fibre in the plane of bending.

Since only the component of the  $M_B$  vector parallel to the axis  $z$  contributes to the torque in the cord, for two fibres, the total torque available from fibre bending is then:

$$M_{Bz} = 2M_B \sin \theta = \frac{2E_f I_f \sin^3 \theta}{r_f} \quad \dots(4.2)$$

### **b) Torque due to fibre torsion**

For the assumed perfect helix arrangement of each fibre (ply) about the cord axis, the equivalent twist of the fibres as they lie in the cord,  $T_f$ , is related to the cord twist  $T_c$  through the following equation [89]:

$$T_f = T_c \cos^2 \theta$$

For linearly elastic fibres, the torque from fibre torsion,  $M_T$ , is given as below [89]:

$$M_T = K_f G_f 2\pi T_f = K_f G_f 2\pi T_c \cos^2 \theta$$

where  $K_f G_f$  = the torsional rigidity of a fibre. The component of fibre torque parallel to the axis  $z$ ,  $M_{Tz}$ , contributes to the total torque in the cord; for two fibres, it is:

$$M_{Tz} = 2M_T \cos \theta = 2K_f G_f 2\pi T_c \cos^3 \theta$$

By substituting equation (4.1), the above equation can be rewritten as a function of  $\theta$ :

$$M_{Tz} = 2K_f G_f \frac{\tan \theta}{r_f} \cos^3 \theta = 2 \frac{K_f G_f}{r_f} \sin \theta \cos^2 \theta \quad \dots(4.3)$$

### **c) Torque due to fibre tension**

If a tensile force  $F_{ZR}$  is applied to the fibres in the direction of axis z, the torque the two fibres contribute due to this tensile force will be [90]:

$$M_{Fz} = 2 \frac{F_{ZR}}{2} r_f \tan \theta = F_{ZR} r_f \tan \theta \quad \dots(4.4)$$

### **d) Total torque**

Summing up equations (4.2), (4.3), and (4.4), the total torque,  $M_\theta$ , for any cord helix angle  $\theta$  is:

$$M_\theta = 2 \frac{E_f I_f}{r_f} \sin^3 \theta + 2 \frac{K_f G_f}{r_f} \sin \theta \cos^2 \theta + F_{ZR} r_f \tan \theta \quad \dots(4.5)$$

## **4.2.4 Effect of Pin Movement on Helix Angle**

From the model in Figure 4.2, if the end has rotated through an angle  $\phi$  after time  $t$ , the total twist number in the cord at time  $t$  will become:

$$N = N_0 - \frac{\phi}{2\pi} \quad \text{.....(4.6)}$$

Also according to the geometry in Figures 4.2(a) and (b) and equation (4.1):

$$\tan \theta = 2\pi r_f \frac{N}{h} = 2\pi r_f \frac{N_0 - \frac{\phi}{2\pi}}{l_0 - V_p t - \frac{R_p}{\sin \theta}} \quad \text{.....(4.7)}$$

where  $R_p$  is the pin radius.

Rearranging equation (4.7), the expression for fibre end rotation angle can be obtained as:

$$\phi = 2\pi N_0 - \frac{l_0 - V_p t}{r_f} \tan \theta + \frac{R_p}{r_f \cos \theta} \quad \text{.....(4.8)}$$

Recalling that the initial helix angle  $\theta_0$  does not contribute any torque in the cord as mentioned in the previous section, the net torque which could cause any fibre end rotation should be:

$$\sum M = M_\theta - M_{\theta_0} - M_{ZR} \quad \text{.....(4.9)}$$

where  $M_{ZR}$  is the 'restraint torque' from surrounding fibres, as represented in Figure 4.2.

Applying the classical theoretical mechanics for solid bodies [86]:

$$I_z \frac{d^2 \phi}{dt^2} = \sum M = M_\theta - M_{\theta_0} - M_{ZR} \quad \text{.....(4.10)}$$

The cord helix angle ( $\theta$ ) at any time  $t$  can therefore be expressed by the following set of equations:

$$\left\{ \begin{array}{l} \phi = 2\pi N_0 - \frac{l_0 - V_p t}{r_f} \tan \theta + \frac{R_p}{r_f \cos \theta} \\ M_\theta = \frac{2E_f I_f}{r_f} \sin^3 \theta + \frac{2K_f G_f}{r_f} \sin \theta \cos^2 \theta + F_{ZR} r_f \tan \theta \\ I_z \frac{d^2 \phi}{dt^2} = M_\theta - M_{\theta_0} - M_{ZR} \end{array} \right\} \quad \dots(4.11)$$

The boundary conditions for this set of equations are:

$$\left\{ \begin{array}{l} 0 \leq \phi \leq 2\pi N_0 \\ 0 \leq t \leq \frac{l_0}{V_p} \end{array} \right\} \quad \dots(4.12)$$

Note here that the effect of any ply elongation or twist contraction on the time the pin takes to pass through the twisted fibres is assumed to be negligible.

With some mathematical manipulation, equation set (4.11) can be reduced to a single non-linear 2nd order differential equation as below:

$$f_1(\theta, t, V_p, I_z) \frac{d^2 \theta}{dt^2} + f_2(\theta, V_p, I_z) \frac{d\theta}{dt} + f_3(\theta, t, V_p, I_z) \left( \frac{d\theta}{dt} \right)^2 = M_\theta - M_{\theta_0} - M_{ZR} \quad \dots(4.13)$$

where



$$f_1(\theta, t, V_p, I_z) = \frac{I_z \sec \theta}{r_f} \left( R_p \tan \theta + \frac{V_p t - l_0}{\cos \theta} \right)$$

$$f_2(\theta, V_p, I_z) = 2 \frac{I_z \sec \theta}{r_f} V_p \sec \theta$$

$$f_3(\theta, t, V_p, I_z) = \frac{I_z \sec \theta}{r_f} [R_p (\tan^2 \theta + \sec^2 \theta) + 2(V_p t - l_0) \sec \theta \tan \theta]$$

To find the solution for  $\theta$  according to equation (4.13), the initial value of  $d\theta/dt$  (at  $t=0$ ) is needed.

Differentiate both sides of equation (4.8) with respect to time  $t$ , noting that both  $\phi$  and  $\theta$  are functions of  $t$ ,

$$\frac{d\phi}{dt} = \frac{R_p \sin \theta + V_p t - l_0}{r_f \cos^2 \theta} \left( \frac{d\theta}{dt} \right) + \frac{V_p}{r_f} \tan \theta \quad \dots(4.14)$$

Now, at  $t = 0$ ,

$$\theta = \theta_0 \quad \dots(4.15)$$

Also, because of the inertia of the system and possible external restraint, the change in fibre end rotation angle ( $\phi$ ) due to the initial pin movement would be negligible, so

$$\left. \frac{d\phi}{dt} \right|_{t=0} = 0$$

and thus from equation (4.14),

$$\left. \frac{d\theta}{dt} \right|_{t=0} = \frac{V_p \sin \theta_0 \cos \theta_0}{l_0 - R_p \sin \theta_0} \quad \dots(4.16)$$

It should be noted that the above analysis of the changes in the cord helix angle is based on the assumption that the idealized geometry of the cord remains unaffected during the pin action. Practically, this might not be true, as can be seen later.

#### 4.2.5 Tension in the Fibres Behind the Pin

The maximum fibre tension occurs behind the pin, amplified by capstan friction against the pin. Fibre breakage could occur here if the tension exceeds the fibre breaking strength.

Before the cord becomes unstable, the tension in each fibre ahead of the pin,  $T'$ , can be easily represented as:

$$T' = \frac{F_{ZR}}{2 \cos \theta} \quad \dots(4.17)$$

If the kinetic coefficient of friction between the fibre and the pin is  $\mu_k$ , the tension in each fibre behind the pin,  $T$ , would then be:

$$T = T' e^{\mu_k \theta} = \frac{F_{ZR}}{2 \cos \theta} e^{\mu_k \theta} \quad \dots(4.18)$$

Since the solution to equation (4.13) is to be obtained numerically, it is convenient to solve equation (4.18) numerically as well.

Differentiate with respect to time  $t$  both sides of equation (4.18),

$$\frac{dT}{dt} = \frac{F_{ZR} e^{\mu_k \theta}}{2 \cos^2 \theta} (\mu_k \cos \theta + \sin \theta) \frac{d\theta}{dt} \quad \dots(4.19)$$

The initial fibre tension value should be,

$$T|_{t=0} = \frac{F_{ZR} e^{\mu_s \theta_0}}{2 \cos \theta_0} \quad \dots(4.20)$$

where  $\mu_s$  is the static coefficient of friction between the fibre and the pin. (Note that in many cases, the pin may already be moving prior to engagement at  $t = 0$ ; in such cases  $\mu_k$  should be used instead of  $\mu_s$ .)

#### 4.2.6 Limit of the Helix Angle

In a study of the geometrical twist limits in multi-ply cords, Gracie [93] presented a general equation predicting the maximum twist that can be put into a cord as below:

$$b T_{limit} \leq \frac{1}{2} \sqrt{\frac{1}{n_p^2} - \frac{b^2}{\pi^2 a^2}} \quad \dots(4.21)$$

where

$T_{limit}$  = maximum cord twist in turns per unit length,

$n_p$  = number of plies in the cord,

$a$  = radius of ply axis helix,

$b$  = radius of ply as it lies in the cord.

For a 2-ply cord as in the present case,  $a = b = r_f$ , and  $n_p = 2$ ; also note that  $\tan\theta = 2\pi r_f T_c$ , so that equation (4.21) reduces to:

$$\tan \theta_{limit} \leq \pi \sqrt{\frac{1}{4} - \frac{1}{\pi^2}}$$

or

$$\theta_{limit} \leq 50.47^\circ \quad \dots(4.22)$$

Any attempt to put in more twist must, for geometrical reasons, lead to snarling, which strongly violates the idealized geometry assumed in the present study.

Although snarling must occur above the twist limit, it can also occur below the twist limit: it may occur at a low twist level owing to the flexural stiffness of the filaments if the twist has not been set in any way, especially if the twisted structure is not held taut through some tensile force [93]. In practice, snarling may occur earlier due to mechanical buckling [94].

An analysis of buckling [95] shows that the values of tensile force  $F$  and torque  $M$  at which lateral buckling occurs for an assumed elastic filament of length  $l'$  and bending rigidity  $EI$  are given by the following equation:

$$\frac{M^2}{4EI} = F + \frac{\pi^2 EI}{l'^2} \quad \dots(4.23)$$

Equation (4.23) indicates that if the torque  $M$  were increased, a higher tensile force  $F$  would be required to prevent the filament from lateral buckling. In other words, for a given tensile force  $F$ , when the torque is increased to a certain level, buckling will certainly occur. Relating this to the present study, where the torque  $M$  is a

function of the helix angle  $\theta$ , and the tensile force  $F_{ZR}$  is assumed to be a constant, there should be a critical value for the cord helix angle at which buckling occurs, and this could be calculated if necessary.

When the cord twist reaches its geometrical limit, or when buckling occurs, the symmetrical geometry of the cord is destroyed. Generally, a rod free to buckle in any direction will buckle in the plane of smallest flexural rigidity [95], which indicates that in the present case, the twisted structure will tend to buckle into a helix with a maximum number of turns and minimum radius, just like the buckling of a highly twisted yarn [96]. Such buckled configuration will not untwist readily and leads to the inevitable consequence that at least one of the fibres must break ultimately due to the pin action.

#### 4.2.7 Fibre Breakage and Maximum Pin Speed

Fibre breakage normally occurs when the tension in the fibre exceeds its breaking strength. The analyses in the previous sections suggest that the development of fibre tension in the present case can be complicated by the fact that the cord helix angle  $\theta$  itself has an upper limit, and there might also be lateral buckling. However, before these events happen, fibre tension can be represented by equations (4.17) and (4.18) which show that fibre tension increases with both  $\theta$  and  $F_{ZR}$ . Suppose  $\theta=50.47^\circ$  (the twist limit predicted in Equation (4.22)), and  $\mu_k=0.3$ , then from equation (4.18),

$$\frac{F_{ZR}/2}{T} = \frac{\cos \theta}{e^{\mu_k \theta}} = \frac{\cos 50.47^\circ}{e^{0.3 \cdot 50.47 \cdot \pi / 180}} \approx 0.5 \quad \dots(4.24)$$

Table 4.1: Details of fibre and pin

Pin	Fibre			
$R_p$ (m)	$r_f$ (m)	$E_f I_f$ (N m <sup>2</sup> )	$K_f G_f$ (N m <sup>2</sup> )	$\rho$ (g/mm <sup>3</sup> )
$5 \times 10^{-4}$	$10 \times 10^{-6}$	$4.66 \times 10^{-11}$	$3.3 \times 10^{-11}$	$1.32 \times 10^{-3}$

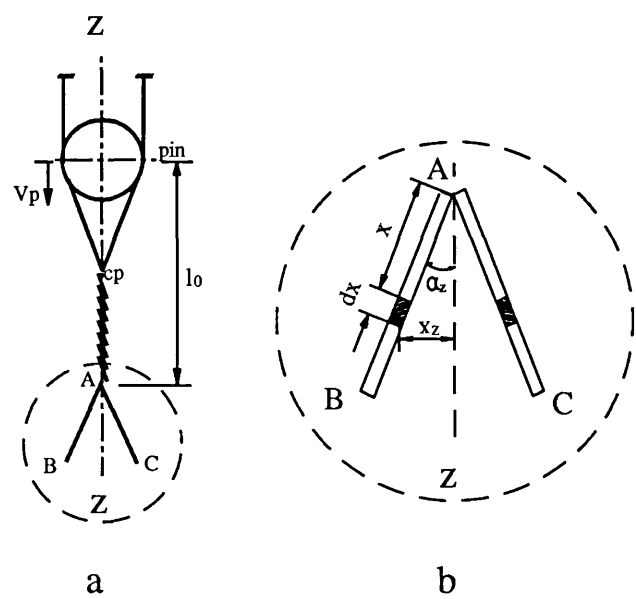


Figure 4.3: Two twisted fibres engaged by a pin  
(Typical case)

This indicates that, for the fibre tension behind the pin ( $T$ ) to exceed the fibre breaking strength before the twist limit is reached, the tensile load applied to each fibre in the cord below the convergence point ( $F_{ZR}/2$ ) has to be at least half of the fibre breaking strength. This is normally unlikely in real combing and other similar opening processes according to the information provided in chapter two and some other sources [9, 77]. It is therefore reasonable to consider that fibre breakage will only occur if snarling of the cord occurs.

The cord helix angle  $\theta$  at any particular time during the pin action is given by equation (4.13); it clearly is a function of the pin speed  $V_p$ . There should therefore be a critical pin speed at which the twisted structure will be just unable to untwist quickly enough, so that the limiting value of  $\theta$  will be reached during the passage of the pin. Below this critical pin speed, the pin should disentangle the twisted fibres without breaking them.

When snarling occurs due to either mechanical buckling or the cord helix angle exceeding its limit, the fibres can no longer separate to allow the pin to pass; therefore fibre breakage could happen in a way similar to that of a looped fibre engaged by a fast moving pin. To be able to quantitatively examine this situation, the following analysis will mainly consider the maximum cord helix angle as the criterion for fibre breakage to occur.

### 4.3 CASE ANALYSIS

Based on the foregoing analyses, a simple case as represented in Figure 4.3a, can be theoretically examined, where two twisted fibres with initial helix angle  $\theta_0$  are to be

engaged by a round combing pin at a speed of  $V_p$ . There are no other fibres attached to the end of the twisted fibres. Furthermore,  $F_{ZR}$  is very small, only due to the fibre mass, and so its contribution to the torque is negligible and can be omitted. Note however, that the consequently low value of tension in the cord would also mean that buckling of the cord could occur at lower values of  $\theta$  than the geometrical limit. The objective is to analyze how to separate these two twisted fibres without breaking them, with the criterion for fibre breakage to occur being the cord helix angle exceeding its geometrical limit ( $50.47^\circ$ ). Details of the fibres (typical for 20  $\mu\text{m}$  merino wool) and the combing pin are listed in Table 4.1. The length  $l_0$  is set at 4 cm.

To simplify the analysis, it is assumed that prior to any lateral buckling or snarling, the 'triangle' ABC can only rotate around axis z and that it maintains its shape during the pin action (although in practice point A may be expected to move down and shorten AB and AC as the pin moves down). Therefore the moment of inertia  $I_z$  of this 'triangle' about axis z can be reasonably calculated according to Figure 4.3b as follows:

$$dI_z = 2(\rho\pi r_f^2 dx)x_z^2 = 2\rho\pi r_f^2(x^2 \sin^2 \alpha_z)dx$$

$$I_z = 2(\rho\pi r_f^2 \sin^2 \alpha_z) \int_0^{\overline{AB}} x^2 dx \quad \dots(4.25)$$

If length AB = 10 mm, and BC = 5 mm so that  $\sin \alpha_z = 0.25$ , then

$$I_z = \frac{1}{8}(\rho\pi r_f^2) \int_0^{10} x^2 dx = 1.728 \times 10^{-5} (gmm^2) \quad \dots(4.26)$$

This value, together with  $l_0$  and those given in Table 4.1, are then used in equation (4.13).



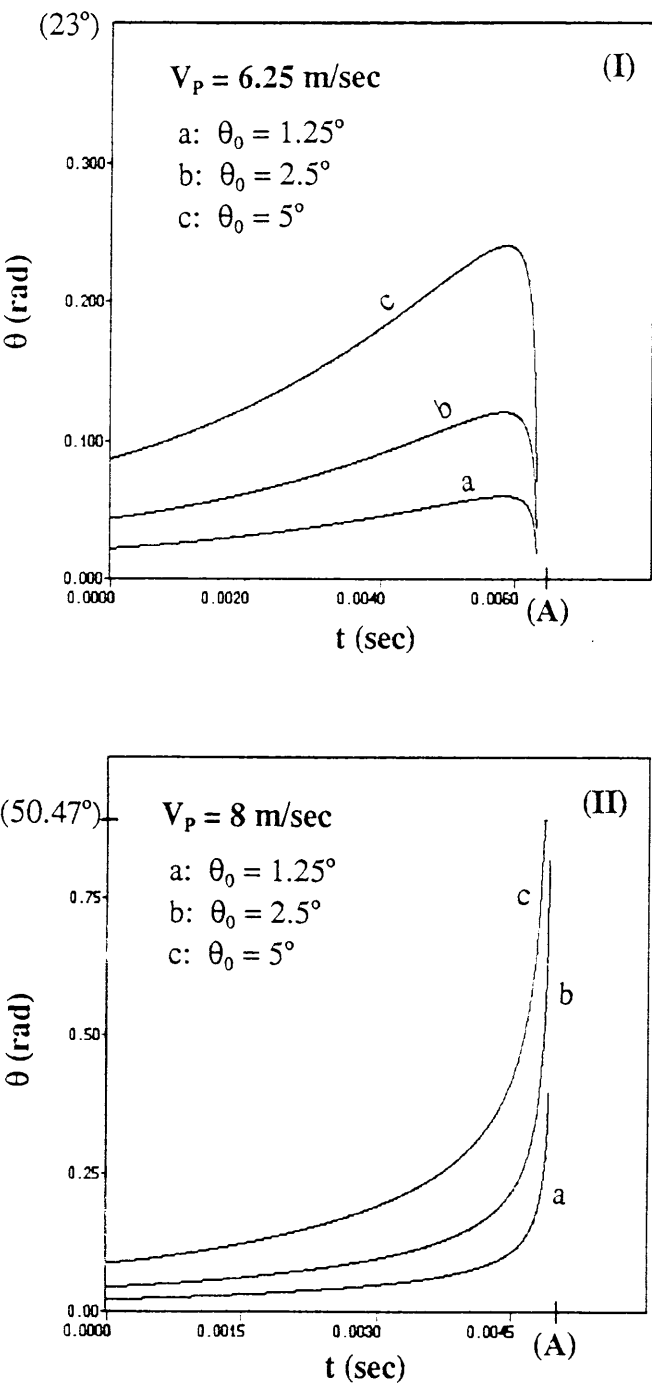


Figure 4.4: Helix angle changes over time for two pin speeds at different initial twist levels

(A is time at which pin reaches point A in Figure 4.3)

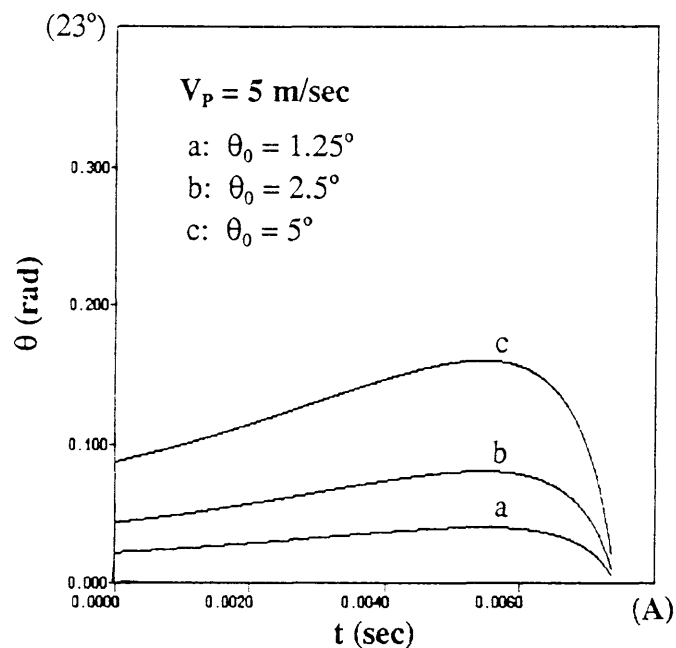


Figure 4.5: Helix angle changes over time at different initial twist levels

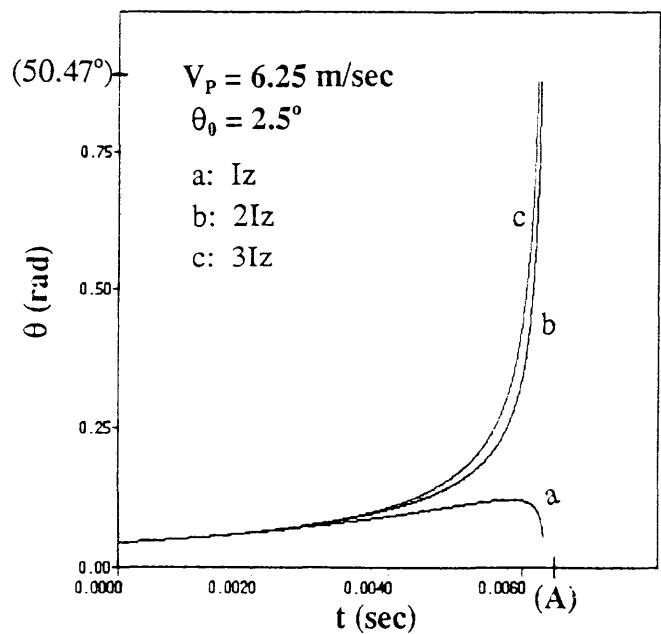


Figure 4.6: Effect of moment of inertia on helix angle changes

(A is time at which pin reaches point A in Figure 4.3)

A computer program has been developed to find a numerical solution to equation (4.13), so that a set of graphs representing the change in helix angle with time during the pin action can be obtained at various pin speed levels. From these graphs, the threshold pin speed value can be predicted.

Figure 4.4 shows how the helix angle changes over time for different pin speeds and initial twist levels<sup>1</sup>. At the pin speed of 6.25 m/sec (Figure 4.4(I)), the helix angles at each initial twist level first increase gradually during the pin engagement (Figure 4.4(I)), then they begin to drop before the pin reaches point A in Figure 4.3a and before they reach the limit value of  $50.47^\circ$ , indicating the pin has been able to untwist the two twisted fibres without breaking them. However, at a higher pin speed of 8 m/sec (Figure 4.4(II)), the twisted section is unable to untwist quickly enough and the helix angles eventually reach the limit, especially at higher initial twist level; in such case, fibre breakage is inevitable. Also from these graphs, a threshold pin speed value between 6.25 and 8 m/sec can be estimated, below which the combing pin could have disentangled the twisted fibres without breaking them, which also agrees with the qualitative description. More accurate estimation of the critical pin speed could be achieved by plotting more graphs at finer steps in speed levels between 6.25 and 8 m/sec. Figure 4.5 shows the change in helix angle at a pin speed of 5 m/sec; it is very obvious that no fibre breakage would have occurred at this pin speed which is much lower than its critical value.

The effect of the moment of inertia about axis z in Figure 4.3 of the 'triangle' ABC is also very interesting, as shown in Figure 4.6. It reflects the effect on helix angle changes of the length of the untwisted fibre end and its configuration and shows that

---

<sup>1</sup> For the dimensions used in this case, the values of  $1.25^\circ$ ,  $2.5^\circ$  &  $5^\circ$  for  $\theta_0$  correspond to about 6, 20 & 47 turns in the twisted section.

the moment of inertia is also a critical parameter. There is a critical inertia value above which the twisted fibres might not be separated without breakage. Figure 4.6 also indicates that, above the critical inertia value, further increase in the inertia value, such as from  $2I_z$  to  $3I_z$ , has little effect on the helix angle changes, because the inertia value of  $2I_z$  in the present case is already too high.

## 4.4 EXPERIMENTAL VERIFICATION OF THE THEORY

Since empirical evaluation of the effect of pin movement on helix angle changes (equation (4.13)) and fibre tension variations (equation (4.19)) is extremely difficult using the wool fibres modelled in the case analysis, a coarse monofilament and a relatively large pin have been used to verify the model.

### 4.4.1 Material

Nylon 6 filaments were used to simulate the fibres. The filaments have the following relevant physical properties:

- (1) Diameter:  $2r_f = 0.25 \text{ mm}$
- (2) Bending rigidity:  $E_f I_f = 1.3 \times 10^{-8} \text{ Nm}^2$  (measured on KES-FB2 pure bending tester [97])
- (3) Torsional rigidity (previously determined [98]):  $K_f G_f = 1.42 \times 10^{-7} \text{ Nm}^2$
- (4) Frictional coefficients (filament vs pin, measured using the capstan principle on an Instron extensometer)
  - Static:  $\mu_s = 0.4$  (average value)
  - Kinetic:  $\mu_k = 0.35$  (average value)

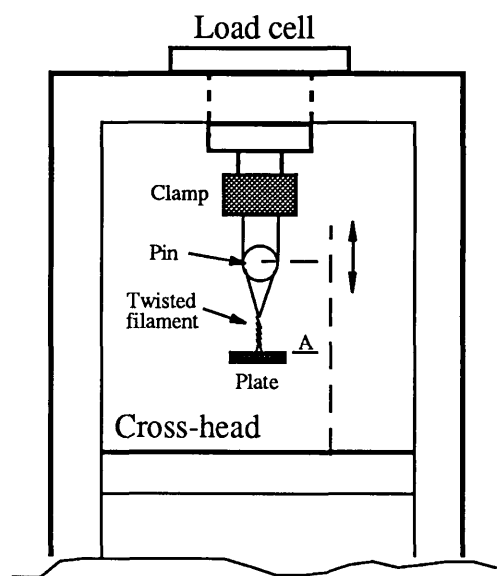


Figure 4.7: Diagram of the experimental set-up on Instron Tensile Tester

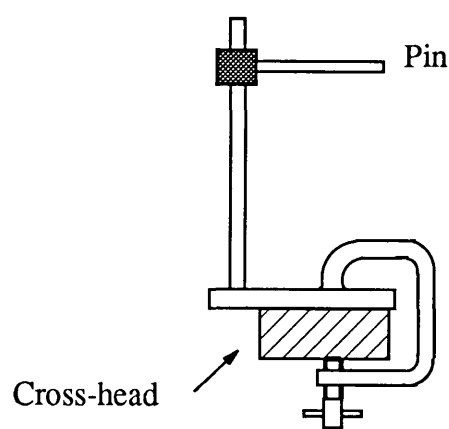


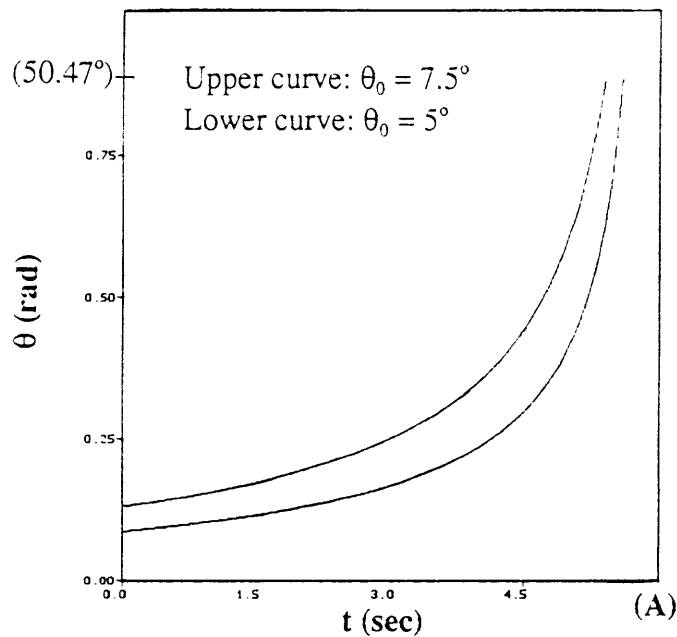
Figure 4.8: Connection between the pin and cross-head

### 4.4.2 Apparatus

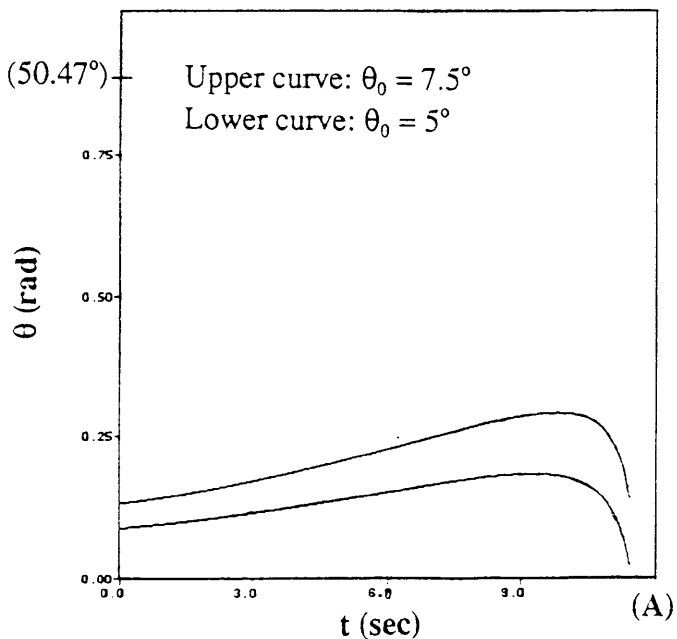
Two of the nylon filaments, each about 20 cm long, were prepared as follows. A steel plate with known weight and dimension was attached near its centre of mass to one end of each filament. A certain amount of initial twist was then 'cabled' into the two filaments by hand, so that no torsion was created in the individual filaments; the other ends of the filaments were firmly gripped and connected to a load cell on top of an Instron extensometer 1122 (Figure 4.7); a round steel pin with a diameter of 8 mm was mounted on a frame, which was fixed on the cross-head of the Instron (Figure 4.8). Before testing, the pin was positioned between the filaments above their convergence point, and the initial distance between the pin centre and the steel plate was set at 10 cm. Initially, there was a slight untwisting of the cord and rotation of the plate due to the torque generated by the weight of the plate; tests were carried out after the plate became stable. During each test, the pin moved downwards at a constant speed with the Instron cross-head, simulating a pin combing through two twisted fibres.

### 4.4.3 Parameters Examined

With this experimental set-up, many of the parameters in equations (4.13) and (4.19) could be examined, to confirm their effects on fibre tension and the likelihood of fibre breakage. For the purpose of this verification however, only the parameter of most concern, viz. the pin speed, is examined in detail.

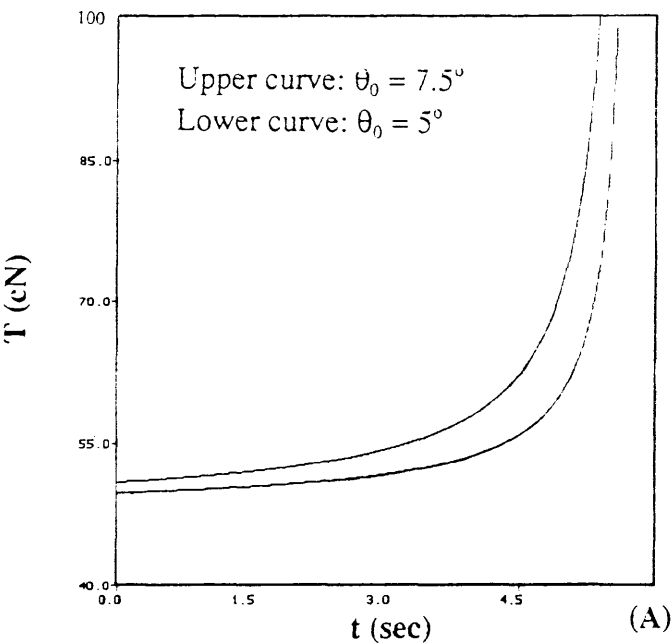


(a) Pin speed: 1000 mm/min

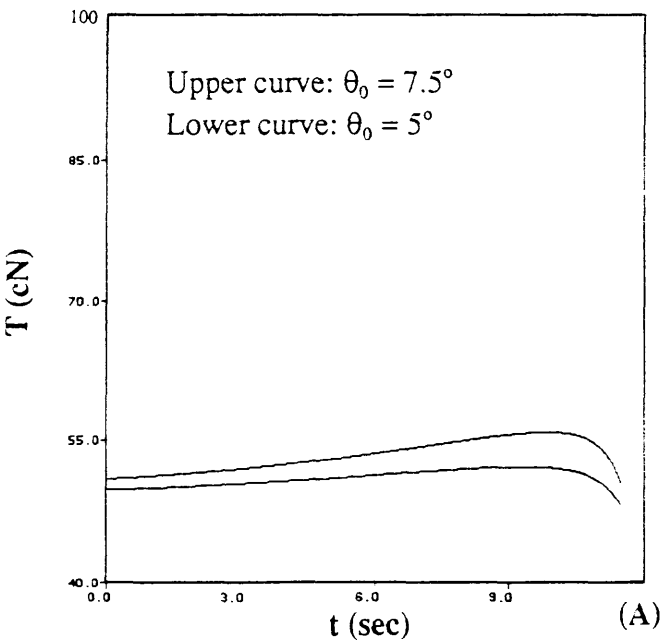


(b) Pin speed: 500 mm/min

Figure 4.9: Helix angle changes over time for two pin speeds at different initial twist levels



(a) Pin speed: 1000 mm/min



(b) Pin speed: 500 mm/min

Figure 4.10: Tension changes over time for two pin speeds at different initial twist levels



#### 4.4.4 Theoretical Predictions

Theoretical predictions of the behaviour of this experimental arrangement were made in the form of various graphs of helix angle  $\theta$  or tension  $T$  versus time, obtained numerically according to equations (4.13) and (4.19). The initial parameters<sup>2</sup> used for the numerical solution were those regarding the physical properties of the nylon filament, as listed in section 4.4.1, and the weight ( $F_{ZR} = 48 \text{ cN}$ ) and moment of inertia about axis  $z$  ( $I_z = 8 \times 10^{-5} \text{ kgm}^2$ ) of the steel plate that was attached to the end of the filaments. The 'restraint torque' in Equation (4.13),  $M_{ZR}$ , was reasonably assumed to be negligible and was not considered in obtaining these theoretical graphs. Figure 4.9 shows the predicted changes in helix angle with time at two different pin speeds, 500 mm/min and 1000 mm/min. It can be noted from Figure 4.9a that at the pin speed of 1000 mm/min, the two filaments cannot untwist rapidly enough, so that the cord helix angle eventually increases quite sharply; it exceeds its geometrical limit before the pin reaches the steel plate (denoted by point A), indicating that snarling and eventually 'breakage' of the filament are inevitable during the pin engagement. However, at the slower pin speed of 500 mm/min, the cord helix angle drops as the pin approaches the steel plate (Figure 4.9b), implying that the filaments are able to untwist and that no snarling or breakage is expected in this case. The corresponding predictions of tension variations in the filaments above the pin during the pin action, which will be used to compare with tension values obtained empirically, are given in Figure 4.10.

---

<sup>2</sup> For the dimensions used in this case, the values of  $5^\circ$  &  $7.5^\circ$  for  $\theta_0$  correspond to about 5 & 11 turns in the twisted section.

---

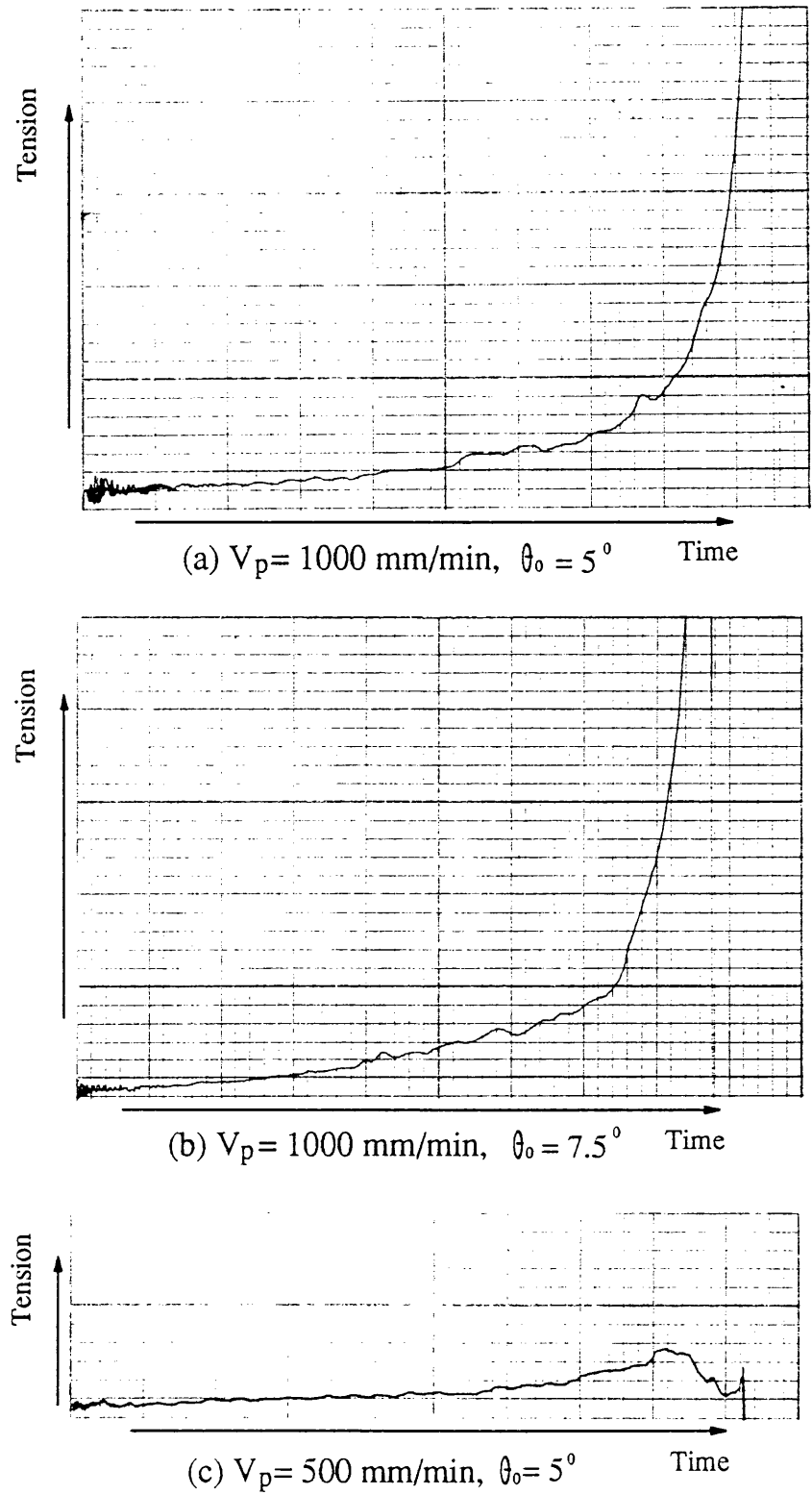


Figure 4.11: Typical tension curves

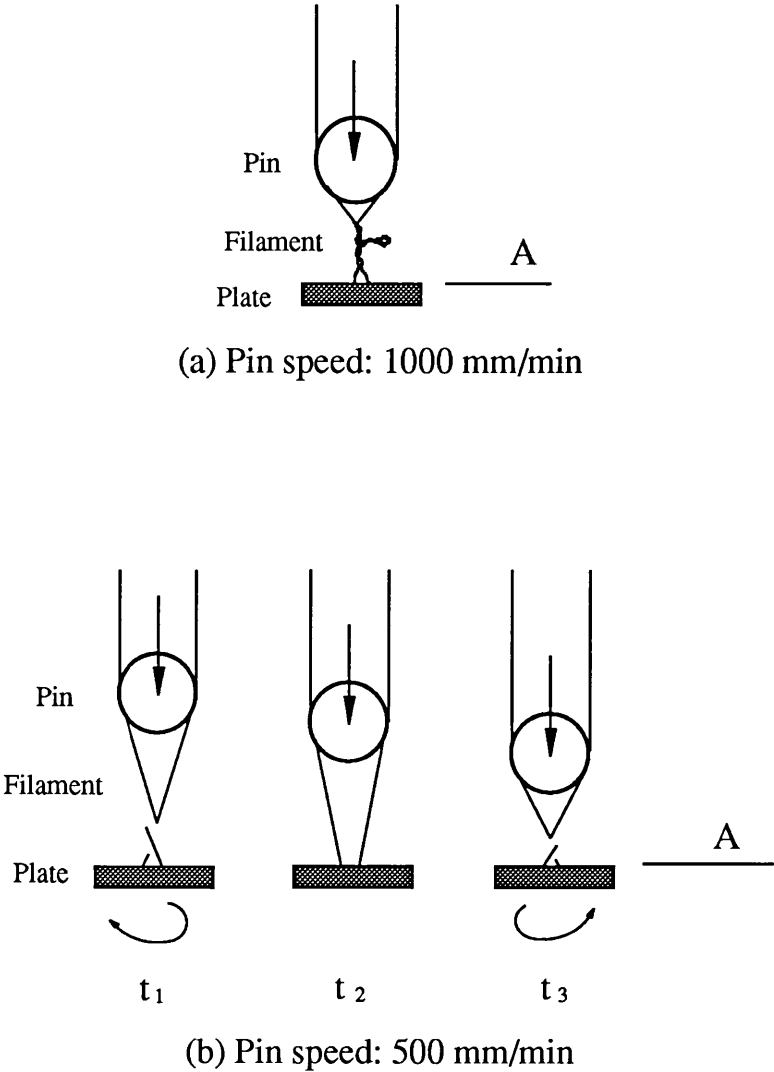


Figure 4.12: Snarling and untwisting observed in experiments

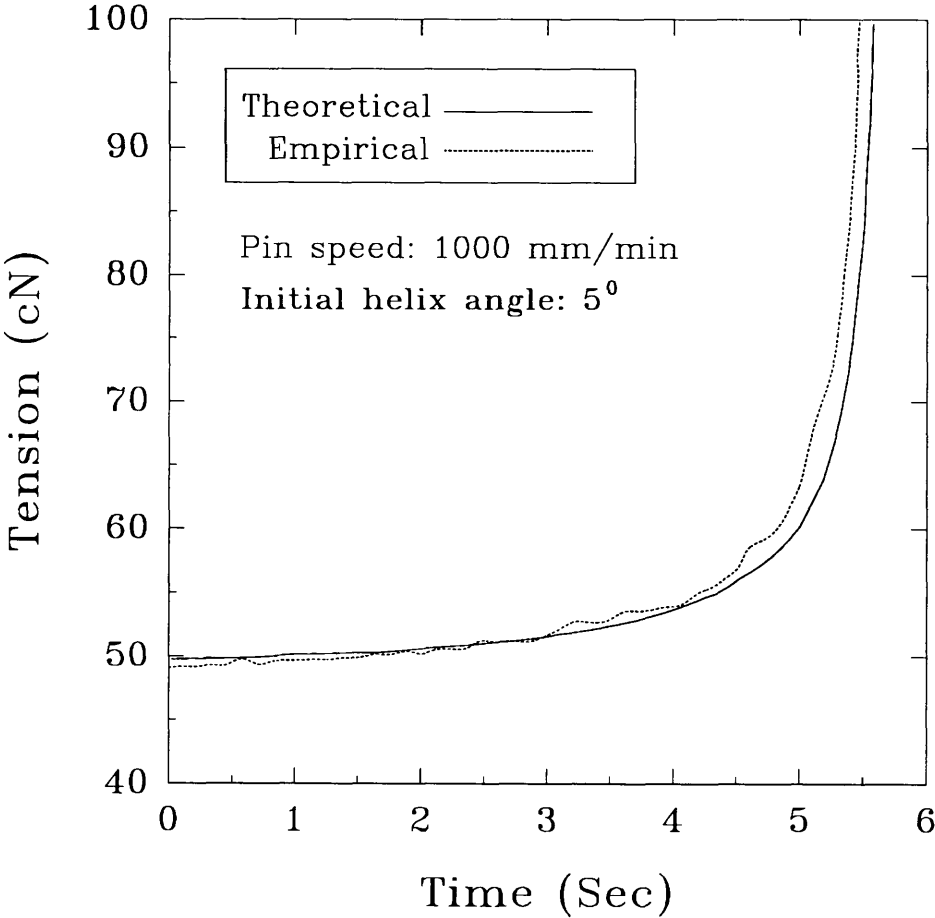


Figure 4.13: Comparison between theoretical and empirical curves (Fast speed)

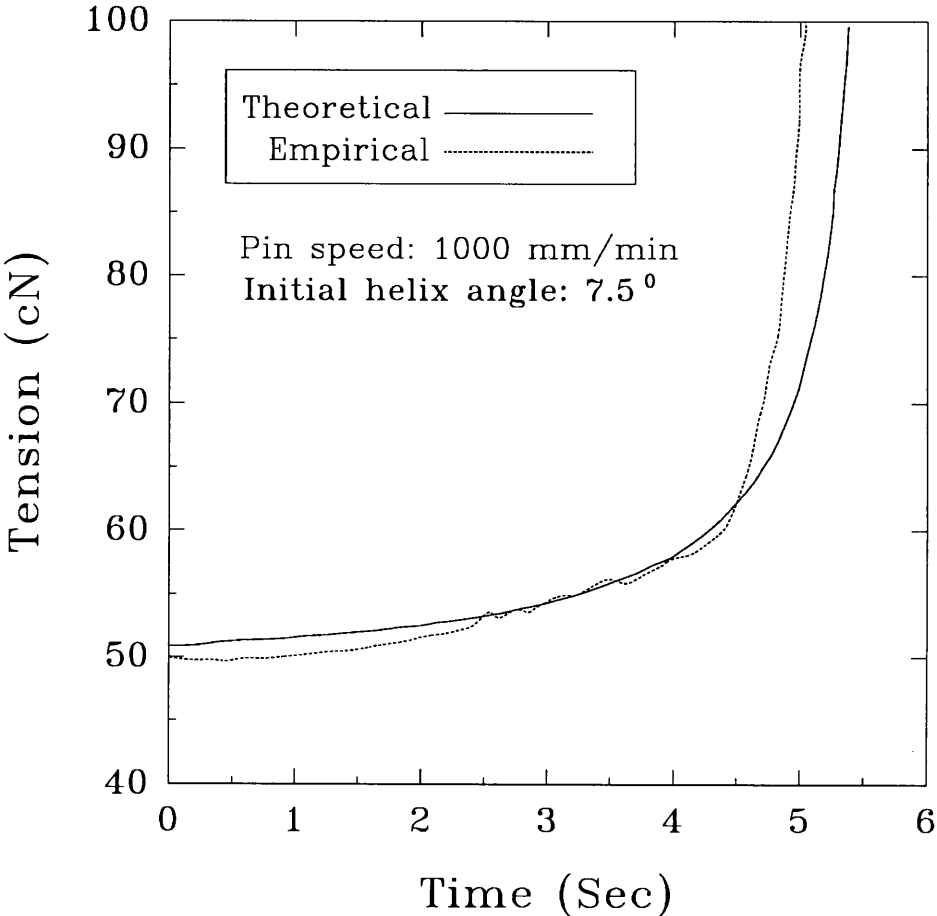


Figure 4.14: Comparison between theoretical and empirical curves (Fast speed)

## 4.4.5 Empirical Results and Discussion

### 4.4.5.1 Fast speed

Typical recorded tension signals for two different initial helix angles ( $\theta_0$ ) are shown in Figures 4.11a & 4.11b, for a pin speed corresponding to the maximum cross-head speed on the extensometer of 1000 mm/min. A digitiser has been used to combine these empirical curves with the theoretical curves of Figure 4.10a in Figures 4.13 & 4.14 (Note that the digitising has smoothed the empirical curves). There is very good general agreement between theory and experiment, with a sharp increase in the tensions before the pin reached the steel plate (at 6 sec.), indicating the helix angle must have increased dramatically, leading to the onset of snarling. This snarling of the nylon filaments was clearly observed during the experiment, as the pin approached the steel plate attached to the filaments (Figure 4.12a). However, both of the empirical curves show the tension increasing earlier than theoretically predicted. This discrepancy is discussed later.

### 4.4.5.2 Slow speed

A typical tension curve obtained at the slower pin speed of 500 mm/min is shown in Figure 4.11c. No filament snarling was observed in this case. The tension slowly increased at the beginning, then it started to drop.

There are two reasons for the sharp tension increase near the very end of the tension curve in Figure 4.11c. Firstly, after the twist has been fully removed through rotation of the steel plate, the pin still has to force the filaments apart because their spacing

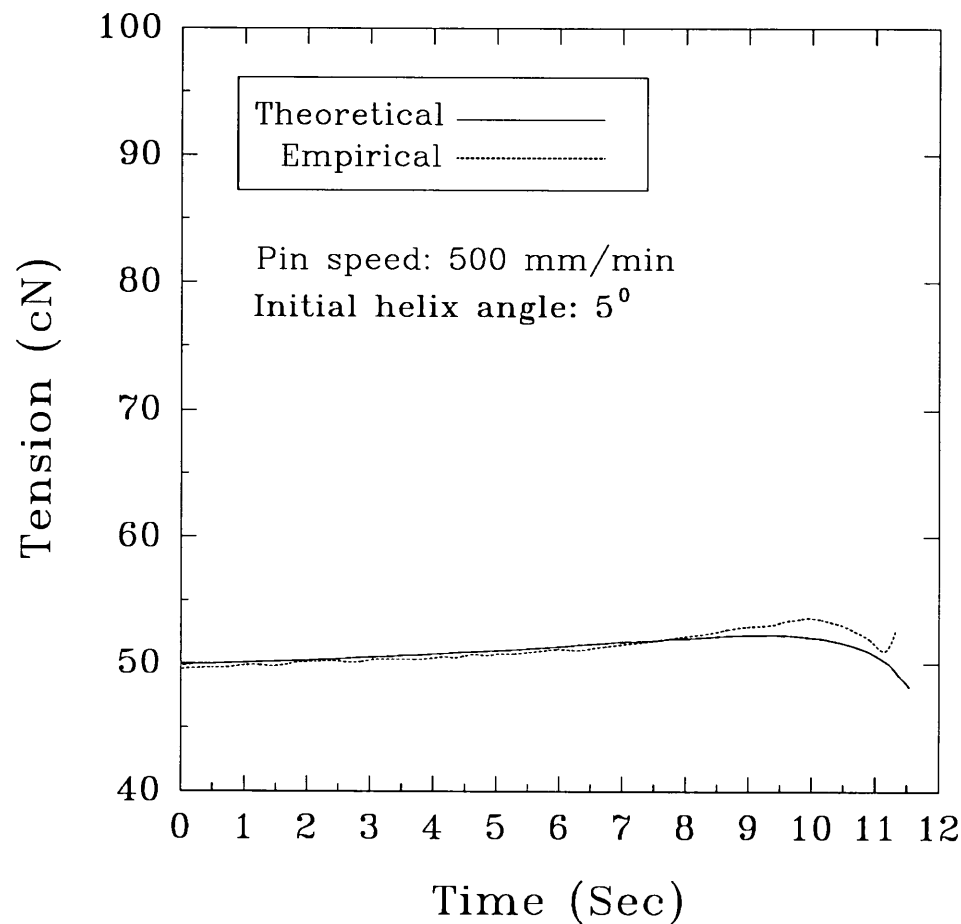


Figure 4.15: Comparison between theoretical and empirical curves (Slow speed)

on the plate is narrower than the pin diameter, as is shown at  $t_2$  in Figure 4.12b; and secondly, the plate continues to rotate after the twist has been removed, due to its angular momentum, thereby twisting the filaments in the opposite direction (Figure 4.12b).

Comparison of this empirical curve with one of the theoretical curves in Figure 4.10b is given in Figure 4.15. Consideration of why the experimental curve reaches a higher tension before decaying is given below.

#### 4.4.5.3 Discrepancies

In both cases of fast and slow pin speeds, the experimental values of tension eventually drift higher than the predicted values, the difference being more noticeable at a higher initial helix angle. Furthermore, there are fluctuations in the experimental curves which are not reproduced by the theory. These discrepancies suggest that the actual case departs from some of the assumptions of the theoretical model.

The departure arises mainly because, as the helix angle of the twisted structure increases, the angle between the axis of the twisted structure and each filament above the convergence point becomes greater than the helix angle, especially as the helix angle approaches its geometrical limit. This difference stems from the fact that transmission of the torque generated by the pin movement is affected by the viscoelastic losses and frictional resistance of the filaments; moreover, the higher the twist level in the twisted structure, the greater these effects would be. Thus, for a certain helix angle during the pin engagement, a higher angle of wrap between the



filament and pin occurs, leading to a higher measured tension. The fact that the difference between empirical tension and its predicted value is more noticeable at a higher initial helix angle (Figure 4.14) is also consistent with this explanation.

Some other factors, such as the filaments being not perfectly elastic and possible small deviations from the assumed ideal helical geometry during the pin movement, etc., may also contribute to these discrepancies.

The viscoelastic losses and small deviations from the assumed ideal helical geometry might be responsible for the fluctuations in the experimental curves as well.

## 4.5 CONCLUSION

A theoretical model of disentangling two twisted fibres by a combing pin has been presented in this chapter. The postulated model represents the first attempt at theoretically investigating the critical pin speed in combing, below which breakage of twisted fibres could be avoided.

In this model, it has been elucidated that the pin engagement increases the twist level and develops torque in the twisted structure in a way similar to the torque generation in the twisting of textile yarns and cords. The torque thus developed could untwist the fibres without breaking them if the untwisted fibre ends are not subjected to much restraint and have a relatively small moment of inertia about the axis of the twisted structure, and if the pin speed is not very high. Otherwise, the helix angle of the twisted structure increases very sharply towards its geometrical limit, leading to the

inevitable consequences of fibre breakage because of buckling or snarling of the twisted structure. Such breakage is then analogous to that of a looped fibre engaged by a combing pin.

The various mathematical formulae derived from this model can be used to predict the threshold pin speed value below which fibre breakage could be avoided, which was the main objective of this study. They could also be used to examine the effects on fibre breakage of different parameters such as initial twist level, fibre length, fibre physical properties, etc. The effects of other processing variables, such as fringe density, pin geometry and friction, etc., could also be inferred from this model.

Although the theoretical model requires several assumptions about the geometry of the twisted fibres, the various empirical curves obtained in the experimental evaluation of this model, using nylon 6 filament to simulate the twisted fibres, have shown general agreement with those predicted by the postulated model.

The simple case analysis presented in this chapter is a typical application of the mathematical modelling. The threshold pin speed value between 6.25 and 8 m/sec under the particular circumstances is also quite informative, corresponding to a comb cylinder speed between about 800 rpm to 1000 rpm for a typical rectilinear comb (about 4 to 5 times current comb speeds). Of course, twisted fibres in a real pre-combed sliver are unlikely to be perfectly twisted as assumed in the model, and would probably not untwist as readily, thus lowering the critical pin speed.

## **Chapter 4                      The Behaviour of a Pin Disentangling Two Twisted Fibres**

---

Since the twisted fibre form of entanglement exists not only in fringes subjected to combing, but also in fibre assemblies subjected to other opening actions such as carding and sliver opening for open-end spinning, the findings of this chapter should help explain the fibre disentangling behaviour in those opening processes as well.

## CHAPTER 5

# CONCLUSION

---

### 5.1 SUMMARY

The work reported in this thesis is concerned with the incidence and mechanisms of fibre breakage in woolcombing, and how to eliminate fibre breakages without jeopardizing the combing production rate. It can be summarized in two major areas: 1) investigation of various combing forces; and 2) mathematical modelling of the disentangling of two twisted fibres.

Two sets of apparatus have been developed, using real time data acquisition and strain gauge techniques, to investigate different forces involved in the rectilinear combing process. Direct force measurements were made of individual wool fibres lying in a fringe during the combing action of a comb cylinder, and also of a single pin on a comb cylinder as it combed through different fibre fringes. Early attempts in combing force investigation were confined to the study and measurement of withdrawal forces only through the top comb and feed gill; moreover, only average force levels were obtained in such measurements.

In the fibre tension investigation reported in chapter two, both the average and the peak fibre tension values were obtained. The development of tension peaks in fibres and the difference in behaviour between fibres which do, or do not, protrude beyond the fibre fringe were studied. It was found that the average tension (in test fibres) generally increased with fringe length, fringe density, and test fibre length. This was

predicted by the postulated simple hypothesis, based on earlier quantitative analyses of fibre-fibre, and fibre-pin contacts. The effect of combing speed (within the examined speed range) on test fibre tension, was not found to be very significant, which agrees with previous works in other similar areas.

One important point arising from the fibre tension investigation is the incidence of fibre breakage during combing. Although in this investigation, parallel fibre fringes free of short fibre and fibre entanglements were used, and in most cases the test fibres were initially laid straight in those fringes, the test fibres could still be broken. The measured average fibre tension values were simply too small, compared with fibre breaking strength, to account for the breakage. Instead, tension peaks appear to provide the explanation, because those tension peaks did coincide with the occurrence of most forms of test fibre breakage.

Positions of fibre breakage were identified mainly in two places, behind the combing zone and near the end of the combing zone. Fibre breakages behind the combing zone were always associated with tension peaks. These were sometimes induced by a fibre hook, or perhaps by fibre entanglements; the relatively higher accumulated tensile stress in that region (the tension built up from all contacts in the combing zone) could also contribute to the forces causing this breakage. Fibres extending beyond the fringe usually broke near the end of the fringe, but there was not always a high tension peak to account for the breakage; breakage here was probably due to either a cutting of the protruding free fibre end by the saw-teeth, or a defect in the fibre, or repeated wrapping of the protruding free end around the saw-teeth.

The significant implication of this fibre tension investigation is that, in terms of determining the extent of fibre breakage, conclusions drawn from average fibre

tension only may be misleading; detailed analysis of fibre breakages requires knowledge of the tension peaks experienced by individual fibres lying in a fringe in different combing processes. This argument may also apply to the withdrawal process through top comb and feed gill; re-evaluation of the forces involved in this process is necessary.

It is difficult to measure the tension experienced by individual fibres involved in different fibre entanglements during combing. In order to assess the forces and fibre breakages associated with combing entangled fibre fringes, forces acting on a single pin were measured as it combed through carded, 1st gilled, and 3rd gilled fringes, using the constructed simulating device described in chapter three.

The average peak values of the "pin force" recorded by this device increased with increase in fringe density, increase in fringe length, and decrease in number of gillings. These results are in general agreement with the related findings of other workers.

However, the individual pin force profiles obtained in this investigation can indicate how the forces build up as the pin penetrates the fringe, dislodges entanglements, breaks fibres and separates the fringe. These individual pin forces can also indicate the degree of fibre entanglement, ease of disentangling, and level of fibre breakage in a fringe.

It should be noted that in the pin force investigation, only fringes of constant linear density (or ideal 'rectangular' fringes) were used, which had the advantages of making fringes of different length and density more definable, and their effects on pin forces more comparable. The results and predictions thus obtained, on the effect

on pin forces of individual parameters defining an ideal fringe, can also be utilised to interpret and predict the effect on pin forces of other non-ideal fringes, such as a normal 'tapered fringe', which usually would require more parameters to define than that required by an ideal 'rectangular' fringe. The measurement technique used in this investigation could also be used to evaluate other factors, such as fibre type, pin geometry, and fibre lubricants.

The mathematical model of the disentangling of two twisted fibres, which was presented in chapter four, represents the theoretical attempt at investigating the critical pin speed in combing, below which fibre breakage could be avoided. This model is also an extension of the above-mentioned investigation of combing forces and related fibre breakage. It elaborates the point that the fibres themselves, rather than the mechanism, should provide the factor limiting the ultimate combing speed, and examines in detail the effect on fibre breakage of combing speed, mechanical properties of the fibres, etc., while previous theories on combing have mainly considered the machine settings and fibre length. The twisted fibre form of entanglement has been selected for detailed study because, although it is one of the major entanglement forms that can be found in a fibre assembly, very little theoretical analysis has ever been carried out to unravel the behaviour of twisted fibres in combing and other similar opening actions.

In the mathematical modelling, idealized twist geometry has been assumed for the twisted section of the two fibres. It has been elucidated that the pin engagement increases the twist level and develops torque in the twisted structure in a way similar to the torque generation in the twisting of textile cords. If the pin speed is not too high, the torque thus developed is able to untwist the fibres without breaking them, provided the twisted section is relatively free to rotate. Otherwise, the helix angle

of the twisted structure increases very sharply towards its geometrical limit, leading to the inevitable consequences of fibre breakage because of the lateral buckling or snarling of the twisted structure. Such breakage is then analogous to that of a looped fibre engaged by a combing pin.

The model further demonstrates that the pin speed is one of the critical parameters in determining whether the two fibres would be able to untwist quickly enough to allow the pin to pass through without breaking them. It also suggests that the major mode of fibre breakage in this case is due to the helix angle of the twisted structure exceeding its geometrical limit.

The various mathematical formulae derived from this model can be used to predict the critical pin speed value, below which fibre breakage could be avoided. They could also be used to examine the effects on fibre breakage of different parameters such as initial twist level, fibre length, fibre physical properties, etc. In the typical case analyzed in chapter four, where two identical fibres with some initial twist 'cabled' in them were engaged by a round pin, a critical pin speed equivalent to about 4 to 5 times the present maximum combing speed on existing combs was predicted by the model. This obviously would have practical implication to the increase in combing production rates.

Predictions from this model have been confirmed by experiments, using nylon filament to simulate the fibres. The effects of other processing variables, such as fringe density, pin geometry and friction, etc., could also be inferred from this model.



## **5.2 FURTHER WORK**

Relevant further work is suggested in the following areas:

### **(1) Measurement of Withdrawal Forces**

Previous works on withdrawal force measurement during drawing-off through top comb and feed gill only provided the average fibre tension values. These average tension values are not sufficient to justify the extent of fibre breakage known to occur during the drawing-off process in combing. Therefore, it would be useful to know the magnitude of peak tensions experienced by individual fibres in a fringe, in order to re-evaluate the contribution of the drawing-off process to the total fibre breakage in combing. Attempts to reduce fibre breakage could then sensibly concentrate on reducing these peaks.

### **(2) Investigation of the Sources of Fibre Tension Peaks**

In the fibre tension study in chapter two, infrequently-occurring tension peaks were found in a fibre being combed, and it has been proposed that these tension peaks might be caused by a wrapping action of the fibre around the tooth. While the mechanism of a fibre wrapping around a pin at very high pin speed can be successfully explained by Yan and Johnson's theory with the assumption of the fibre being perfectly flexible [78], the postulated wrapping phenomenon at the rather low speed in combing is certainly something different, especially when the fibre stiffness is taken into consideration. Similar tension peaks were also observed in single,

tensioned fibres by Young and Johnson [83]. The specific sources of these tension peaks should be found in the hope of reducing fibre breakage in combing and other fibre separation processes.

### **(3) Disentangling of Neps and Related Fibre Breakage**

There are about five major fibre entanglement types that can be found in a fibre assembly, i.e. parallel fibres, hooked fibres, looped fibres, twisted fibres, and neps. Among them, the first four entanglement types have so far been analyzed mathematically. The last and probably the most important one, fibre neps, has not yet been investigated theoretically. It would be desirable in future study to examine theoretically how, and to what extent, fibre neps cause fibre breakage in combing and other similar opening processes.

After such individual analysis of all these major fibre entanglement types, certain parameters involved in different stages of various opening processes, such as the combing (opening) speed, can be more rationally maximized, based on the percentage level of different types of entanglement in a fibre assembly at different processing stages, and the theoretically predicted critical values for those parameters.

### **(4) Fundamental Studies of Fibre Damage Caused by Saw-teeth**

Many theoretical works on the interaction between wool fibres and clothing elements in various opening processes have considered either round pins or saw-teeth with a rounded front face. These works include the recent study by Yan and Johnson [78] on a fast moving pin striking a single fibre, the present study reported in chapter four

on a round pin disentangling twisted fibres, and the work reported by Siersch [77] about a decade ago on saw-teeth related opening forces. Empirical works on saw-tooth related fibre breakage carried out by Wood et al [68] and Xu and Zhou [74] at slow speed, and by Yan [75] at fast speed indicated that the mean breaking load for a saw-tooth to break a fibre was significantly lower than that for a round pin, and fibre breakages occurred mainly at the teeth. In the fibre tension investigation reported in chapter two, it was also found that the tension peak experienced by an individual fibre, which coincided with its breakage, was lower than the average fibre breaking strength. The bending stress concept employed by Xu and Zhou [74] is quite helpful in understanding these phenomena, but more fundamental work on contacts between a fibre and a saw-tooth (especially its sharp edges), such as analysis of Herzian stresses and their relation to different morphologies of fibre damage, is necessary; the effect of tooth shape could also be incorporated in these analyses.

APPENDIX I

**PIN ARM DESIGN**

---

**(a) Introduction**

Chapter three described a device for measuring forces acting on a single pin as it combs through different fibre fringes. A key component of that device is the pin arm, which supports the combing pin, as well as the strain gauges used to detect any pin force variations. Designing the pin arm involved choosing the right material for it and determining its dimensional values. Normally, three criteria should be considered regarding its performance:

- 1). high sensitivity,
- 2). good stability,
- 3). fast dynamic response.

Generally, the pin arm should have large deformation within its elastic limit when acted upon by a given pin force, so that even small pin force variations can be detected, i.e. the pin arm should be highly sensitive. For good stability, the maximum working stress of the pin arm should be below its elastic limit. The fast dynamic response of the pin arm requires that its natural frequency should be as high as possible, in other words, the pin arm should be highly rigid. These three requirements for the pin arm sometimes conflict each other; for example, a highly rigid pin arm can satisfy its requirement for a fast dynamic response, but not necessarily for a high sensitivity; similarly, a highly sensitive pin arm has a large deformation under a given force, but this could jeopardize its stability. Therefore, the design of the pin arm is actually a

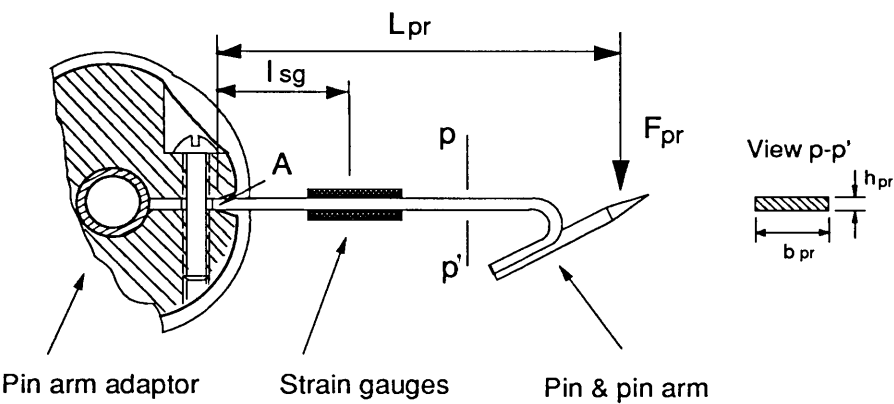


Figure A1.1: Diagram of the pin arm assembly

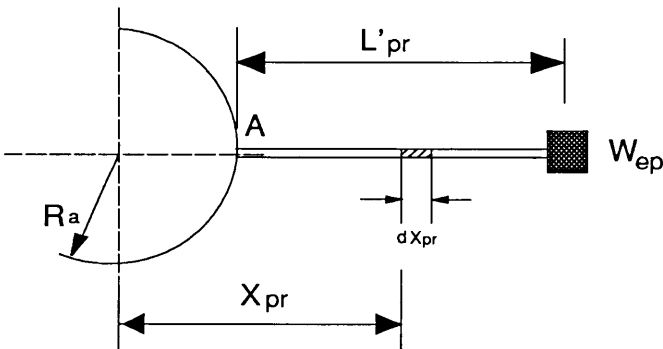


Figure A1.2: Simplified diagram of the pin arm assembly

process of trial and error, with the purpose of achieving a reasonable compromise between different requirements. Furthermore, considerations should also be given to the availability of the various types of material, and the feasibility of processing the material in the available workshops.

### **(b) Material Used for the Pin Arm**

A widely used stainless steel was selected as the material for the pin arm. It has the following relevant physical properties:

Modulus of elasticity in tension,  $E_{pr} = 19000 \text{ kg/mm}^2$ ,

Density,  $\rho_{pr} = 8060 \text{ kg/m}^3$ ,

Maximum elastic stress,  $\sigma_{prm} = 165 \text{ N/mm}^2$ .

### **(c) Maximum Pin Force, $F_{pr}$**

In a real combing process, the maximum pin force may be realized when the pin causes excessive fibre breakage while making its way through heavily entangled fibres. In the present design calculations, a maximum pin force value of 150 cN was chosen, which represents possible breakage of about 10 to 15 fibres simultaneously during the pin action.

### **(d) Pin Arm Stability**

For the pin arm to be stable, its maximum working stress should be lower than its maximum elastic stress. Figure AI.1 is a diagram of the pin arm assembly. According

to classical mechanics of material, the tensile stress due to force  $F_{pr}$  at the point A is the largest, and it is given by the following formula:

$$\sigma_{AF_{pr}} = \frac{6F_{pr}L_{pr}}{b_{pr}h_{pr}^2} \quad \dots(AI.1)$$

To conform with the dimensions of the beater, length  $L_{pr}$  is set to be 23.5 mm. Since  $F_{pr} = 150$  cN, the unknown variables now are  $b_{pr}$  and  $h_{pr}$ . Practically, the width of the pin arm should be as large as possible, otherwise, mounting the strain gauges on it would be quite difficult. However, a large pin arm width would reduce the sensitivity of the pin arm. By choosing  $b_{pr} = 4$  mm first, and giving a preliminary value for  $h_{pr}$  of 0.65 mm, the tensile stress at point A then is:

$$\sigma_{AF_{pr}} = \frac{6F_{pr}L_{pr}}{b_{pr}h_{pr}^2} = \frac{6 \times 1.5 \times 23.5}{4 \times 0.65^2} \approx 125 \text{ N/mm}^2$$

which is less than the maximum elastic stress of 165 N/mm<sup>2</sup>. The corresponding tensile strain at point A is:

$$\epsilon_{AF_{pr}} = \frac{\sigma_{AF_{pr}}}{E_{pr}} \approx \frac{125}{190000} \approx 0.066\%$$

Note that additional tensile stress and strain could also arise from the centrifugal force on the pin arm if the beater rotated at very high speeds. This centrifugal force might have some effect not only on the maximum tensile stress at point A, but also on the elongation of the strain gauge grid attached to the pin arm, which in turn could affect the real pin force values detected by the strain gauges. To examine this effect, a simplified representation of Figure AI.1 is shown in Figure AI.2; the equivalent

weight ( $W_{ep}$ ) of the pin plus the part of the pin arm holding it is about 0.2 grams. Suppose the beater rotates at an angular velocity of  $\omega_b$ , the centrifugal force caused by  $W_{ep}$  is:

$$F_{C_{W_{ep}}} \approx W_{ep} \omega_b^2 (L'_{pr} + R_a) \quad \dots (AI.2)$$

where  $R_a$  is the radius of the pin arm adaptor.

To calculate the centrifugal force due to the pin arm, take an infinitesimal length  $dX_{pr}$  of the pin arm (Figure AI.2); it has a small mass of  $b_{pr}h_{pr}\rho_{pr}dX_{pr}$ , and the centrifugal force can be calculated as:

$$F_{C_{pr}} = \int_{R_a}^{L'_{pr} + R_a} (b_{pr}h_{pr}\rho_{pr}dX_{pr})\omega_b^2 X_{pr} = (b_{pr}h_{pr}\rho_{pr}\omega_b^2) \int_{R_a}^{L'_{pr} + R_a} X_{pr}dX_{pr} \quad \dots (AI.3)$$

The stress at point A due to the total centrifugal forces would then be:

$$\sigma_{AC} = \frac{(F_{C_{W_{ep}}} + F_{C_{pr}})}{b_{pr}h_{pr}} \quad \dots (AI.4)$$

The dimensions of the beater and the combing pin to be used determine the values of  $L'$  and  $R_a$  to be  $L'_{pr} = 18.2$  mm, and  $R_a = 11$  mm. If certain values for other variables are given as below:

beater speed  $n_b = 100$  rpm,

$b_{pr} = 4$  mm,

$h_{pr} = 0.65$  mm (preliminary),



and also noting that  $\omega_b = 2\pi n_b$ , then, from equations (AI.2) & (AI.3),

$$F_{C_{W_{ep}}} \approx 6.47 \times 10^{-4} N$$

$$F_{C_{pr}} \approx 8.64 \times 10^{-4} N$$

Putting these values into equation (AI.4), the total stress at point A is:

$$\sigma_{AC} \approx 5.81 \times 10^{-4} N/mm^2$$

and the corresponding strain is:

$$\epsilon_{AC} = \frac{\sigma_{AC}}{E_{pr}} \approx 3.06 \times 10^{-7} \%$$

Thus, it can be noted that the centrifugal force at the beater speed of 100 rpm contributes very little to the total tensile stress and strain at point A. At any beater speed below 100 rpm, such as 60 rpm used in the pin force measurement (refer to Chapter 3), the effect of the centrifugal force can be neglected without affecting the final magnitude of pin force.

According to these calculations, the pin arm should be stable with the chosen preliminary dimensions. Next, the natural frequency of the pin arm was calculated to check its dynamic response.

### (e) Natural Frequency of The Pin Arm

The natural frequency of the pin arm,  $f_n$ , can be calculated from the equation below:

$$f_n = \frac{1}{4\pi} \sqrt{\frac{E_{pr} g_{pr} b_{pr} h_{pr}^3}{L'_{pr}{}^3 (W_{ep} + 0.236 W_{pr})}} \quad \dots (AI.5)$$

where  $W_{pr}$  is the weight of the pin arm.

In practical design, this frequency should be more than ten times the signal frequency.

Values for some parameters in the above equation are listed below:

$$L'_{pr} = 18.2 \text{ mm}, b_{pr} = 4 \text{ mm}, h_{pr} = 0.65 \text{ mm},$$

$$W_{pr} = b_{pr} h_{pr} L'_{pr} \rho_{pr} = 4 \times 10^{-4} \text{ kg},$$

$$g = 9800 \text{ mm/s}^2,$$

$$W_{ep} = 2 \times 10^{-4} \text{ kg}.$$

Putting these values into equation (AI.5), the natural frequency of the pin arm can be calculated as being,

$$f_n \approx 854 \text{ Hz}$$

If the beater rotates at a speed below 100 rpm, its frequency is less than 2 Hz, but this frequency is not exactly the frequency of the pin force variation. During each passage of the pin through a fibre fringe, the frequency of pin force variation will be dependant on the extent of fibre entanglement in that fringe. It is reasonable to assume that in each passage of the pin through a fringe no longer than 40 mm in the combing zone (refer to Chapter 3), the total number of entanglements encountered by the pin would be no more than 10. Therefore, the frequency of pin force variation at a beater speed below 100 rpm should be less than 20 Hz. Since ten times this frequency (i.e. 200 Hz) is much less than the natural frequency of the pin arm (i.e.

854 Hz), the pin arm should satisfy the requirement for a fast dynamic response. However, when the strain gauges are mounted on the pin arm, additional weight from the strain gauges, the adhesive material used, and the electrical wires connected to the strain gauges will be added to the pin arm, which could reduce its natural frequency slightly. Nevertheless, these preliminary dimensional values for the pin arm can still be used as a theoretical foundation for the design of the pin arm.

### **(f) Strain Gauges**

For accurate measurements, the strain gauges should have no effect on the test object, the gauge grids should be properly protected, and if possible, the gauges should be large enough to make their handling easier. Based on the pin arm dimension values given in the previous sections, strain gauges were selected having the following important standard specifications:

Base dimensions: length 6mm, width 2.5mm,

Measurable strain: 2 to 4% maximum,

Temperature range:  $-30^{\circ}$  to  $+80^{\circ}$ ,

Gauge factor: 2.0 (nominal).

The distance from the centre of the strain gauges to point A ( $l_{sg}$ , Figure A2.1) is about 7 mm.

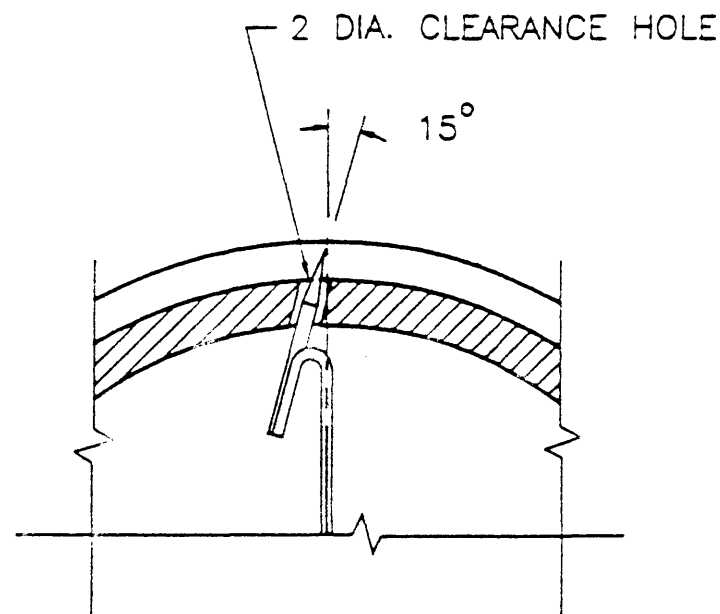
**(g) Modifications**

The pin arm was constructed with its dimensions selected mainly according to the calculations in the previous sections. One modification was the pin arm thickness value ( $h_{pr}$ ), which in section (b) is given the preliminary value of 0.65 mm. Since the stainless steel sheet of 0.72 mm thickness was more easily available in the market, and much easier to be worked with in the available workshop, the thickness of the pin arm was therefore finally chosen as 0.72 mm. This obviously would have very little adverse effect on the pin arm performance during the pin force measurement, as is indicated in Chapter three. Other minor modifications to the pin arm dimensions are also allowed based on the calculations presented here. Details of the final pin arm assembly are given in the attached drawings.

---

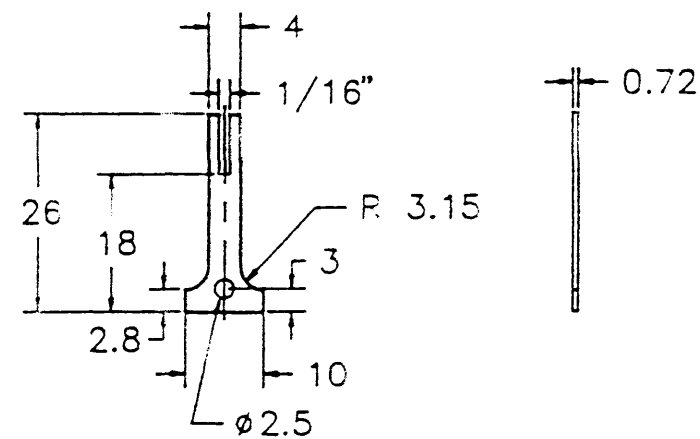
**References:**

1. Potma, T.  
"Strain gauges: Theory and application".  
ILIFFE Books Ltd., London, 1967.
2. Higdon, A.  
"Mechanics of material (2nd edition)".  
John Wiley & Sons, Inc., New York, 1967.
3. Zhu, J., Tong, Z., Yu, H. and Dai, G.  
"Electrical measurement techniques in textiles".  
Textile industry press, Beijing, 1983. (in Chinese)



DETAIL OF BEATER AND PIN

SCALE 2:1




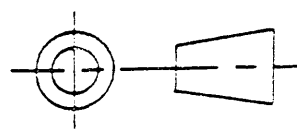
PIN ARM

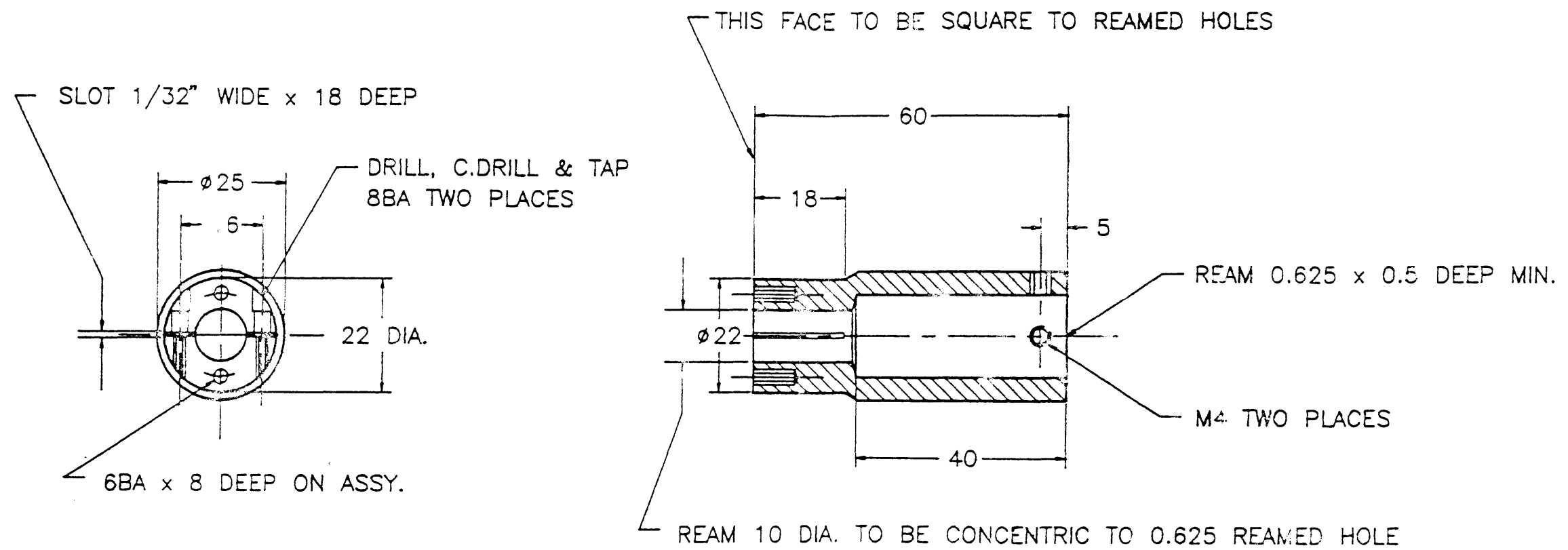
MATERIAL STAINLESS STEEL SHEET 0.72 THICK

QTY. 1.

THE UNIVERSITY OF NEW SOUTH WALES  
FACULTY OF APPLIED SCIENCE  
DEPARTMENT OF TEXTILE TECHNOLOGY

# PIN FORCE EXPERIMENT

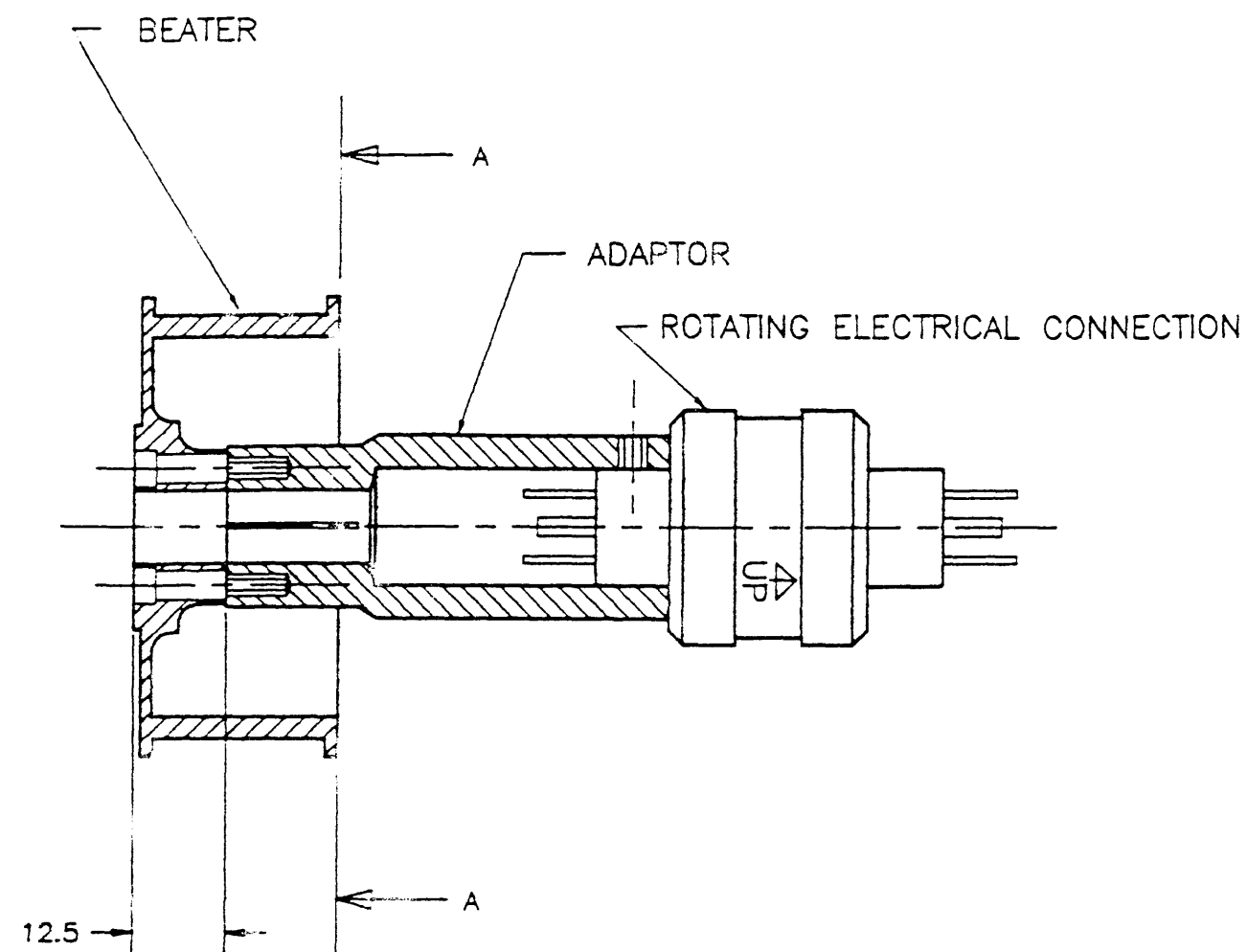
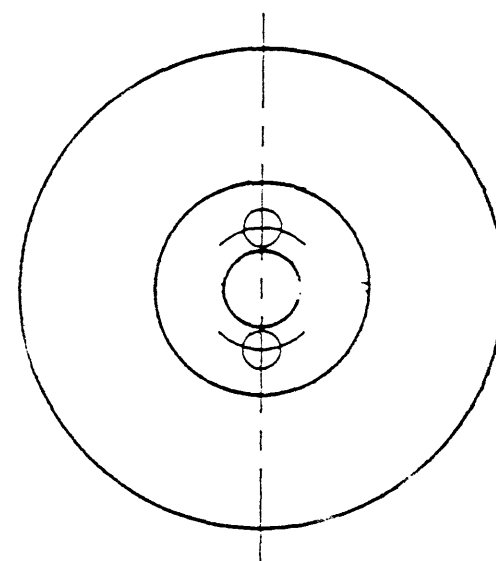
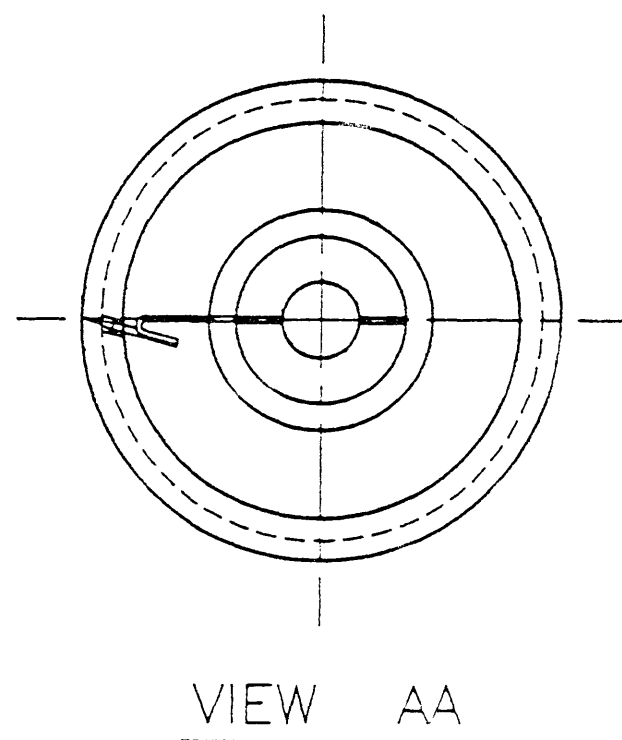
Unless otherwise stated all dimensions in millimeters  Tolerances except as stated  Linear Angular			Design WANG/FISK Drawn A.J.FISK Approved	Date 27-11-89 Scale 1:1 OR AS SHOWN Sheet Size A0	DRG. No. 10-1052-01
--	---	---	--	---	------------------------



## PIN FORCE ADAPTOR

MATERIAL ALUMINIUM

QTY. 1



## SUB ASSEMBLY

BEATER MODIFY TO DRAWING.

ADAPTOR MAKE AS PER DRAWING

ROTATING ELECTRICAL CONNECTION SUPPLIED

PIN ARM MAKE AS PER DRAWING

PIN 1 DIA.x 12.7 LONG SUPPLIED

APPENDIX II

TABLES OF EXPERIMENTAL DATA

Table AII.1: Raw data for Figure 2.5

Combing speed (rpm)	800				1000				1200			
Test fibre length (mm)	20	30	40	50	20	30	40	50	20	30	40	50
Individual test fibre tension values (cN)	0.17	0.19	0.43	0.60	0.28	0.45	0.60	0.77	0.29	0.44	0.61	0.92
	0.10	0.20	0.48	0.63	0.20	0.46	0.58	0.93	0.30	0.55	0.53	0.77
	0.08	0.13	0.42	0.61	0.21	0.43	0.58	0.78	0.26	0.53	0.61	0.80
	0.12	0.20	0.31	0.67	0.17	0.35	0.53	0.71	0.29	0.61	0.68	0.78
	0.14	0.30	0.46	0.68	0.20	0.37	0.55	0.62	0.26	0.44	0.69	0.79
	0.14	0.24	0.46	0.52	0.21	0.31	0.51	0.67	0.30	0.55	0.68	0.82
	0.10	0.22	0.21	0.64	0.18	0.43	0.57	0.66	0.24	0.43	0.67	0.81
	0.13	0.21	0.47	0.51	0.15	0.41	0.54	0.68	0.35	0.56	0.66	0.82
	0.12	0.20	0.27	0.61	0.18	0.39	0.53	0.67	0.28	0.53	0.61	0.78
	0.08	0.18	0.42	0.58	0.16	0.42	0.51	0.66	0.27	0.61	0.65	0.82
Mean	0.12	0.21	0.39	0.61	0.20	0.40	0.55	0.72	0.28	0.53	0.64	0.81
Std Dev.	0.03	0.04	0.09	0.06	0.03	0.05	0.03	0.09	0.03	0.07	0.05	0.04
95% C.I.	0.02	0.03	0.07	0.04	0.02	0.03	0.02	0.06	0.02	0.05	0.04	0.03

Fringe length 25 mm; fringe density 1.8 Ktex.



Table AII.2: Raw data for Figure 2.6

Fringe density (Ktex)	1.0				0.5			
Test fibre length (mm)	20	30	40	50	20	30	40	50
Individual test fibre tension values (cN)	0.62	0.72	1.01	1.18	0.27	0.31	0.45	0.56
	0.46	0.67	0.94	1.17	0.26	0.45	0.54	0.60
	0.51	0.81	0.86	1.07	0.29	0.32	0.38	0.55
	0.56	0.81	0.88	1.06	0.31	0.44	0.54	0.68
	0.59	0.72	0.91	0.94	0.23	0.35	0.54	0.58
	0.61	0.65	0.95	1.11	0.24	0.41	0.50	0.59
	0.56	0.74	0.79	0.99	0.28	0.42	0.54	0.60
	0.32	0.62	0.89	1.16	0.26	0.40	0.48	0.56
	0.48	0.65	0.95	0.91	0.27	0.43	0.44	0.50
	0.36	0.61	0.92	0.91	0.24	0.31	0.41	0.53
Mean	0.51	0.70	0.91	1.05	0.26	0.38	0.48	0.58
Std Dev.	0.11	0.07	0.06	0.11	0.02	0.06	0.06	0.05
95% C.I.	0.08	0.05	0.04	0.08	0.02	0.04	0.04	0.04

Fringe length 50 mm; combing speed 800 rpm.

Table AII.3: Raw data for Figure 2.9

Test fibre length (mm)	20			30			40			50		
Combing speed (rpm)	800	1000	1200	800	1000	1200	800	1000	1200	800	1000	1200
Individual test fibre tension values (cN)	0.17	0.28	0.29	0.19	0.45	0.44	0.43	0.60	0.61	0.60	0.77	0.92
	0.10	0.20	0.30	0.20	0.46	0.55	0.48	0.58	0.53	0.63	0.93	0.77
	0.08	0.21	0.27	0.13	0.43	0.53	0.42	0.58	0.61	0.61	0.78	0.80
	0.12	0.17	0.29	0.20	0.35	0.61	0.31	0.53	0.68	0.67	0.71	0.78
	0.14	0.20	0.26	0.30	0.37	0.61	0.46	0.55	0.69	0.68	0.62	0.79
	0.14	0.21	0.30	0.24	0.31	0.44	0.46	0.51	0.68	0.52	0.67	0.82
	0.10	0.18	0.24	0.22	0.43	0.55	0.21	0.57	0.67	0.64	0.66	0.81
	0.13	0.15	0.35	0.21	0.41	0.43	0.47	0.54	0.66	0.51	0.68	0.82
	0.12	0.18	0.28	0.20	0.39	0.56	0.27	0.53	0.61	0.61	0.67	0.78
	0.08	0.16	0.26	0.18	0.42	0.53	0.42	0.51	0.65	0.58	0.66	0.82
Mean	0.12	0.20	0.28	0.21	0.40	0.53	0.39	0.55	0.64	0.61	0.72	0.81
Std Dev.	0.03	0.03	0.03	0.04	0.05	0.07	0.09	0.03	0.05	0.06	0.09	0.04
95% C.I.	0.02	0.02	0.02	0.03	0.03	0.05	0.07	0.02	0.04	0.04	0.06	0.03

Fringe length 25 mm; fringe density 1.8 Ktex.

Table AII.4: Raw data for Figure 2.11

Fringe length (mm)	15	25	35	50
Individual test fibre tension values (cN)	0.48	0.51	0.92	1.18
	0.44	0.61	0.79	1.17
	0.32	0.35	0.84	1.07
	0.29	0.40	0.81	1.06
	0.30	0.56	0.83	0.94
	0.34	0.60	0.77	1.11
	0.42	0.44	0.82	0.99
	0.32	0.71	0.73	1.16
	0.30	0.51	0.77	0.91
	0.31	0.50	0.75	0.91
	0.28	0.54	0.71	-
	0.32	0.53	0.68	-
	0.28	0.41	0.66	-
	0.26	0.31	0.69	-
	0.32	0.30	0.76	-
Mean	0.33	0.48	0.77	1.05
Std Dev.	0.07	0.12	0.07	0.11
95% C.I.	0.04	0.07	0.04	0.08

Test fibre length 50 mm; fringe density 1 Ktex; combing speed 800 rpm.

Table AII.5: Raw data for Figure 2.12

Fringe density (Ktex)	0.2	0.6	1.0	1.4	1.8	2.2
Individual test fibre tension values (cN)	0.39	0.51	0.51	0.61	0.60	0.60
	0.35	0.43	0.61	0.50	0.63	0.61
	0.37	0.39	0.35	0.52	0.61	0.78
	0.20	0.52	0.40	0.53	0.67	0.59
	0.20	0.42	0.56	0.72	0.68	0.69
	0.15	0.42	0.60	0.49	0.52	0.83
	0.38	0.41	0.44	0.56	0.64	0.72
	0.37	0.36	0.71	0.49	0.51	0.61
	0.43	0.50	0.51	0.48	0.61	0.65
	0.24	0.49	0.50	0.58	0.58	0.61
	0.33	0.42	0.54	0.53	-	0.69
	0.40	0.33	0.53	0.55	-	0.65
	0.31	0.30	0.41	0.49	-	0.68
	0.24	0.25	0.31	0.50	-	0.60
	0.20	0.36	0.29	0.50	-	0.58
Mean	0.30	0.40	0.48	0.54	0.61	0.66
Std Dev.	0.09	0.07	0.12	0.06	0.05	0.07
95% C.I.	0.05	0.02	0.07	0.04	0.03	0.04

Fringe length 25 mm; test fibre length 50 mm; combing speed 800 rpm.

Table AII.6: Raw data for Figure 3.6

Fringe density (Ktex)	0.5	1.0	1.5
Individual pin force values (cN)	29.01	29.67	142.86
	16.26	21.98	153.85
	12.75	26.37	145.06
	19.12	64.40	44.84
	23.70	76.26	100.00
	18.24	63.74	124.84
	17.58	25.71	61.10
	34.29	21.54	47.91
	17.14	40.22	81.98
	21.54	38.24	40.22
	14.51	44.84	51.43
	13.19	56.70	97.36
	14.95	25.71	117.80
	25.93	27.03	79.34
	19.12	78.24	129.01
	22.64	36.04	56.92
	17.14	50.77	44.62
	14.07	43.52	92.53
	26.15	33.19	74.07
	13.85	94.51	54.51
	14.51	32.31	60.22
	18.24	46.59	70.55
	17.80	23.30	41.54
	19.78	21.54	94.95
	39.34	28.13	58.90
Mean	20.03	42.02	82.66
Std Dev.	6.65	20.10	35.52
95% C.I.	2.75	8.30	14.66

Fringes: after 3 gillings, 40 mm in the combing zone.

Table AII.7: Raw data for Figure 3.7

Number of gillings	one			three		
Fringe length (mm)	20	30	40	20	30	40
Individual pin force values (cN)	23.16	18.32	72.97	17.42	13.63	29.67
	17.47	50.46	34.29	12.43	17.14	21.98
	15.15	37.51	67.25	7.86	66.59	26.37
	14.37	20.34	49.45	5.32	30.33	64.40
	21.88	21.37	66.15	6.97	30.77	76.26
	53.25	45.82	21.98	21.72	21.54	63.74
	47.36	71.10	83.52	8.51	27.25	25.71
	9.99	67.33	66.81	9.90	29.89	21.54
	7.85	29.42	35.17	22.82	30.33	40.22
	12.42	33.15	34.73	7.94	36.92	38.24
	32.60	42.17	50.33	11.96	26.37	44.84
	37.17	44.82	79.78	6.37	19.12	56.70
	11.43	63.90	37.80	16.72	16.26	25.71
	9.41	55.13	67.25	16.30	13.85	27.03
	8.32	75.92	109.89	8.55	29.00	78.24
	7.76	77.36	45.93	19.22	23.08	36.04
	13.54	23.62	51.43	7.73	45.50	50.77
	32.74	31.91	105.05	8.31	18.24	43.52
	35.42	34.74	93.85	9.42	14.73	33.19
	32.67	53.92	72.09	9.30	32.75	94.51
	14.93	66.32	66.15	6.88	14.29	32.31
	21.51	56.55	60.66	10.43	17.14	46.59
	8.17	44.80	62.20	12.25	24.62	23.30
	7.82	37.92	42.42	8.62	22.64	21.54
	7.73	20.88	39.12	8.14	14.07	28.13
Mean	20.16	44.99	60.65	11.24	25.44	42.02
Std Dev.	13.39	18.26	22.57	4.93	11.87	20.10
95% C.I.	5.53	7.54	9.32	2.04	4.90	8.30

Fringe linear density: 1 Ktex.

Table AII.8 Raw data for Figure 3.8

Number of gillings	zero	one	three
Individual pin force values (cN)	103.72	72.97	29.67
	57.34	34.29	21.98
	49.52	67.25	26.37
	49.03	49.45	64.40
	83.10	66.15	76.26
	147.82	21.98	63.74
	73.77	83.52	25.71
	59.25	66.81	21.54
	76.80	35.17	40.22
	85.42	34.73	38.24
	63.16	50.33	44.84
	43.25	79.78	56.70
	54.90	37.80	25.71
	74.84	67.25	27.03
	103.28	109.89	78.24
	43.52	45.93	36.04
	62.72	51.43	50.77
	67.55	105.05	43.52
	78.04	93.85	33.19
	57.45	72.09	94.51
	51.32	66.15	32.31
	74.08	60.66	46.59
	65.22	62.20	23.30
	73.67	42.42	21.54
	101.19	39.12	28.13
Mean	72.24	60.65	42.02
Std Dev.	23.86	22.57	20.10
95% C.I.	9.85	9.32	8.30

Fringes: 1.0 Ktex, 40 mm in the combing zone.

## REFERENCE

---

1. Australian Wool Corporation.  
Guide to Wool Textiles.  
About Wool, No. 3, July, 1988.
2. Brearley, A. and Iredale, John A.  
"The Worsted Industry (2nd Edition)".  
Wira, Leeds, 1980.
3. Brearley, A. and Iredale, John A.  
"The Woollen Industry (2nd Edition)".  
Wira, Leeds, 1977.
4. Dyson, E. and Happey, F.  
An Experimental Study of Woolcombing.  
J. Text. Inst., 51, T1016, 1960.
5. Ross, D.A., Carnaby, G.A. and Lappage, J.  
Woollen-yarn Manufacture.  
Textile Progress, Vol. 15, No. 1/2, 1986.
6. Townend, P.P. and Spiegel, E.J.  
Fibre Breakage in Worsted Carding.  
J. Text. Inst., 37, T58, 1946.
7. Kraus, K.  
Über die Ursachen der Noppenbildung in Kammwollen.  
Melliand Textilber. (German Ed.), 14, 169, 1933.
8. Townend, P.P. and Spiegel, E.  
Nep Formation in Worsted Carding.  
J. Text. Inst., 35, T17, 1944.



9. Aldrich, De V.  
"A Study of the Rectilinear Combing of Fibres".  
Ph.D. Thesis, University of Port Elizabeth, South Africa, 1971.
10. Belin, R.E., Taylor, D.S. and Walls, G.W.  
Some Comparisons between Noble and Rectilinear Combing.  
Third Int. Wool Text. Res. Conf., Paris, IV-71, 1965.
11. Ogden, A.J.  
The Relative Merits of the Noble and French Combs in Recombing.  
J. Text. Inst., 57, T520, 1966.
12. Aldrich, De V., Kruger, P.J. and Turpie, D.W.F.  
The Carding and Combing of Wools of Different Fibre Lengths.  
SAWTRI Techn. Rep. 136, Jun. 1970.
13. Chaikin, M. and Collins, J.D.  
In "Contemporary Textile Engineering" (Editor: Happey, F.).  
Academic Press, London, 1982.
14. Gore, C.E. and Lee, C.S.P.  
Increased Efficiency and Quality.  
Textile Horizons, vol. 2, No. 7, July, 1989.
15. Needham, H. and Parkin, W.  
Principles of the Rectilinear Comb.  
Wool Textile Industry, 40, 14, April 1966.
16. Walker, R.  
The Rectilinear Comb.  
Textile Manufacturer, 53, 69, 1957.
17. Spibey, H. (Editor).  
"The British Wool Manual (2nd Edition)".  
Columbine Press, 1969.

18. Belin, R.E. and Walls, G.W.  
A Preliminary Investigation of the Rectilinear Combing of Wool.  
J. Text. Inst., 54, T171, 1963.
19. Belin, R.E. and Verhagen, A.M.  
The Rectilinear Combing of Wool.  
J. Text. Inst., 56, T349, 1965.
20. Kruger, P.J.  
Carding and Combing of Mohair - Part III: Rectilinear Combing.  
SAWTRI Techn. Rep., No.118, 1969.
21. Kruger, P.J. and Aldrich, De V.  
Fibre Breakage in Rectilinear Combing.  
Applied Polymer Symposium, No. 18, 1375, 1971.
22. Godawa, T.O., Kruger, P.J. and Veldsman, D.P.  
The Behaviour of the Rectilinear Comb.  
SAWTRI Techn. Rep. 49, 1965.
23. Kruger, P.J.  
Withdrawal Forces in the Processing of Wool Slivers - Part I: The Determination of the Withdrawal Force.  
J. Text. Inst., 58, 463, 1967.
24. Kruger, P.J.  
Withdrawal Forces in the Processing of Wool Slivers,  
Part II: The Influence of Variations in Gilling on the Withdrawal Forces.  
J. Text. Inst., 58, 472, 1967.
25. Kruger, P.J.  
Withdrawal Forces in the Processing of Wool Sliver,  
Part III: The Influence of Pin Density Variations.  
J. Text. Inst., 58, 478, 1967.

26. Belin, R.E.  
Residual Grease in the Gilling and Rectilinear Combing of Wool.  
J. Text. Inst., 58, 169, 1967.
  
27. Belin, R.E.  
Mineral Lubricants and the Effect of Backwashing in the Preparing of Combing Wools.  
J. Text. Inst., 59, 575, 1968.
  
28. Kruger, P.J.  
The Influence of Lubricants in Rectilinear Combing.  
J. Text. Inst., 58, 158, 1967.
  
29. Turpie, D.W.F. and Klazar, J.  
The Effect of Comb Speed on Rectilinear Combing Performance.  
SAWTRI Bulletin, 11, 19-21, Dec. 1977.
  
30. Belin, R.E. and Taylor, D.S.  
Directional Effects in Worsted Rectilinear Combing.  
J. Text. Inst., 58, 145, 1967.
  
31. Belin, R.E.  
Some Observations on Neps and Vegetable Particles in the Rectilinear Combing of Wool.  
J. Text. Inst., 58, 626, 1967.
  
32. Verhagen, A.W.M. and Belin, R.E.  
The Equilibrium Distribution of Vegetable Particles in The Beard of a Worsted Rectilinear Comb.  
J. Text. Inst., 59, 557, 1968.
  
33. Belin, R.E. and Verhagen, A.W.M.  
The Transfer of Vegetable Particles from Beard to Sliver in Worsted Rectilinear Combing.  
J. Text. Inst., 59, 567, 1968.

34. Wood, G.F.  
The Effect of Some Precarding Conditions on Wool Combing.  
J. Text. Inst., 61, 56, 1970.
  
35. Aldrich, De V.  
The Combing Performance of Different Types of Comb Cylinders For Rectilinear Combs.  
SAWTRI Technical Report, No. 145, 1971.
  
36. Atkinson, K.R., Harrowfield, B.V., Plate, D.E.A. and Robinson, G.A.  
Increasing Card Productivity.  
CSIRO Division of Textile Industry Symposium on Wool Scouring & Worsted Carding, Geelong, Australia, Nov., 1986.
  
37. Chaikin, M.  
New Methods in the Processing of Wool Tops.  
Applied Polymer Symposium No. 18, 1215-1227, 1971.
  
38. Alexander, P., Hudson, R.F and Earland, C.  
"Wool, Its Chemistry and Physics".  
Chapman & Hall Ltd., London, 1963.
  
39. Onions, W.J.  
"Wool: An Introduction to Its Properties, Varieties, Uses and Productions".  
E. Benn Ltd., London, 1962.
  
40. Hearle, J.W.S  
"Fibre Structure".  
The Textile Institute, Manchester, 1963.
  
41. Leeder, J.D.  
Wool Science Review, 63, 1986.

42. Ferry, J.D.  
"Viscoelastic of Polymer (2nd Edition)".  
John Wiley & Sons, Inc., New York, 1970.
43. Postle, R., Carnaby, G.A., and Jong, S.de.  
"The Mechanics of Wool Structures".  
Ellis Horwood Limited. Chichester, England, 1988.
44. Morton, W.E. and Hearle, J.W.S.  
"Physical Properties of Textile Fibres (2nd edition)".  
Wm Heinemann and The Textile Institute, Manchester, 1975.
45. Harrowfield, B.V., Plate, D.E.A. and Eley, J.R.  
From Raw Wool to Top.  
CSIRO Division of Textile Industry Symposium on Wool Scouring and  
Worsted Carding, Geelong, Australia, Nov. 1986.
46. Tobolsky, A.V. and Eyring, H.  
J. Chem. Phys., 11, 125, 1943.
47. Halsey, G., White, H.J. and Eyring, H.  
Mechanical Properties of Textile, I.  
Text. Res. J., 15, 295, 1945.
48. Meredith, R.  
"The Mechanical Properties of Textile Fibres".  
NorthHolland Publishing Company, Amsterdam, pp. 87 et seq., 1956.
49. Leaderman, H.  
"Elastic and Creep Properties of Filamentous Materials and Other  
High-Polymers"  
The Textile Foundation, Washington, D.C., 1943.

50. Dickson, J.B. and Davieau, L.A.  
Impact Tester for Textiles.  
ASTM Bulletin 198, 85-90, 1954.
  
51. Meredith, R.  
The Effect of Rate of Extension on the Tensile Behavior of Viscose and Acetate Rayons, Silk, and Nylon.  
J. Text. Inst., 45, T30, 1954.
  
52. McCrackin, F.L., Herbert, F.S., Smith, J.C., and Stone, W.K.  
Stress-Strain Relationships in Yarns Subjected to Rapid Impact Loading, Part II: Breaking Velocities, Strain Energies, and Theory Neglecting Wave Propagation.  
Text. Res. J., 15, 529, 1955.
  
53. Smith, J.C., McCrackin, F.L., and Schiefer, H. F.  
Stress-Strain Relationships in Yarns Subjected to Rapid Impact Loading, Part III: Effect of Wave Propagation.  
Text. Res. J., 25, 701, (1955).
  
54. Lyons, W.J.  
"Impact Phenominon in Textiles".  
The M.I.T. Press, Cambridge, Massachusetts, 1962.
  
55. Timoshenko, S.  
"Elements of Strength of Materials".  
van Nostrand-Reinhold, New York, 1968.
  
56. Koch, P.A.  
Textil-Rdsch., 4, 199, 1949, and 6, 111, 1951.
  
57. Lincoln, B.  
The Frictional Properties of Wool Fibres.  
J. Text. Inst., 45, T92, 1954.

58. Mercer, E.H. and Makinson, K.R.  
The Frictional Properties of Wool and Other Textile Fibres.  
J. Text. Inst., 38, T227, 1947.
59. Makinson, K.R.  
Trans. Faraday Soc., 44, 279, 1948.
60. Lindberg, J. and Gralen, N.  
Measurement of Friction Between Single Fibres - II. Frictional Properties of  
Wool Fibre Measured by the Fibre-Twist Method.  
Text. Res. J., 18, 287, 1948.
61. Shooter, K.V. and Tabor, D.  
Proc. Phys. Soc., B65, 661, 1952.
62. Makinson, K.R.  
"Surface Characteristics of Fibres and Textiles Part I".  
Editor M. J. Schick, Marcel Dekker, Inc., New York, 109, 1975.
63. Young, M.D. and Johnson, N.A.G.  
Wool Fibre Damage in Feeding Devices for Open-end Spinning.  
Proc. Text. Inst. Conf. Sydney, 389, 1988.
64. Howell, H.G., Mieszkis, K.W. and Tabor, D.  
"Friction in Textiles".  
Butterworths Publications Ltd., London, 1959.
65. Taylor, D.S.  
The Determination of Contacts Between the Constituents of the Fibre  
Assemblies.  
J. Text. Inst., 47, T141, 1956.
66. Grosberg, P.  
The Strength of Twistless Slivers.  
J. Text. Inst., 54, T223, 1963.

67. Maltin, G.  
Simplified Analysis of the Disentanglement of a Fibre Clump.  
Text. Res. J., 41, 685-691, 1971.
  
68. Wood, E.J., Stanley-Boden, P. and Carnaby, G.A.  
Fibre Breakage During Carding - Part II: Evaluation.  
Text. Res. J., 54, 419, 1984.
  
69. Carnaby, G.  
Fibre Breakage During Carding - Part I: Theory.  
Text. Res. J., 54, 366, 1984.
  
70. Henshaw, D.E.  
The Role of a Lubricant and Its Viscosity in Worsted Carding.  
J. Text. Inst., 52, T537, 1961.
  
71. Eley, J.R. and Harrowfield, B.V.  
Reduced Fibre Breakage in Continental Worsted Carding as a Result of Wool Lubrication.  
J. Text. Inst., 77, 274, 1986.
  
72. Landwehrkamp, H.  
Preparation and Spinning of Wool with the Rotor-Spinning System.  
Text. Res. J., 49, 137, 1979.
  
73. Harrowfield, B.V., Robison, G.A. and Eley, J.R.  
The Removal of Entanglements in Carding.  
CSIRO Devision of Textile Industry Symposium on Wool Scouring and Worsted Carding, Geelong, Australia, Nov. 1986.
  
74. Xu, L. and Zhou, Q.  
A Method of Abating Fibre Breakage in the Taker-in Part.  
J. China Text. University (English Edition), No.1, 1986.



75. Yan, Y.  
"Wool Fibre Damage Caused by Clothed Surfaces".  
Ph.D Thesis, The University of New South Wales, Australia, 1991.
76. Salhotra, K.R. and Chattopadhyay, R.  
Incidence and Mechanism of Fibre Breakage in Rotor Spinning.  
Text. Res. J., 52, 317-320, 1982.
77. Siersch, E.  
"Contribution to the Mechanism of the Fibre Transport in OE rotor Spinning".  
Ph.D Thesis, Rhine-Westfalian Technical University, Aachen, Germany,  
1980.
78. Yan, Y. and Johnson, N.A.G.  
The Behaviour of Fibres Struck by High Speed Pins - Part I: Theory.  
J. Text. Inst., (accepted for publication).
79. Chaikin, M. and Chamberlain, N.H.  
The Propagation of Longitudinal Stress Pulses in Textile Fibres - Part I.  
J. Text. Inst., 46, T25, 1955.
80. Halliday, D. and Resnick, R.  
"Physics".  
John Wiley & Sons, Inc., 1966.
81. Postle, L.J., Ingham, J. and Cox, D.R.  
The Measurement of Inter-fibre Friction in Slivers.  
J. Text. Inst., 43, T77, 1952.
82. Yan, Y. and Johnson, N.A.G.  
The Effect of Opening Roller Speed on Wool Fibre Damage in Open-end  
Spinning.  
Proc. 8th Int. Wool Text. Res. Conf. Christchurch, III 267, 1990.

83. Young, M.D. and Johnson, N.A.G.  
Abrasion of Wool Fibres by Pinned Surfaces.  
Proc. 8th Int. Wool Text. Res. Conf. Christchurch, III 389, 1990.
84. Malachowski, G.C. and Hall, B.R.  
"DAOS Reference Manual (for PC/MS-DOS, Version 7.0)".  
Interface Publications Pty. Ltd., Australia, 1986.
85. Shannon, C.E.  
"The Mathematical Theory of Communication".  
University of Illinois Press, Urbana, 1949.
86. Light, G.S. and Higham, J.B.  
"Theoretical Mechanics".  
Longman, London, 1975.
87. Wilson, N. and Treloar, L.R.G.  
British Journal of Applied Physics, 12, 147, 1961.
88. Emmanuel, A. and Plate, D.E.A.  
An Alternative Approach to Two-Fold Weaving Yarn Part II: The  
Theoretical Model.  
J. Text. Inst., 3, 107, 1982.
89. Platt, M.M., Klein, W.G. and Hamburger, W.J.  
Mechanics of Elastic Performance of Textile Materials - Part XIII: Torque  
Development in Yarn Systems: Singles Yarn.  
Text. Res. J., 28, 1, 1958.
90. Postle, R., Burton, P. and Chaikin, M.  
The Torque in Twisted Singles Yarns.  
J. Text. Inst., 55, T448, 1964.

91. Hearle, J.W.S., Grosberg, P. and Backer, S.  
"Structural Mechanics of Fibres, Yarns, and Fabrics (Vol. 1)".  
John Wiley & Sons, New York, p66, 1969.
92. Emmanuel, A. and Plate, D.E.A.  
An Alternative Approach to Two-Fold Weaving Yarn Part III: Testing of  
The Theoretical Model.  
J. Text. Inst., 3, 117, 1982.
93. Gracie, P.S.  
Twist Geometry and Twist Limits in Yarns and Cords.  
J. Text. Inst., 51, T271, 1960.
94. Postle, R., The University of New South Wales.  
Personal communication, 1991.
95. Timoshenko, S.  
"Theory of Elastic Stability".  
McGraw-Hill, New York, p169 and p67, 1936.
96. Bennett, J.M.  
"The Mechanics of Yarn Structures in Torsion".  
Ph.D Thesis, The University of New South Wales, Australia, 1977.
97. Kawabata, S.  
"The Standardization and Analysis of Hand Evaluation (2nd Edition)".  
The Textile Machinery Society of Japan, 1980.
98. Dhingra, R.C.  
"Bending and Torsional Properties of Textile Yarns".  
Ph.D Thesis, The University of New South Wales, Australia, 1975.
99. Holmes-Brown, R.L. and Carnaby, G.A., J. Soc. Dyers Col., 98, 243, 1982.
100. El-Shiekh, A., D.Sc Thesis, Massachusetts Institute of Technology, 1965.

L

P  
T677.31  
40

>009523243



